Novel Imaging and Circulating Biomarkers in Hepatic Malignancies

Helen S Winter

Green Templeton College, University of Oxford

A Thesis Submitted for the Degree of Doctor of Philosophy

Michaelmas Term 2019

Acknowledgements

To the many people who have supported me throughout this thesis and especially:

- The patients who gave informed consent to take part in this clinical research
- My wise and supportive academic supervisors Professors Sharma, Bulte, Kerr and Gleeson
- Colleagues in the Department of Oncology and at the OUH NHS Trust
- My supportive and wonderful family

Declaration of the work of others

1. The motion correction and PK modelling discussed in Chapter 3 were carried out by Dr Bartlomiej Papiez and Dr Benjamin Irving, Department of Engineering.
2. T1 mapping scanning was supervised in collaboration with Dr Michael Pavlides at the Oxford Centre for Magnetic Resonance. Histological samples were prepared by Dr Lai Mun Wang (LW).
3. The mass spectroscopy was performed by Dr Joe Harvey, Mass Spectrometry Research Facility, Chemistry Research Laboratory, University of Oxford, Mansfield Rd, Oxford.

Novel imaging and circulating biomarkers in hepatic malignancies

Abstract

Colorectal cancer (CRC) that has metastasised to the liver has a median survival of less than 24 months unless patients have resectable disease. Liver-directed therapies target disease to improve hepatic disease-control. Selective internal radiation therapy (SIRT) exploits the arterial blood supply to the liver to deliver yttrium-90 (^{90}Y) microspheres. Optimising radiation delivery whilst sparing normal liver is an important part of the work-up. Imaging biomarkers to determine vascularity and microcirculation may improve patient selection for liver-directed therapies. This research project studied the following imaging modalities to optimise patient selection for liver-directed therapy: perfusion computerized tomography (pCT); dynamic contrast enhanced magnetic resonance imaging (DCE MRI); T1 mapping (native and oxygen-enhanced) MRI.

Patients were recruited in three clinical trials, each exploring tissue and imaging biomarkers of potential response to therapy: FOXFIRE; PERFORM and NICOLA studies. The PERFORM trial investigated the feasibility of multi-parametric imaging to measure hepatic perfusion and generate parameter maps pre- and post-SIRT treatment through pCT and DCE MRI. The distribution and location of microspheres were described through the histopathological analysis of patients from the FOXFIRE study in patients who had hepatic resection post-SIRT. T1 mapping pre- and during high flow oxygen inhalation in the NICOLA study explored the role of this emerging technique for the characterisation of liver lesions having a hepatic resection.

The potential role of complimenting imaging biomarkers with circulating biomarkers was also explored. Circulating tumour DNA (ctDNA) was extracted at three time-points having pCT and DCE MRI after SIRT. Ion Torrent Amplicon sequencing detected multiple somatic mutations associated with CRC and the quantification of these mutations over time. This was also expanded to include patients with intrahepatic cholangiocarcinomas (ICC) and included some measurements of circulating metabolites with liquid chromatography mass spectrometry.

The PERFORM study recruited 58 patients to examine the feasibility of pCT and DCE MRI to generate perfusion parameters pre- and post-SIRT. The hypothesis was that baseline perfusion parameters reflecting high blow flow would increase delivery of SIRT microspheres and would predict for response. The second hypothesis was that a reduction in perfusion parameters would act as a biomarker for the response to the targeted delivery of ^{90}Y, at four weeks rather than the standard imaging at 12 weeks.

The acquisition and analysis of pCT parameters was completed via 4D perfusion software. Specific parameters measured were – blood flow; blood volume; mean transit time and permeability surface area product. Pharmacokinetic modelling post DCE MRI acquisition supported the generation of K^{trans}, K_{ep} and V_{ep} mapping. Measurement of each parameter at a range of time intervals failed to demonstrate a specific imaging predictive biomarker of response to SIRT. DCE MRI analysis did reveal parameter changes over time, although the mean values did not discriminate treatment responders from non-responders.

Quantitative T1 mapping using shortened Modified Look-Locker Inversion recovery (shMOLLI) was performed on 11 patients and explored oxygen as a non-invasive contrast agent. The feasibility of this technique for quantitative T1 mapping in malignant hepatic lesions was demonstrated for the first time and analysis of data supported the need for further research into the role of T1 mapping pre and post oxygen-enhancement for patients receiving neo-adjuvant chemotherapy.

The analysis of the resected tumour specimens from the FOXFIRE study demonstrated that the density of microspheres was highest 0-1 mm within the tumour margin. The location of microspheres also showed clustering around the endothelium. The analysis of macrophages revealed giant cell reactions around microspheres with increased numbers of tumour-associated macrophages.

The results from the ctDNA revealed high concordance of *KRAS* status up to 1127 days from primary CRC to ctDNA results. Variant allele frequencies were measured during treatment with SIRT and detected common genes associated with CRC including *APC*, *AKT* and *BRAF*. The exploration of ctDNA and metabolites in four patients with ICC confirmed the presence of elevated circulating 2-hydroxyglutarate in a patient with an IDH1 mutation.

In summary, the feasibility of pCT and DCE MRI is shown, but further work is required to validate these techniques as a measure of vascularity that will predict for SIRT delivery. The findings from FOXFIRE resection analysis confirmed the changes and deposition from microsphere delivery. T1 mapping has been used for one of the first times to assist in the characterisation of suspected hepatic malignancies and suggests

that the role of oxygen as a non-injectable contrast agent is worth pursuing. The addition of circulating biomarkers in helps to integrate multiple biomarkers into cancer care, pairing biology with imaging. It is likely a combined approach like this may need to be adopted in this emerging era of precision medicine.

List of Tables

List of Figures

List of Abbreviations

2HG	2 hydroxyglutarate
AIF	arterial input function
BF	blood flow
BOLD	blood oxygenation level dependent
BV	blood volume
CA	contrast agent
CA19-9	carbohydrate antigen 19-9
CAPOX	capecitabine, oxaliplatin
CEA	carcinoembryonic antigen
cfDNA	cell free DNA
CI	confidence interval
CT	computed tomography
CRC	colorectal cancer
CRCLM	colorectal cancer liver metastases
ctDNA	circulating tumour DNA
CTE	Commissioning Through Evaluation
DCE MRI	dynamic contrast enhanced nuclear magnetic resonance
DFS	disease-free survival
ECV	extracellular volume
EGFR	epidermal growth factor receptor
FFPE	formalin-fixed, paraffin-embedded
FOXFIRE	an open-label randomized phase III trial of 5-fluorouracil, oxaliplatin, and folinic acid +/- interventional radioembolisation as first-line treatment in unresectable liver-only or liver-predominant metastatic colorectal cancer
FOLFIRI	Folinic acid, fluorouracil, irinotecan
FOLFOX (4)	Folinic acid, fluorouracil, oxaliplatin
FOLFOXIRI	Folinic acid, fluorouracil, oxaliplatin, irinotecan
g	gravitational force
Gd-EOB-DTPA	gadoxetic acid
gDNA	germline DNA
H & E	haematoxylin and eosin
HCC	hepatocellular carcinoma
HR	hazard ratio
HRFS	hepatic recurrence free survival
IB	imaging biomarker
ICC	intrahepatic cholangiocarcinoma
IC-MS	ion chromatography mass spectrometry

IDH	isocitrate dehydrogenase
IV	intravenous
KRAS	Kirsten rat sarcoma viral oncogene
LAVA	Liver acquisition with volume acquisition
LCMS	liquid chromatography mass spectrometry
LV	left ventricle
MBq	mega Becquerel
MDT	multidisciplinary team
MOLLI	modified look-locker inversion recovery
mRECIST	modified Response Evaluation Criteria in Solid Tumour
MSI	microsatellite instability
MSS	microsatellite stability
MTT	mean transit time
MVD	microvessel density
NAFLD	non-alcoholic fatty liver disease
NET	neuroendocrine tumour
NICOLA	non-invasive comprehensive liver assessment
OCMR	Oxford Centre for Clinical Magnetic Resonance Research
OE MRI	oxygen- enhanced MRI
OS	overall survival
pCT	perfusion CT
PD	progressive disease
PDGF	platelet derived growth factor
PERFORM	perfusion CT pilot study in the FOXFIRE clinical trial to determine blood flow to liver metastases
PETCT	positron emission tomography - computed tomography
PFS	progression free survival
PR	partial response
PS	permeability surface area product
PVE	portal vein embolisation
RCT	randomised controlled trial
RECIST	Response Evaluation Criteria in Solid Tumour
RFA	radiofrequency ablation
ROI	region of interest
RPLC-MS/MS	reversed phase liquid chromatography mass spectrometry
rpm	revolutions per minute
RV	right ventricle

SBRT	stereotactic body radiotherapy
sd	standard deviation
SD	stable disease
shMOLLI	shortened modified look-locker inversion recovery
SIRT	selective internal radiation therapy
SOS	Sinusoidal obstruction syndrome
SSFP	steady-state free precession
T	Tesla
T1	longitudinal relaxation time
T2	transverse relaxation time
T2*	effective T2 relaxation time
TACE	trans arterial chemoembolization
TE	echo time
TGF	transforming growth factor beta 1
TNF	tumour necrosis factor
TNM	tumour, node, metastases
TR	repetition time
TSR	two stage resection
VAF	variant allele fraction
VEGF(R)	vascular endothelial growth factor (receptor)
VOD	veno-occlusive disease
WGS	whole genome sequencing

Chapter 1: Introduction

1.1 Motivation

The outcome from colorectal cancer liver metastases (CRCLM) remains poor. CRCLM commonly cause death within two years, despite access to new agents and more radical approaches to hepatic metastatic disease. Selective Internal Radiation Therapy (SIRT) is one option for patients with liver predominant disease aimed at disease-control. Currently, response to chemotherapy and other treatments is evaluated with the use of computed tomography (CT) scans. The RECIST criteria classify response in to four classes. Complete response (CR) is defined as a complete response with the disappearance of all target lesions; partial response (PR) as a decrease of >30% in the sum of diameters of target lesions; and progressive disease (PD) defined as an increase of >20% in the sum of diameters of target lesions or the appearance of a new cancer lesion. Stable disease (SD) is attributed to patients when change is not sufficient to be considered as PR or PD (Eisenhauer et al., 2009).

For patients with CR, PR and SD treatment will usually be continued, while patients with PD are considered for a change in definitive treatment, if more options are available. RECIST criteria have been validated and show acceptable inter- and intra-observer variability. However the value of radiologic response assessment following SIRT is frequently unclear. Treatment responses are not only reflected by a decrease in tumour size and following radiation it can be challenging to differentiate between PD and radiation effects. Attempts to define the patients that are most likely to benefit from SIRT are ongoing.

Therefore, predictive biomarkers for chemotherapy and or SIRT response would be of great value in patient-selection, sparing patients from potentially toxic treatments who are unlikely to benefit and to more accurately assess the need for a change in the definitive management plan.

A biomarker is a measurable characteristic that can be used as an indicator of physiologic and pathologic processes. Two main categories are distinguished: prognostic and predictive biomarkers. Prognostic biomarkers provide insight into patient outcome, independent of the received treatment. These biomarkers can give an estimation of survival, type of progression and may indicate to a patient the potential life expectancy despite treatments.

Predictive biomarkers identify subsets of patients who would benefit from specific cancer treatment, and thus guide treatment decisions. A biomarker can only be termed predictive if its predictive value is confirmed in a study with at least two treatment comparison groups, preferably a randomised controlled trial. An ideal biomarker is cheap to obtain, easy to analyse, non-invasive for the patient, and can be collected repeatedly.

The ability to assess perfusion parameters as a predictive marker may better guide patients' selection for procedures such as SIRT. Whereby, high perfusion parameters may indicate a more vascular tumour, with high blood flow and the hypothesis of increased delivery of SIRT microspheres carried in this circulation.

Circulating biomarkers are gaining interest in cancer research due to the many advantages over tumour tissue biomarkers. "Liquid biopsies" are popular with patients and researchers in the search of predictive and prognostic biomarkers, because the procedure is less hazardous than percutaneous tumour biopsies, easier and safer to obtain and can be repeated on multiple occasions e.g. with each cycle of chemotherapy. Intra-tumoural heterogeneity has been identified as a key contributing factor to the emergence of resistance and liquid biopsies may overcome the selective nature of tissue biopsies at one time point from one site.

Blood samples, e.g., plasma or serum, are a great source of cell-free DNA, proteins, RNA, exosomes, and metabolites. By combining imaging biomarkers looking at the baseline structural and functional changes within tumours, with these circulating biomarkers this research seeks to define a comprehensive picture of the predictive nature of these potential biomarkers and the change in tumour biology and tumour response to SIRT treatment.

New imaging and circulating biomarkers are urgently needed, to add prognostic and predictive accuracy for individuals. These biomarkers require biological and clinical validation to ensure that any decisions made on the basis of them, have a positive impact on patient outcomes. The ability of biomarkers to address the translational and clinical gaps offer the potential for therapeutic, quality of life and cost effectiveness benefits in patients with advanced cancer. These patients have acute needs given their limited prognosis, finite treatment options and a short window of opportunity for active therapy.

1.2 Thesis Outline

The theory behind perfusion CT, DCE MRI and T1 mapping (native and oxygen-enhanced) is discussed. This focuses on the justification for these techniques to be researched in the context of patients with hepatic malignancy. The challenge of treating CRCLM and one of the specific approaches to liver dominant, unresectable disease - Selective Internal Radiation Therapy is considered. The development of new imaging biomarkers is discussed in more detail from three clinical trials; PERFORM (perfusion CT pilot study in the FOXFIRE clinical trial to determine blood flow to liver metastases), NICOLA (Non-Invasive COmprehensive Liver Assessment) and FOXFIRE (randomised III trial of 5-fluorouracil, oxaliplatin, and folinic acid +/- interventional radioembolisation). The results from these trials are from clinical data from 58, 11 and 71 patients, respectively.

All FOXFIRE and PERFORM patients had advanced cancer, the majority with CRCLM and a smaller number with ICC. These patients were all being considered for SIRT for unresectable hepatic malignancy as part of a large randomised-controlled trial or Commissioning Through Evaluation ((Sharma et al., 2017; White et al., 2019). Patients receiving SIRT have a number of radiological investigations as part of the work-up and delivery of SIRT, PETCT does not form part of the standard of care for these and therefore PETCT was not included in this study. The feasibility of perfusion CT and DCE MRI for the assessment of tumour perfusion are examined and discussed within the context of SIRT, as an arterially-infused treatment. Perfusion parameters were generated from imaging patients with hepatic malignancies to explore these as potential biomarkers in patients receiving SIRT. Exploratory analysis of the underlying histology after hepatic resection in patients after SIRT and the complimentary sampling of circulating biomarkers are discussed. The measurement of circulating tumour DNA, as a non-invasive circulating biomarker, in parallel to the assessment of imaging biomarkers is justified on the basis of the limitations of imaging biomarkers in determining the underlying molecular profile of tumours.

For participation in the NICOLA study, patients were included who were considered for liver surgery with known or suspected malignancy or those patients with indeterminate liver lesions. A collaboration with the Oxford Centre for Clinical Magnetic Resonance Research (OCMR) enabled the exploration of native and oxygen-enhanced T1 mapping in patients with hepatic lesions planned for surgery. T1 mapping values were measured in hepatic lesions and compared to the background liver. As these patients were all identified as suitable candidates for resection, the opportunity for a comparison with histology from the resected liver specimen was available. The development of

shMOLLI, a T1 weighted MRI sequence, as a tool to assess these hepatic lesions is presented. The role of oxygen enhancement in T1mapping as a non-invasive arterial contrast is also explored. Quantitative T1 mapping as a potential imaging biomarker in malignant disease is considered with the results of T1 mapping using shMOLLI for the first time in patients with metastatic CRC and the inclusion of oxygen-enhanced MRI. The adaptation of this sequence from the OCMR Siemens scanner (Tim Trio, Siemens Healthcare, Germany) to the GE scanners (Signa HDxt, GE Healthcare) at the Churchill Hospital site, demonstrated the challenges of ensuring generalisability and clinical utility of new sequences. This adaptation requires use of phantoms, healthy volunteers before piloting on patients. T1 mapping supported the exploration of the role of OE MRI, as a non-injectable contrast agent looking at arterial perfusion.

In the analysis of hepatic resections following SIRT the safety, histological changes and microsphere distribution are examined. The delivery and presence of microspheres in relation to hepatic blood vessels supplying the tumour are demonstrated. The changes in the tumour microenvironment including macrophage migration are described. The hypotheses for this study were:

1. Hepatic resection is as safe after SIRT as after chemotherapy alone. Overall survival and post–surgery complication rates are not worsened by the addition of SIRT to chemotherapy.
2. Down-staging after SIRT will be improved compared to chemotherapy alone.
3. Histological examination of hepatic resection after SIRT with chemotherapy will demonstrate the microsphere distribution within tumour vasculature.
4. Changes to the local tumour microenvironment differ after chemotherapy and SIRT when compared to chemotherapy alone.

Chapter 6 explores additional information acquired from non-invasive circulating biomarkers, namely ctDNA and metabolites, as complimentary biomarkers to imaging studies. ctDNA was used to detect somatic mutations at three time-points in patients receiving SIRT. Concordance of ctDNA with historical tissue KRAS status is demonstrated in heavily pre-treated patients with CRCLM. The role of the variant allele frequency (VAF) of mutations as a biomarker of response to SIRT is explored. The potential to detect emerging mutations following high dose irradiation from SIRT is considered. The sequencing of ctDNA from patients with ICC coupled with the measurement of plasma metabolites highlights the potential of dual biomarkers and the role of metabolomics in determining the functionality of oncogenes.

The detection of an IDH1 mutation, from the ctDNA from a patient with ICC was correlated with plasma 2 hydroxyglutarate (2HG) measurement. The analysis of circulating metabolites, using mass spectroscopy, from plasma of patients with advanced ICC adds to the small number of studies of

sequencing data of ctDNA in ICC. This offers proof of principle that combining the analysis of circulating genomic and metabolite data is feasible in patients with ICC. The detection of high concentrations of new potential oncometabolites from these patients suggests this may be helpful for investigation in a prospective multi-centre study.

In conclusion, the learnings, limitations and suggestions for future work and the development of the findings are considered.

1.3 **Introduction to colorectal cancer liver metastases and SIRT**

Colorectal cancer (CRC) is the third most common cause of cancer death in the UK (Ferlay et al., 2013). Mortality is predominantly from liver metastases (LM), and patients with metastatic disease treated with modern chemotherapy regimens have a median survival of less than two years (Maughan et al., 2011). Perioperative chemotherapy typically leads to longer progression free survival (PFS) in resectable metastases (Nordlinger et al., 2008). Liver-directed therapy in unresectable disease include microwave and radiofrequency ablation (RFA) (Ruers et al., 2010) (Tanis et al., 2014), stereotactic body radiotherapy (SBRT) (Rusthoven et al., 2009) and SIRT.

SIRT, also termed radio-embolisation, delivers yttrium-90 (Y90) microspheres to tumour vasculature by exploiting the preferential arterial blood supply of hepatic tumours. In a pre-clinical model, the development of the arterial supply of hepatic metastases demonstrated arterialised micrometastasis with feeding dilated arterioles surrounding the avascular centre (Dezső et al., 2009).

In clinical practice the arterial supply to hepatic tumours is mapped and during a work-up procedure, before microsphere delivery, adjacent vessels are coiled (embolised) to avoid microspheres entering normal adjacent structures (Figure 1.1).

Figure 1.1. Radioembolisation under CT guidance for the targeted delivery of SIRT. Coils are seen within the gastric artery (thin arrow) and the gastroduodenal artery (thick arrow) to ensure no off-target delivery of yttrium-90.

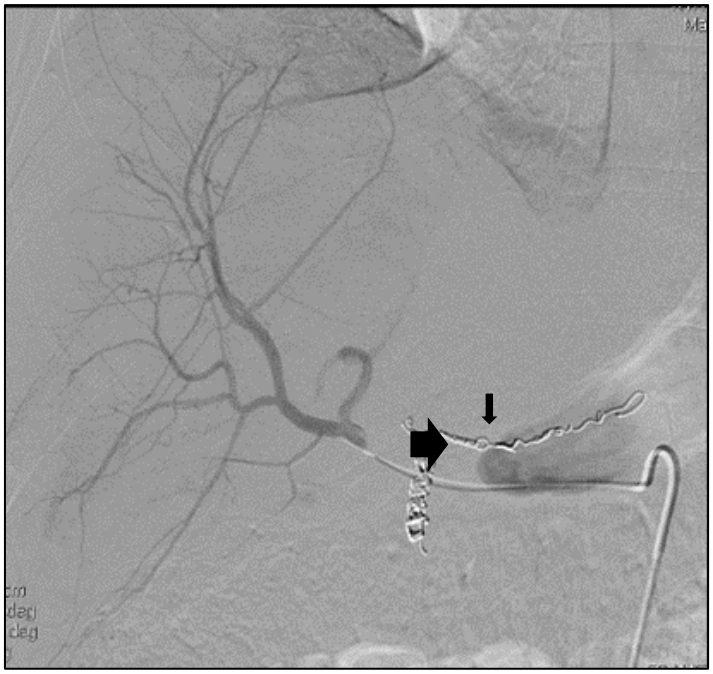

Radioactive resin or glass microspheres are subsequently injected via cannulation of branches of the hepatic arterial supply, allowing accurate tumour–directed therapy (Benson et al., 2013; Kennedy et al., 2007). The primary objective is to selectively irradiate malignant lesions whilst sparing adjacent normal liver parenchyma (Archetti, 2013; Nicolay, Berry, & Sharma, 2009; Townsend, Price, & Karapetis, 2009). Yttrium, physical half-life 64 hours, is delivered in a steep dose gradient, 1 GBq yttrium-90 delivers β-radiation to a mean tissue penetration of 2.5 mm (maximum 11 mm).

Concurrent chemotherapy was added as a radiosensitiser and showed to be safe (R. A. Sharma et al., 2007). Two first-line randomised controlled trials of SIRT have been completed (Dutton, Kenealy, Love, Wasan, & Sharma, 2014; van Hazel et al., 2016). The effect of SIRT within the liver of patients with CRCLM was demonstrated with an increased proportion of patients achieving an overall response and prolonged hepatic progression free survival. However, the locoregional effect did not translate into improved overall progression-free survival or overall survival, even in patients with liver–only metastases. This suggests that the biology of the disease is only transiently changed by the delivery of locoregional SIRT treatment (Wasan et al., 2017).

CT imaging is the standard assessment tool for evaluating the impact of chemotherapy. Response Evaluation Criteria in Solid Tumour (RECIST) and the revised RECIST v1.1 (Eisenhauer et al., 2009) have been established as biomarkers of response to chemotherapy. However, limitations exist in the clinical utility of the RECIST tools because of their inability to assess tumour activity and the underlying tumour biology. The criteria fail to reflect tumour responses resulting from new therapeutic strategies including immunotherapy, vascular disrupting agents and specific targeted

therapies. The development of new criteria for assessing response to immunotherapy (iRECIST) reflects a changing paradigm in assessments of tumours by imaging in the era of new (non-chemotherapy) treatments (Seymour et al., 2017). The iRECIST assessment guideline describes a standard approach for change in tumour size for use in trials using immunotherapy. Consideration to similar approaches are needed for localised radiotherapy treatments and novel targeted therapies.

The current challenges for imaging technology for image acquisition, analysis and computer modelling is complicated by the imperative of managing volume effects, registration, motion correction, inter- and intra-scanner reliability, different key platform vendors and timing of scanning protocols. When combined with the effective standardisation of protocols, biological validation may finally be assured. This ensures that response assessment is reproducible and is independent of the target lesion selection: size; location; background tissues and patient variables. It is important to also acknowledge the additional performance criteria of the ability to determine intra- and inter-tumour heterogeneity independent of patient phenotype or changing biology.

Imaging techniques currently employed cannot be relied upon to adequately assess liver function or liver toxicity. This is a crucial limitation as both are greatly influential in the physician's management of liver-directed therapies for patients with liver predominant malignancy (Sharma, Maitland, & Ratain, 2012).

Chapter 2 Theory

2.1 Hepatic Circulation

The liver is highly vascular with a predominant portal venous system supplying blood to the sinusoids (a series of porous vascular channels within the liver) with small openings (fenestrae). The The hepatic artery supplies approximately 25% of blood flow (Chiandussi et al., 1968). The blood from both vessels mix within the sinusoids to supply the liver cords. The Space of Disse, (an interstitial space), separates the sinusoids from the tightly ordered hepatic cords which are formed from two rows of hepatocytes. These sinusoids have large fenestrae that support the requirement of a high flow circulation and allow free exchange of low-molecular weight compounds including the contrast agent gadolinium, between the vascular space and the interstitial Space of Disse.

In hepatic malignancies the tumour blood supply is initially derived from the proliferation of sinusoidal cells. These capillarised sinusoidal cells form new basement membranes. These new basement membranes may impedes the free exchange of low molecular weight compounds such as gadolinium between the sinusoidal space and the Space of Disse. The sinusoids appear to permit the "outside-in" blood flow from sinusoids into tumour vasculature. As tumours grow, the tumour

recruits additional blood vessels supplied from the hepatic artery. This process of arterialisation of the vascular supply is typical within hepatic malignancies and is referred to as neoarteriogenesis. The new vessels are typically seen in peritumoural areas of CRCLM and are a prominent feature of the highly vascular HCC.

The first investigations of the arterial blood supply of liver malignancies was with the injection of Indian ink. When injected into the hepatic circulation via the portal vein, tumour tissue failed to stain. When a similar injection was introduced via the hepatic artery both the hepatic tumours and liver tissue became stained (Breedis & Young, 1954). Since this time, studies have investigated the blood supply using varying methods including corrosion casting (Yamamoto, Sherman, Phillips, & Fisher, 1985), in vivo fluorescent microscopy (Liu & Matsui, 2007) and radiolabeled tracers (Archer & Gray, 1989; Ridge, Bading, Gelbard, Benua, & Daly, 1987). Each have verified the key Breedis and Young conclusion that *"malignant neoplasms growing in the liver tend to acquire an exclusively arterial blood supply".*

The mechanism for the development of arterial blood supply in liver metastases has since been described in a pre-clinical model. Five steps in the arterialisation process of liver metastases have been identified:

Step 1. Distortion of hepatic microcirculation

Step 2. Fusion of the sinusoids at the tumour/parenchyma interface

Step 3. Fusion at base leads to "burst pipe" disruption of vascular sphincter

Step 4. Dilated artery and fused sinusoids are incorporated into tumour

Step 5. Arterial tree of tumour vessels develops by proliferation, remodeling and ongoing incorporation of fused sinusoids at the interface between tumour and parenchyma. This "burst pipe" with reduced resistance, due to the dilatation of arteries and fused sinusoids, allows the supply of multiple metastases from one artery (Dezső et al., 2009).

More studies are required to further understand this process in human livers. However, the discovery of arterial blood supply to hepatic tumours facilitated the study of arterially liver-directed therapies including hepatic arterial chemotherapy (Mocellin, Pilati, Lise, & Nitti, 2007) and more recently immunotherapy (Katz et al., 2015), transhepatic chemoembolisation (TACE) (Aliberti et al., 2016; Fiorentini et al., 2014) and SIRT (Salem & Thurston, 2006; R. A. Sharma et al., 2007; van Hazel et al., 2016). These therapies exploit the predominant arterial blood supply by selectively targeting liver malignancies and sparing the normal liver.

2.2 Background to perfusion CT and dynamic contrast enhanced MRI

Precision medicine - right treatment for the right patient at the right time requires validated molecular diagnostics and predictive biomarkers. Accurate methods for the early assessment of response, for the specific therapy, are essential. Quantitative imaging must accurately reflect the tumour and normal tissue biology. Clinical and biological validation of imaging parameters as biomarkers of tumour physiology, vascularity, perfusion and hypoxia are needed. Parameters for perfusion may be particularly important for cancer treatments delivered via the intra-arterial route and for those that acts as antiangiogenic or vascular disruptive agents. Predictive imaging biomarkers that would accurately determine the response to SIRT may include perfusion parameters. Perfusion imaging of blood flow may determine tissue vascularity. Perfusion computed tomography (pCT) and dynamic contrast-enhanced magnetic resonance imaging (DCE MRI) are two perfusion techniques that may be incorporated into standard imaging protocols. These techniques track a bolus of injected contrast over time as it passes through the liver vasculature. For SIRT, these blood perfusion parameters may acts as surrogates of radiation dose delivery and likelihood of response. Liver malignancy characteristics have shown to correlate with an increase in perfusion relative to normal tissue and treatment responses has shown to correlate with the normalisation of perfusion parameters ((Kim, Kamaya, & Willmann, 2014). As ^{90}Y SIRT is delivered into the hepatic artery, there is a good reason to believe that perfusion imaging could be a predictor of microsphere deposition as well as treatment response (Morsbach et al., 2014). Dosimetry may be helpful as an indicator of response in patients treated with SIRT (Kappadath et al., 2018).

2.3.1 Perfusion CT

Perfusion is defined as the transport of blood, usually at capillary level, to tissues. The changes in the haemodynamics of arterial and venous blood supplying the liver are complex (Zhong, Wang, & Xu, 2009). However, these changes may be detected in perfusion imaging of the liver and assist in the assessment of tumours considered for arterially-delivered therapies. The first published reports of pCT described the application of CT in producing colour perfusion imaging and the measurement of tissue perfusion (Miles, 1991). More recent research has focused on the correlation of perfusion parameters, with tumour vascularity on histopathology (Goh et al., 2008; Ippolito, Capraro, Casiraghi, Cestari, & Sironi, 2012; Jiang et al., 2009; Miles et al., 1998).

pCT requires the serial scanning of a pre-specified area of the liver across time, using an intravenous (IV) contrast agent (CA), typically iodinated, pre, during and post administration. Imaging following the injection of CA serial scans allow temporal changes to be visualised.

Initial uptake and decrease (washout) of the agent provides a measurable change in the concentration as a function of time. Tissue attenuation is proportional to the concentration of contrast agent and is measured in Hounsfield units (HU). pCT provides both qualitative and quantitative data on the perfusion of the liver. Quantitative colour perfusion maps are generated from dynamic CT and allows the calculation of discrete values of perfusion parameters, which include blood flow (BF), blood volume (BV), mean transit time (MTT) and permeability surface area (PS) (Jiang et al., 2009). Early pCT in liver imaging was limited by motion artefacts, limited coverage and radiation dose. Rapid advances in both CT hardware and software have addressed many of these technical factors. Motion correction algorithms, the use of wide area detectors and reconstruction developments have led to the wider integration of this imaging into clinical practice and research. Standardisation of pCT protocols have improved consistency (Miles, 2003). pCT is a proposed biomarker for the assessment of liver cancer therapies (Liapi, Mahesh, & Sahani, 2015). Research in pCT has developed in the era of liver-directed (Morsbach et al., 2014) and antiangiogenic agents in the treatment of primary malignancies (Sahani, Holalkere, Mueller, & Zhu, 2007). However, the major role for pCT may be in the ability to assess secondary lesions arising from common cancers (Kim et al., 2014; Meijerink et al., 2009).

Despite the advent of PETCT, conventional CT of chest, abdomen and pelvis remains the gold standard for the baseline and follow up in the management of many malignancies and is widely available and accessible for most patients. Standardised protocols have ensured the reproducibility of this technique. pCT can now be integrated into these standard protocols within the same scanning visit. Hepatic pCT has yet to be prospectively validated for use as either a prognostic or predictive tool. The potential advantages of pCT as an imaging biomarker include it is relatively quick to acquire, supports a functional assessment of normal and affected tissues, minimally

invasive, reliable with high spatial and temporal resolution. Also the scans can be integrated into standard CT protocol. However, disadvantages include the requirement for a long breath-hold, increased radiation exposure, limited cranio-caudal range, need for standardisation of analysis and reproducibility (Ogul et al., 2014).

2.3.2 DCE MRI

DCE MRI is a T1-weighted sequence that requires the injection of a low molecular weight gadolinium-chelate contrast agent. Rapid measurements of image signal intensity follow as gadolinium first enters tumour capillary beds via the arterioles and then washes out from the tumour. DCE MRI in patients with CRCLM has been identified as having potential to enhance diagnostic and prognostic assessments of hepatic lesions. The future applications of DCE MRI in liver predominant metastatic disease may lead to describing the heterogeneity of tumour vascularity, change of blood flow and permeability.

Originally adapted from measuring renal blood flow DCE MRI has now become the mostly commonly adopted perfusion technique in cancer patients (O'Connor, A. Jackson, G. Parker, C. Roberts, & G. Jayson, 2012). Through tracer kinetic modelling DCE MRI supports quantitative characterisations of changes in parenchyma and tumour microcirculation. DCE MRI has been proposed as a tool to assess vascular physiology of lesions with anatomical detail and the quantitative measurement of these vascular parameters may act as an indirect measure of angiogenesis (Prezzi & Goh, 2016).

Relative changes in the blood supply of the hepatic artery and portal vein may lead to the earlier detection of CRCLM (Leggett, Kelley, Bunce, & Miles, 1997); (Thng, Koh, Collins, & Koh, 2010). Significantly, the sensitivity to differences in vascular permeability and blood volume suggests that DCE MRI has a potential use as a biomarker for antiangiogenic therapy (Dowlati, 2005; Galbraith, 2002; Miller, 2005). Gadolinium ions are paramagnetic and therefore shorten T1, the longitudinal relaxation time (Figure 2.1). This results in an increased signal in T1-weighted images. Signal enhancement reflects the tissue perfusion: capillary surface area; capillary permeability; volume of extracellular extravascular leakage space (EES) and concentration-time course of contrast agent in the artery that is supplying the vascular bed (arterial input function (AIF).

Figure 2.1. T1, the longitudinal relaxation time, is shortened with the use of paramagnetic agents such as gadolinium and oxygen. The signal is increased from lower curve (long T1) pre-contrast to the short T1 curve post contrast. x axis time in msec, y axis longitudinal magnetisation.

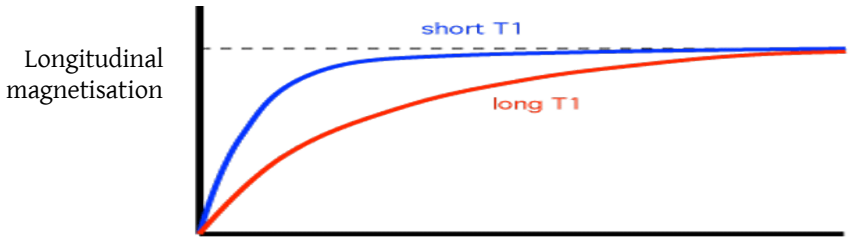

Signal intensity changes in proportion to the concentration of the contrast agent in the measured volume or voxel and analysed using a tracer kinetics model (Tofts et al., 1999). K^{trans} is measured as the contrast agent rapidly diffuses into the extracellular space (Figure 2.2).

Figure 2.2. A tracer kinetic model applied to DCE MRI used to estimate K^{trans}, v_e and k_{ep}. K^{trans} represents the volume transfer constant between the blood plasma and the EES (thin black arrow). ve represents the volume of the EES / unit volume of tumour. kep is the flux rate constant between the EES and the blood plasma ($k_{ep} = K^{trans}/v_e$)

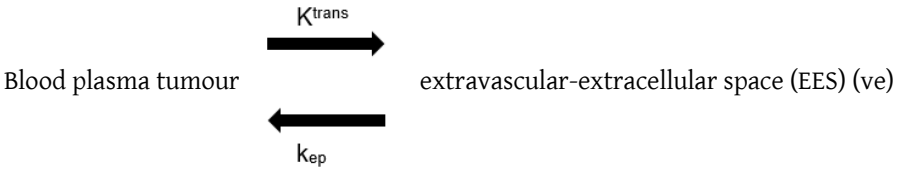

The quantitative kinetic parameters derived provide information on the microcirculation of tumours; that are indirectly related to vessel surface area and vascular permeability (d'Arcy et al., 2006).

Over one hundred early-phase trials have investigated the role of DCE MRI in patients receiving antivascular therapies, including those with advanced CRC (J. P. B. O'Connor, A. Jackson, G. J. M. Parker, C. Roberts, & G. C. Jayson, 2012). However, functional MRI has not found an established role as an assessment tool (Collins, 2003). Research has demonstrated the role of measuring tumour plasma volume and led to improved understanding of the changes in microvascular function and structure (J. P. O'Connor, Jackson, Parker, & Jayson, 2007; Zweifel & Padhani, 2010) but few have examined DCE MRI within the context of arterially delivered liver directed therapy.

In localised rectal cancers how DCE MRI correlates with rectal carcinoma angiogenesis has been examined. Significant findings included that higher peak enhancement ratio and time to peak (T_p)

were evident in rectal cancer when contrasted with normal rectal tissue. The microvascular density (MVD) and vascular endothelial growth factor (VEGF) expression were determined in rectal tissue after resection. It was found that T_p was negatively correlated with MVD and the mean T_p (peak) was significantly earlier for the patients with VEGF-positive tumours compared to the VEGF-negative tumours (Zhang et al., 2008). DCE MRI was therefore suggested as a predictor of rectal tumour angiogenesis with the capability of distinguishing malignant from benign tissue.

2.4 Background to T1 mapping and oxygen enhanced MRI

There is a clinical need for non-invasive imaging biomarkers. T1 mapping has been proposed as an MRI technique that helps characterise the liver in benign liver disease. Each tissue exhibits a characteristic range of normal T1 relaxation times at a particular magnetic field strength (Bottomley, Foster, Argersinger, & Pfeifer, 1984). This technique adapted from cardiovascular imaging has been developed for imaging of the liver and allows imaging in shorter time frames for patients. The ability to use native T1 mapping and the development of oxygen-enhanced T1 mapping may provide information on the extent of oxygen delivery to tumour tissue and potentially tumour hypoxia. In the liver, the ability to characterise the background liver and tumour hypoxia would help in optimising treatment strategies including the delivery of SIRT. New imaging biomarkers are required to assess the impact of liver-directed therapies on the underlying tumour biology and effects on background liver parenchyma.

2.3.1 Quantifying T1 and histological correlation in benign disease of the heart and liver

The ability to quantify myocardial fibrosis with non-contrast T1 has been shown to characterise cardiac disease and correlate with histology findings of diffuse myocardial fibrosis (DMF) (Bull et al., 2013). Methods to acquire T1 values after intravenous contrast are time consuming, require complex and non-standardised processing and risk nephrogenic systemic fibrosis in patients with severe renal impairment (Mewton, Liu, Croisille, Bluemke, & Lima, 2011). A technique for measuring tissue fibrosis without the need for contrast agent offers the potential to reduce scan time, costs and application for patients with renal disease without concern. Non-contrast T1 values have been acquired from patients with the development of the shortened modified Look–Locker inversion recovery (shMOLLI) T1 mapping sequence. shMOLLI has already been used successfully in the clinical cardiac setting and showed increased non-contrast T1 values in patients with acute myocardial infarction and acute myocarditis (Dall'Armellina et al., 2012)T1 mapping was adapted for liver imaging and has been shown to correlate with liver fibrosis in non-malignant liver disease (Banerjee et al., 2014). T1 mapping determines the extracellular fluid in parenchymal tissue. The presence of elevated extracellular water, is reflected by increased T1 values. Additional work has attempted to correlate these MRI findings with clinical outcomes in non-malignant hepatic disease (Pavlides et al., 2016).

2.3.2 Oxygen enhanced T1 mapping

OE MRI has been proposed as an emerging technique to quantify and demonstrate the spatial distribution of oxygen delivery to tumours. Pre-clinical work in highly vascular renal cancer xenografts has shown that the signals from OE MRI are precise, accurate and sensitive to changes in pO_2 (O'Connor et al., 2016). T1, the longitudinal relaxation time, is highly sensitive to the increase in dissolved O_2 in plasma and interstitial fluid. When a patient inhales an increased concentration of

O_2 during MRI, there is a decrease in T1, which relates to the increased amount of paramagnetic O_2 dissolved in the plasma (Remmele et al., 2013; Silvennoinen, Kettunen, & Kauppinen, 2003; Young et al., 1981). The change of the longitudinal relaxation rate of protons in well-oxygenated tissues, causes the shortening of T1 (msec). This is demonstrated in the decrease in T1 values (msec) pre- and post- oxygen –enhancement of blood in the left ventricle.

There have been limited studies with the measurement of longitudinal relaxation of tumours with high flow inhaled oxygen (Linnik et al., 2014; O'Connor et al., 2009; Remmele et al., 2013).

Current methods for imaging oxygen delivery to tissues include blood oxygenation level dependent (BOLD) imaging. This has significant limitations which have hindered implementation as a biomarker of hypoxia. BOLD values are affected by vessel geometry, haemorrhage and interface artefacts (Baudelet & Gallez, 2002; Blockley et al., 2008; Young et al., 1981) limited clinical application (Zaharchuk et al., 2006).

2.5 Background to hepatic resection and surgery after SIRT and chemotherapy

2.5.1 Surgery of CRCLM

Half of patients who develop CRCLM have liver only disease (Stangl, Altendorf-Hofmann, Charnley, & Scheele, 1994). However, most patients with CRCLM do not receive surgery. A hepatic resection remains the sole curative treatment for malignant disease confined to the liver and also offers the best chance of survival and continues to demonstrate longer-term disease-free survival (Minagawa et al., 2000) (Malafosse, Penna, Sa Cunha, & Nordlinger, 2001) (E. K. Abdalla et al., 2013; Mattar, Al-Alem, Simoneau, & Hassanain, 2016). Only 20% of patients with CRCLM will be offered hepatic resection with limited or no extrahepatic disease and adequate functional hepatic reserve decisive factors. The 5-year survival rates after hepatectomy is approaching 60% (Eddie K. Abdalla et al., 2004; Pawlik et al., 2005) (Simmonds et al., 2006) (Choti et al., 2002). Early data on 456 patients treated with hepatic resection showed a five year survival of 38% and a median survival of 46 months, after surgery (Fong et al., 1997). Non-surgical liver-directed therapies include RFA, SIRT and these may be used as an adjunct to surgery.

Perioperative chemotherapy is considered the gold standard of care for resectable CRCLM (Bernard Nordlinger et al., 2013). The use of triplet regimens and biological therapy has further increased response rates and R0 resections (Falcone et al., 2007; Loupakis et al., 2014). In a retrospective study in over a 1000 patients, chemotherapy resulted in a conversion rate of unresectable disease of 12.5 % (Adam et al., 2004).

Multiple factors have ensured that liver surgery has become increasingly available. These include: improved surgical techniques and peri-operative management; an improved ability to maximise functional capacity e.g. hypertrophy using portal vein embolisation and SIRT (Garlipp et al., 2014); earlier detection of small volume metastases; new neo-adjuvant approaches; increased availability and a multi-disciplinary team approach.

The Brisbane 2000 Nomenclature of Hepatic Anatomy and Resections is widely adopted to standardise terminology of hepatic surgery (Strasberg, 2007) (Strasberg, 2000) (Strasberg & Phillips, 2013). Factors predictive of a poorer prognosis by multi-variate analysis are: a positive margin; lesions greater than 10cm; a disease-free interval of less than 12 months; extrahepatic disease and multiple tumours. Each are independent predictors of a poorer outcome (Fong et al., 1997).

.

Portal vein embolization (PVE) has been used to increase residual liver volume with similar overall survival rates observed between a dual PVE and resection as compared to resection alone (Elias, Ouellet, De Baere, Lasser, & Roche, 2002). In 23 patients who underwent right portal vein embolization there was an increase of 38% in future liver remnant (Massimino, Kolbeck, Enestvedt, Orloff, & Billingsley, 2012). PVE has become a standard preparatory step in the extended right hemihepatectomy where left segments are small. A common resection is therefore often managed in two stages: left metastectomy followed by right hepatectomy (Brouquet et al., 2011). In a systematic review of 22 observational studies, 1610 patients who had recurrent hepatectomy and had a 5 year survival of 42% (range 31-73%) (Lam et al., 2013).

Associating Liver Partition and Portal vein ligation for Staged hepatectomy (ALPPS) combines portal vein ligation with an intraoperative splitting of the liver to induce a more rapid hypertrophy. In 25 patients who received ALPPS after a median of 9 days the left lateral lobe had increased by a median volume increase of 74% (range = 21%-192%) ($P < 0.001$) (Schnitzbauer et al., 2012).

The CLOCC study examined the outcomes for patients with unresectable CRLM treated with a combination of systemic treatment and local treatment with radiofrequency ablation, with or without, resection. It was the first randomised control trial to demonstrate a survival benefit from surgery and ablation beyond that of systemic therapy. The magnitude of improvement resulted in the progression free survival improving to 16.8 months from 9.9 months with systemic therapy alone (T. Ruers et al., 2012). The combination of ablation and chemotherapy compared to chemotherapy alone was also proven at 10 years to generate a prolonged overall survival advantage, with hazard ratio 0.58, 95% confidence interval 0.38 – 0.88, p= 0.01 (Ruers et al., 2017). Similar evidence was replicated in alternative studies for resection combined with intraoperative RFA. The median hepatic recurrence free survival (HRFS) was 14 months (95%CI 11-18) and PFS was 9 months (95%CI 8-11) (Evrard et al., 2014).

2.5.2 Chemotherapy and hepatic resection

The main chemotherapy agents used in CRCLM include combinations with 5-fluorouracil (5-FU), an irreversible thymidylate synthase inhibitor, combined with leucovorin, usually with the addition of the topoisomerase inhibitor, irinotecan or the platinum derivative oxaliplatin.

Long-term outcomes evaluated for 1104 patients with initially unresectable CRCLM, confirmed a conversion rate of 12.5 % with 138 of patients responding well enough to proceed to resection. In multivariate analysis, the four independent poor prognostic factors were: a rectal primary; maximum tumour size > 10cm; 3 or more metastases and a Ca19-9 over 100 µl/l. The presence of 0,

1, 2, or 3 plus factors led to a mean adjusted 5-year survival of 59%, 30%, 7%, and 0% respectively (Adam et al., 2004). This study included a high number of repeat resections and resection of extrahepatic disease. A follow-up study of 196 initially unresectable patients treated with FOLFOXIRI (fluorouracil/leucovorin, oxaliplatin and irinotecan confirmed it was a safe combination. Nineteen percent of patients were converted to resection with no perioperative mortality and only 5% of patients developing steatohepatitis (Masi et al., 2009). In other studies FOLFOXIRI has increased response and resection rates (Falcone et al., 2007; Loupakis et al., 2014).

Bevacizumab was the chosen targeted agent for 508 patients randomised to FOLFIRI or FOLFOXIRI. These evidenced a significant increase in response rate (RR) from 53% in control to 65% in the triplet chemotherapy (p=0.006). This translated to a median progression free survival from 9.7 months to 12.1 months. The hazard ratio for progression, 0.75 (95% CI 0.6-0.90, p=0.003) (Loupakis et al., 2014). Gruppo Oncologico Nord Ovest studied (GONO) 244 patients with unresectable CRCLM, reached the primary end point of response rate. The overall response rate for the control arm of FOLFIRI was 34%. For the FOLFOXIRI arm the rate was 60%, (p< 0.0001). R0 resection rates were also improved in the triplet arm, reaching 15% compared to 6% in the doublet (p=0.017). This study found both a PFS and OS advantage in the FOLFOXIRI arm. The improvement of median progression free survival PFS from 6.9 months to 9.8 months and overall survival increased from 16.7 months to 22.6 months. However, a less positive finding was an increase number of patients reporting higher febrile neutropenia and peripheral neuropathy toxicity (Falcone et al., 2007).

COIN (Adams et al., 2011) and CAIRO3 (Simkens et al., 2015) both investigated maintenance chemotherapy. Findings suggested a median time period from the point of chemotherapy cessation until disease progression lay between 3 and 4 months. The CAIRO3 was a randomised trial of 558 patients receiving either maintenance capecitabine and bevacizumab or observation, after 6 cycles of CAPOX-B. The primary endpoint of progression free survival was reached and calculated at a second progression of 11.7 months in the maintenance group compared to 8.5 months in the observation group (HR 0.67, 95% CI 0·56-0·81, p<0·0001).

Bevacizumab is a monoclonal antibody against vascular endothelial growth factor (VEGF). When combined with chemotherapy it has become the standard of care when managing CRC. In treating first-line metastatic CRC, bevacizumab when combined with irinotecan and 5FU or 5FU monotherapy has been shown to improve response rates. This is not however the case when combined with FOLFOX (Hurwitz et al., 2004; Kabbinavar et al., 2005; Saltz et al., 2008).

Hurtwitz reported a randomised controlled trial of 813 patients treated in first-line. As well as the observed increased response rate, there was an improvement in median overall survival from 15.6 months in the control arm of irinotecan doublet plus placebo extended to 20.3 months in the

chemotherapy plus bevacizumab arm. The HR for death reported at 0.66, p< 0.001 (Hurwitz et al., 2004).

FOLFIRI and cetuximab have improved outcomes when compared to FOLFIRI alone. RCT had 599 patients in each arm and found that for patients with *KRAS* wild type tumours, there was an increase in the response rate from 43% in the FOLFIRI group to 59% in the cetuximab-FOLFIRI group (odds ratio 1.91; 95%CI 1.24-2.93) (Van Cutsem et al., 2009).

Perioperative chemotherapy, with or without cetuximab, has been trialled within the context of resectable CRCLM. "New EPOC" trial patients fared worse in terms of all survival measurements with the addition of cetuximab (Primrose et al., 2014). The primary endpoint was PFS and 257 patients with *KRAS* exon 2 wild-type tumours were randomised to chemotherapy alone or chemotherapy combined with cetuximab. The progression free survival was reported as 14.1 months when combined with cetuximab compared to 20.5 months with chemotherapy alone. The reported HR 1.48, 95% CI 1.04-2.12, p=0.03. These unexpected outcomes have been the subject of much debate (Nordlinger, Poston, & Goldberg, 2015) as earlier cetuximab had demonstrated the ability to downstage liver dominant CRC, when combined with chemotherapy with improvements in PFS and OS (Folprecht et al., 2010). The current view supports the current standard that cetuximab should be excluded from the management of resectable CRCLM.

2.5.3 Histological changes after chemotherapy

There have been a limited number of studies examining the impact of neo-adjuvant therapy on hepatic resection specimens. The main changes within the non- tumour bearing liver have been described as hepatic steatosis. Sinusoidal dilatation and haemorrhage were described in 50% of patients treated with chemotherapy with some disruption of the sinusoidal barrier (Rubbia-Brandt et al., 2004). Veno-occlusive lesions have also been observed (Aloia et al., 2006). However more recent studies, describe vascular lesions with oxaliplatin based therapy, and irinotecan-associated steatohepatitis (Vauthey et al., 2006) (Rubbia-Brandt et al., 2004) (Karoui et al., 2006).

2.5.4 Histological changes after SIRT

Oxaliplatin-based chemotherapy has been shown to be safely combined with SIRT. In the phase II study of this combination, two out of 20 patients were safely down-staged allowing a subsequent hepatic resection (Sharma et al., 2007). More recent data suggest that 10-15% of those treated may be amenable to resection after receiving SIRT. The results from the SIRFLOX study reported no significant difference in resection rates in the patients receiving chemotherapy alone and those

randomised to receive the addition of SIRT: 13.7 % (36 patients) compared with 14.2 % (38 patients) (p= 0.857) (van Hazel et al., 2016).

SIRT-related hepatic toxicity (radiation hepatitis or hepatic failure) is well described (Sangro et al., 2008). In the SIRFLOX study, five out of the 267 patients within the SIRT arm, developed SIRT-related hepatotoxicity. One patient died from radiation hepatitis. Concerns about the link between pre-operative therapy and liver failure after surgery have existed.

There is limited data available on histopathology from hepatic resections after SIRT. The observation of tumour necrosis, mucinous alteration, aggregates of foamy histiocytes and fibrosis with minimal cellular inflammatory response supported direct radiation injury as a non-immune mediated process (Wang, Jani, Hill, & Sharma, 2013). .

The livers from four patients were analysed after transplant (two hepatoma patients) and death (two patients with CRCLM) (Kennedy et al., 2004b). The microspheres appeared to be preferentially deposited in the tumour periphery. The finding of resin microspheres within the vascular bed of the tumour, and portal fibrosis on the adjacent normal liver has also been described. Tumour regression with central scarring was also reported (Justinger et al., 2015).

2.6 Background to circulating biomarkers in colorectal cancer and intrahepatic cholangiocarcinoma

2.6.1 Circulating tumour DNA

Circulating nucleic acids were first detected in the first half of the twentieth century, however it took almost thirty years to confirm cell free DNA (cfDNA) fragments in the serum from cancer patients (Mandel 1948), (Leon et al., 1977). During this time, these fragments were proposed as a factor in oncogenesis (Bendich et al., 1965). Circulating tumour DNA (ctDNA) is a component of the non-tumour specific, cfDNA. Tumour cells release ctDNA into circulation by secretion, apoptosis and necrosis. Genetic alterations include point mutations, copy number variations, chromosomal rearrangements and methylation patterns are can all detectable from ctDNA (Diaz and Bardelli, 2014). The fraction of ctDNA differs across tumour types, with higher levels found in patients with colon, pancreas, gastrointestinal and melanoma cancers. Variant allele frequency (VAF) enables a quantification of the somatic mutations in the collected cfDNA.

ctDNA has emerged as a non-invasive biomarker with potential utility in prognostication, measuring tumour mutational burden, detection of minimal residual disease and as a predictive biomarker. The ability for serial measurements offers the potential for ctDNA to detect emerging drug resistance and to overcome tissue sampling error caused by tumour heterogeneity (Siravegna Bardelli, 2014; (Gerlinger et al., 2012). The potential for circulating tumour fragments, circulating tumour DNA (ctDNA) and circulating tumour cells (CTC), as non-invasive biomarkers in GI malignancies remains an emerging research area. The measurement of ctDNA has been rapidly adopted into many GI trial protocols to examine the clinical utility of ctDNA as a biomarker. ctDNA may provide comprehensive information of the tumour genome as mutational variants can be detected from multiple tumour sites. The ability to detect ctDNA mutations with precancerous lesions and very early cancers would lead to earlier intervention, with a potential impact on outcome from cancer. Currently there is little evidence of the clinical validity of ctDNA in early stage disease. However, work is ongoing across the disease trajectory – including assessing risk for relapse after surgery, identifying patients most likely to benefit from adjuvant therapies and earlier response assessments to chemotherapy in the metastatic setting.

2.6.2 Role of ctDNA in colorectal cancer

ctDNA analysis from patients with CRC has detected alterations in genes encoding KRAS, BRAF, APC, and TP53 genes involved in the carcinogenesis of colorectal tumours (Thierry et al., 2014) (Wang 2004 (Leary et al., 2012; Chan et al., 2013; Leary et al., 2013). The finding of concordance of KRAS mutations from ctDNA with KRAS mutational status in surgical specimens has supported the

further evaluation of ctDNA (Ryan et al., 2003). It has been suggested that the presence of ctDNA mutations in patients may confer a worse prognosis and found that measurable ctDNA levels increase with CRC stage (Bettegowda et al., 2014)).

The sensitivity of ctDNA in mutation detection in early CRC is relatively low compared to advanced cancer (Lin 20). The proportion of circulating mutated genes is quite small compared to the number of normal circulating DNA fragments, making it more challenging to detect ctDNA in patients with lower disease burdens. Small studies have investigated the combination of ctDNA with other biomarkers, including CEA. These remain research tools and are not validated for the early detection of CRC (Mead R et al 2011; Flamini E et al 2006). Interest persists in the role of ctDNA in early stage CRC to assess minimal residual disease and predict recurrence. For example, patients with detectable ctDNA after surgery for early stage CRC were found to be more likely to recur than patients in whom no ctDNA was detected (Tie et al 2016). However, whether the use of ctDNA will translate into improved outcomes has yet to be determined.

The measurement of ctDNA in patients with CRC has been shown to be of prognostic value (Spindler et al., 2014). In a study of palliative chemotherapy in patients with mCRC, significant reductions in ctDNA (median 5.7-fold; $P < 0.001$) levels were observed before cycle 2 of palliative chemotherapy, which correlated with CT responses at 8-10 weeks. This study suggests ctDNA may a have an emerging role as a biomarker in the early prediction of a response to treatment for mCRC (Tie et al., 2015).

The ability to detect somatic mutations in ctDNA at serial time-points suggests potential as a biomarker of clonal evolution and the detection of new mutations occurring overtime during therapy. This includes the detection of mutations associated with drug resistance (Diaz et al., 2012; Diaz et al., 2013; Murtaza et al., 2013; Bettegowda et al., 2014). The presence of *KRAS*, *BRAF*, *NRAS* and *PIK3CA* mutations on the efficacy of treatment with anti-EGFR drugs such as cetuximab are well described (De Roock et al., 2010; Normanno et al., 2009)).

2.6.3 Justification for the inclusion of complimentary circulating biomarkers within an imaging biomarker study

Establishing the role of ctDNA as a biomarker to monitor the response of metastatic disease to systemic therapies is an emerging area of research in the era of precision medicine. Current standard monitoring techniques include serum CEA measurements and the use of imaging, traditionally CT, the interpretation of which is typically based on the Response Evaluation Criteria In Solid Tumours (RECIST, RECIST 1.1) criteria. These current methods, have several limitations.

The measurement of CEA, in particular, has limitations of non-secreting tumours and potential for falsely elevated CEA levels (Wahlby et al1997).

The use of RECIST, may be challenging, particularly when assessing response to novel therapies including immunotherapy. New response criteria are needed as cancer management evolves to new approaches including IO and novel radiation approaches (Solina et al 2017). Imaging biomarkers are also challenged by intra and inter-observer variation and inter-lesional heterogeneity. Therefore, there have been attempts to establish ctDNA as an effective predictive biomarker to monitor response to systemic treatments (Berger AW at el 2017; Siravegna 2016; Tie et al 2015). From a patient perspective, the convenience of serial blood tests may facilitate more frequent disease assessments and minimise radiation from radiological assessment. Regular assessment of the tumour genomic landscape is currently not usually feasible by multiple biopsies and single biopsies are limited in their ability to capture intra-tumoural heterogeneity.

The clinical utility of ctDNA as a tool to monitor response to systemic treatment remains to be established. However, it is likely to be disease-specific and dependent on specific clinical contexts.

When developing and investigating an imaging biomarker study the parallel collection and evaluation of circulating biomarkers is argued to provide complementary information.

Subsequent analysis of circulating biomarkers from proteomics, genomics, and metabolomics may complement the findings of imaging parameters or give insights into the mechanism of the changes described. More importantly, if when novel imaging biomarkers are being investigated to predict or assess response, it is important that a non-invasive blood test is evaluated to permit a comparison of performance for the specific utility of an imaging biomarker.

The potential in the future of a bedside blood test that assesses tumour burden and genomic changes would be hugely beneficial in particular where access to scan may be limited. The ability of ctDNA to assess early response to treatment in CRC continues to remain an area of active interest. Therefore, in the context of refractory mCRC treated with SIRT or arterially directed therapies where the therapy itself may challenge the interpretation of imaging assessments such as disease progression versus inflammation. The parallel measurements of ctDNA, as a potential biomarker for patients with advanced cancer, may compliment the imaging studies in this area.

2.6.4 ctDNA and circulating metabolomics in intrahepatic cholangiocarcinoma

Intrahepatic cholangiocarcinoma (ICC) is an aggressive cancer arising from the bile ducts with a need for earlier diagnosis and a greater range of treatment options. *KRAS*/*NRAS* mutations are

common in ICC tumours and 6-32% of patients also have isocitrate dehydrogenase 1 and 2 (*IDH*1 and *IDH*2) gene mutations associated with metabolic changes.

Chapter 3 Perfusion imaging blood flow in patients with CRCLM receiving Selective Internal Radiation Therapy

Liver metastases are the main cause of death from metastatic colorectal cancer (mCRC). Liver-directed therapies which can improve control of liver metastases include selective internal radiation therapy (SIRT) with yttrium-90 (^{90}Y) microspheres. The PERFORM study was designed as an imaging sub-study of FOXFIRE (randomised controlled trial in patients receiving first-line therapy for CRCLM). It was subsequently later amended to include patients receiving SIRT as part of a national access programme in refractory disease and dynamic contrast-enhanced (DCE) MRI was added to perfusion CT (pCT) imaging. The aim was to assess the feasibility of perfusion imaging acquisition and the ability to generate perfusion parameters over time in patients receiving SIRT.

Patients with CRCLM were recruited prospectively into the PERFORM clinical trial. The acquisition and analysis of pCT parameters included the measurement of blood flow (BF), blood volume (BV), mean transit time (MTT), and permeability surface area (PS) using GE 4D CT perfusion software (GE Healthcare, Milwaukee, WI, US). DCE MRI acquisition was followed by pharmacokinetic modelling to produce transfer constant (K^{trans}), back flux rate (k_{ep}), and fractional volume (V_{ep}) maps. The arithmetic means of these parameters were assessed at baseline and changes in the mean were assessed at four- and ten-weeks after SIRT.

Fifty-eight patients were recruited. The feasibility of the acquisition of pCT and DCE MRI was demonstrated in patients with CRCLM. DCE MRI parameter maps demonstrated the heterogeneity of tumour vascularity, but no functional parameter was identified as a predictive biomarker of radiological response to SIRT.

The feasibility of performing pCT scans before and after SIRT and/or chemotherapy as part of a large multi-centre randomised control trial was demonstrated. Analysis was limited by the challenges of importing images from different vendor platforms into the GE software, coil artefact from embolisation, motion correction and PK modelling. No one parameter was identified as a predictive biomarker of response to SIRT. No change in a single biomarker suggested an early response to SIRT. In future perfusion CT studies the use of a single imaging platform, ensuring the portal vein is included in the imaging of the lesion, avoidance of larger lesions with central necrosis may allow for improved prediction of biomarkers for SIRT. Further investigations are needed in larger cohorts to confirm that pCT metrics may facilitate patient selection for SIRT.

3.1 Introduction

SIRT delivers ^{90}Y labelled microspheres via the hepatic artery. The microspheres are introduced and are carried by the arterial blood flow to the tumours within the liver.

Data suggests SIRT in third-line or subsequent therapy for mCRC has clinical benefit in patients with colorectal liver metastases with liver-dominant disease after chemotherapy. The FOXFIRE, SIRFLOX, and FOXFIRE-Global randomised studies evaluated the efficacy of first-line chemotherapy combined with SIRT in patients with liver-predominant CRC. The studies were designed for combined analysis of overall survival. The outcomes confirmed SIRT had higher local control rates with an increased hepatic progression free survival of 7.9 months, although no associated overall survival advantage (Sharma et al., 2017; van Hazel et al., 2016; Wasan et al., 2017).

Response Evaluation Criteria in Solid Tumour (RECIST) provides the assessment of tumour response to chemotherapy, however has limitations following liver radiotherapy approaches in which early scans can suggest pseudoprogression in the absence of true progressive disease (Kellock et al., 2018) Predictive imaging biomarkers that would accurately determine the response to SIRT may include biomarkers of perfusion. Perfusion imaging measures of blood flow and may determine tissue vascularity. Perfusion computed tomography (pCT) and dynamic contrast-enhanced magnetic resonance imaging (DCE MRI) are two perfusion imaging techniques that may be incorporated into standard imaging protocols. These techniques track a bolus of injected contrast over time as it passes through the liver vasculature. For arterially-directed therapies and treatments that disrupt the vasculature, blood perfusion parameters may act as surrogates of radiation dose delivery and likelihood of response. Liver tumour malignancy characteristics have shown to correlate with an increase in perfusion relative to normal tissue and treatment response has shown to correlate with the normalisation (decrease) of perfusion parameters (Kim et al., 2014). As ^{90}Y SIRT is delivered into the hepatic artery, there is good reason to believe that perfusion imaging could be a predictor of microsphere deposition as well as treatment response (Morsbach et al., 2014). Several studies have shown that dosimetry is an indicator of response in ^{90}Y SIRT patients. It was therefore postulated that perfusion imaging metrics may be a predictive biomarker of the deposition of ^{90}Y SIRT microspheres and hence tumour response.

In this study, the feasibility of perfusion imaging of patients with liver malignancies pre- and post-SIRT using pCT and DCE MRI was investigated. The change in perfusion parameters from baseline to 4 weeks was also examined to see if this could predict an early response to SIRT.

3.2 Methods

Trial participants

FOXFIRE was an open label multi-centre randomised controlled phase III trial of chemotherapy with and without SIRT (Dutton et al., 2014; Wasan et al., 2017; Helen Winter et al., 2019). PERFORM was a prospective imaging pilot study recruiting patients from three centres across UK with ethical approval from the Berkshire Research Ethics Committee (approval number 10/H0505/95). The primary objective was the feasibility of perfusion parameter acquisition. Eligible patients had RECIST measurable disease and were suitable for SIRT either in the FOXFIRE trial (first-line mCRC) or through the National Health Service Commissioning Through Evaluation programme (CTE) for chemotherapy refractory/intolerant CRC or ICC (White et al., 2019; White et al., 2019) The scanning schedule is shown in Figure 3.1. In Figure 3.1a the schedule for the FOXFIRE patients in PERFORM is presented. These patients were recruited during the randomised first-line SIRT and or chemotherapy trial. In Figure 3.1b the amended schedule which was simplified for the refractory patients accessing SIRT through the CTE access programme. An imaging acquisition protocol capable of inclusion within the standard of care visits was chosen. The scheduling of the additional scan at the four week time-point was paired with the clinical visit to minimise impact on patients with a reduction of one less time-point and minimising the drop-out rate.

It was decided to reduce the number of scans as they had more advanced disease. The inclusion of DCE MRI and complimentary circulating biomarkers was added.

Figure 3.1. PERFORM scanning schedule for FOXFIRE and non-FOXFIRE patients. Figure 3.1a PERFORM imaging schedule for FOXFIRE trial patients with mCRC. The pCT scans were at baseline, after cycle one of chemotherapy and before SIRT, after SIRT then at first follow up. The primary endpoint was the acquisition of sufficient data for perfusion analysis. Arm A – were randomised to oxaliplatin and modified de Gramont chemotherapy (OxMdG). Arm B – were randomised to receive OxMdG with SIRT. Figure 3.1b PERFORM imaging schedule for non-FOXFIRE patients with mCRC and ICC receiving SIRT. pCT perfusion CT, MRI – multiparametric MRI.

(Figure 3.1a)

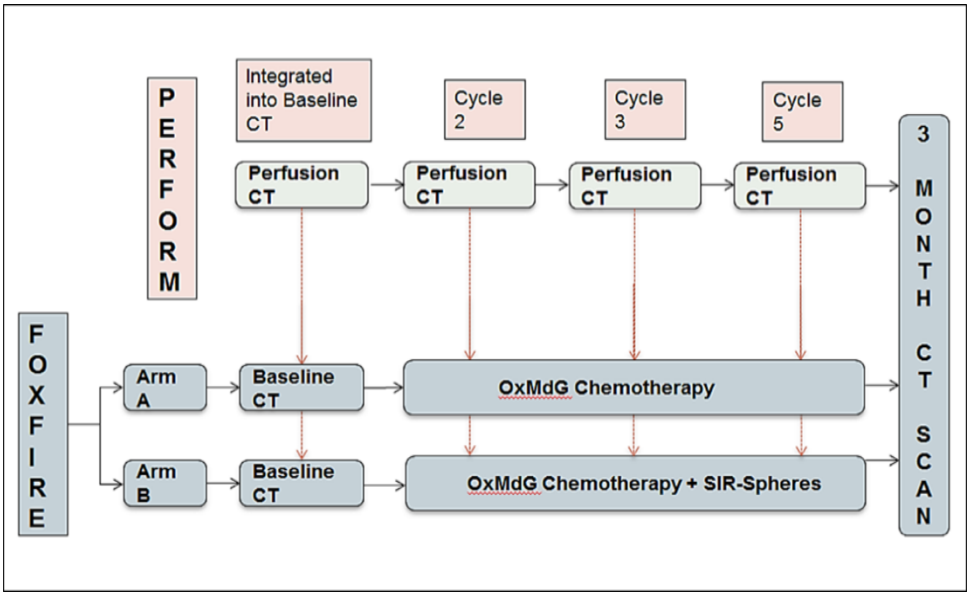

(Figure 3.1b)

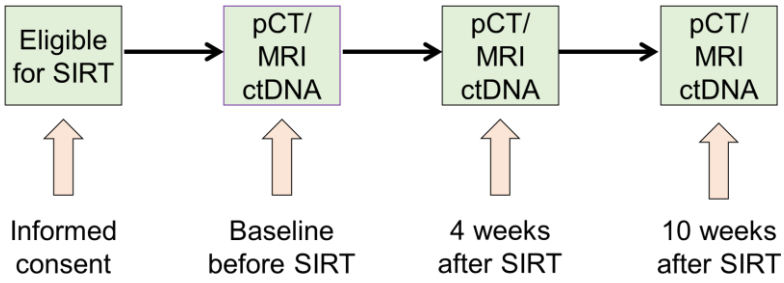

Perfusion imaging

Eligible patients identified through liver multi-disciplinary meetings were screened to ensure suitability for SIRT and the presence of a liver tumour with cranio-caudal coverage of 1-4 cm and including the portal vein. The tumour was annotated on the picture archiving and communication system on a pre-contrast CT study. Dynamic imaging was acquired following the pump-injection of 80 mL iodinated contrast (Omnipaque 300, 4 mL/s). The pCT imaging was acquired using a multi-

slice, multi-detector General Electric (LightSpeed VCT, GE Medical Systems) scanner allowing the acquisition of serial time-resolved images. Once the tumour was identified on the unenhanced scan and eight sections were imaged with 5 mm slices, the delivery process involved a 45-second breath-hold and a rotation time of 1 second. Each rotation included the collection of 8 images at 120 kV on a fixed 60 mA. A portal venous phase was acquired at 60-70 seconds post IV contrast. Images were anonymised and imported into Advantage Workstation 4.2, (GE Healthcare) using commercially available software (CT Perfusion 4D, GE Healthcare, Milwaukee, WI, US). The aorta and portal vein were identified as the dual input vessels for the liver. Regions of interest (ROIs) planned at 20 mm^2 were drawn freehand within the vessels in the tumour periphery (Figure 3.2). To derive functional maps, arterial input curves of the contrast-enhancement over time were measured from the ROIs. Following this, ROIs for the tumour and background liver were delineated and arterial input curves were generated (Figure 3.3). Functional parameter maps were derived for the pCT parameters blood volume (BV), blood flow (BF), mean transit time (MTT), transit time to peak (Tmax), permeability surface area product (PS), time to peak (TTP), positive enhancement integral (PEI), and mean slope of increase (MSI) (Table 3.1) (GE CT perfusion manual, 2014).

For DCE MRI, seven-second breath holds for respiratory gating were repeated over a seven-minute scanning period on a 3T-MRI (Signa HDxt, GE Medical Systems). Calibration images were acquired during three breath-holds prior to injection of gadolinium-chelate contrast at 30 seconds after the third breath-hold, using a programmable pump. Liver imaging was acquired during each seven-second end-expiration breath-hold. Patients were coached with practice breathing techniques and radiographers trained in applying the pulse at end-expiration. Timings of each breath-hold and the application of each pulse were recorded. All scans were repeated 4 and 10 weeks after SIRT. Motion of the liver has challenged perfusion and image registration. Movement was one of the key challenges to overcome to provide high quality hepatic perfusion parameters. Automatic non-linear image registration was applied to dynamic and multi-flip angle sequences. Motion correction applied to MRI sequences ensured the tumour was fixed with minimal movement prior to pharmacokinetic (PK) modelling. Once the gadolinium contrast concentration-time curve in the ROI was known, population-based arterial input function allowed generation and analysis of perfusion parameters. PK modelling was performed as previously described (Tofts, 1999) to generate parameter maps. Parameters (Table 3.1) included the transfer constant (K^{trans}), rate constant of backflux from the extravascular extracellular space (EES) to the blood plasma (k_{ep}), and fractional volume of the EES (v_e).

Figure 3.2. Regions of interest (ROI) were drawn with aorta, portal vein to allow quantification and the generation of tumour and background liver perfusion parameter maps. This shows the ROI 1 in the aorta at 14.5 mm^2, a ROI 2 in the portal vein at 19.2 mm^2 and three delineated ROI with three liver metastases. Images were analysed on CTp 4D software (GE Healthcare, Milwaukee, WI, US). A radioembolisation coil artefact is indicated with the thin arrow.

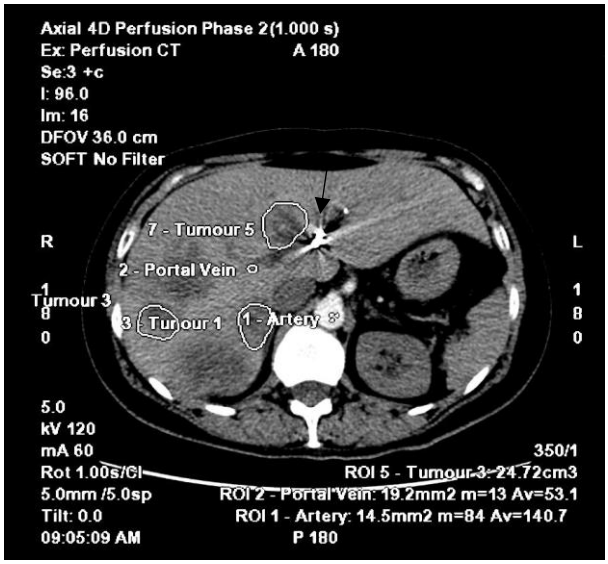

Figure 3.3. Arterial input curves in pCT post image analysis. 1 represents the ROI within the aorta, 2 indicates the ROI within the portal vein, 3- 7 regions of interest from separate lesions. ROI – region of interest.

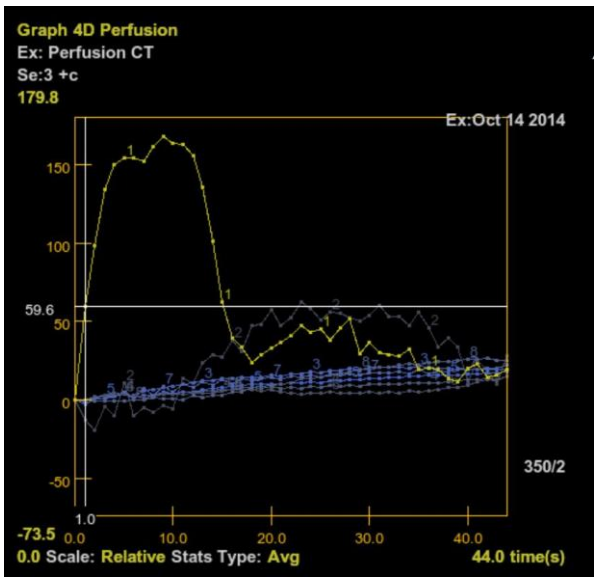

Table 3.1. Liver perfusion imaging modelling parameters

Imaging modality	Parameter	Abbreviation	Units	Description
Perfusion computed tommography (pCT)	Blood flow	BF	mL/min/100g	Value of the fitted enhancement curve at time zero
	Mean transit time	MTT	S	Average residence time of contrast agent in a given tissue location
	Blood volume	BV	mL/100g	BV=BF×MTT
	Permeability-surface area product	PS	mL/min/100g	Diffusion of contrast into the interstitial space
	Hepatic arterial fraction	HAF	None	Contribution of liver blood input from the hepatic artery
	Mean slope of increase	MSI	HU/s	Average slope from the tissue density curve
	Positive enhancement integral	PEI	None	Area under the tissue density curve
	Time to peak	TTP	S	Interval of time between the last pre-enhanced and maximum enhanced values
	Transit time to peak	Tmax	S	TTP of the fitted enhancement curve
Dynamic contrast-enhanced magnetic resonance imaging (DCE MRI)	Extravascular extracellular space (EES)	v_e	None	Tissue volume fraction of the EES
	Transfer constant	K^{trans}	min^{1}	Volume transfer between blood plasma and EES
	Rate constant of backflux from the EES to the blood plasma	k_{ep}	min^{1}	$k_{ep}=K^{trans}/v_e$

Statistical analysis

Analyses were performed using Stata 15. To describe the feasibility of performing pCT and DCE MRI in patients, the number and proportion of patients undergoing scans at each time-point were recorded. Baseline CT and MRI parameters for each group were described separately using means with the standard deviation (sd) and medians with the interquartile range (IQR). Baseline CT and MRI parameters were compared using the Wilcoxon sign rank test for matched groups. The changes in parameters from baseline to follow up were described using means (sd), medians (IQR) and the percentage change for each group. A significance level of 0.05 was imposed for all statistical testing. Means (sd) were used to compare the distribution of each baseline pCT parameter between hepatic responders and non-responders. The arithmetic means of DCE MRI and pCT parameters were assessed at baseline and changes in the mean were assessed at four- and ten-weeks follow-up relative to baseline parameters, defined as the difference.

3.3 Results

From July 2011 to Jan 2014, 58 patients were recruited to the study (Figure 3.4). Twenty-nine of these patients were in the FOXFIRE study and were first-line mCRC patients. Fourteen of these patients were randomised to the chemotherapy alone arm – this allowed a comparison of changes in perfusion parameters in a randomised population when treated with SIRT and chemotherapy compared to chemotherapy alone. One patient withdrew from the study. This patient was randomised to receive SIRT but did not due to prolonged toxicity from the chemotherapy. Of the remaining 28 patients, 14 received SIRT with chemotherapy and 14 patients received chemotherapy alone as part of the FOXFIRE study. Of these 28 patients, 24 had all four pCT scans. Four patients missed one scan because one patient had died before the fourth scan, two patients did not return for their last scan, and one patient missed a scan due to poor IV access (Supplementary Table 1). The total number of scans completed was 109 out a maximum of 116 scans (92% completion). However, the total number of scans available for analysis was significantly lower due to the inability to transfer from another site, no portal vein coverage, inadequate motion correction, or coil artefact. Two patients required delays in protocol, one had their fourth scan with the sixth cycle of chemotherapy (rather than fifth), and one patient had their chemotherapy one week after the second pCT, due to low blood counts.

A further twenty-nine patients with mCRC or ICC were recruited into PERFORM who were not in FOXFIRE and had SIRT as NHS treatment. Only the patients with mCRC are included in the FOXFIRE to non-FOXFIRE comparison. All were eligible to receive SIRT, although four patients were unable to proceed for clinical reasons: two due to technical difficulties, one due to liver dysfunction, and one due to patient performance status. The clinical feasibility and measurement of baseline perfusion parameters in first- and third-line metastatic cancer are provided in Supplementary Table 2.

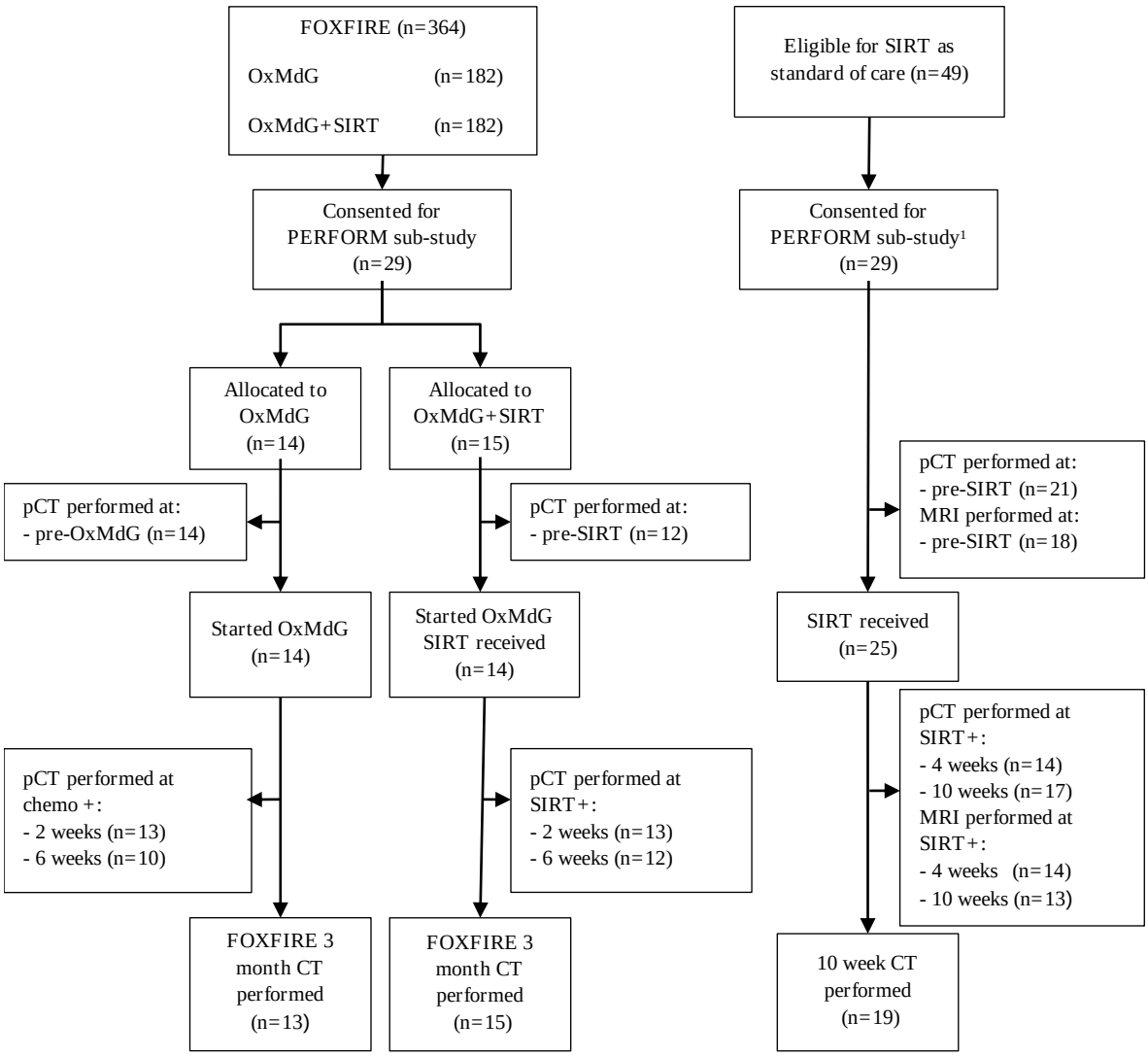

Figure 3.4. PERFORM study flow chart. Five patients did not proceed with SIRT two due to technical difficulties, one due to liver dysfunction, one due to patient performance status and one in the FOXFIRE study due to significant toxicity with first cycle OxMdG. Three patients missed the 4-week scan – due to family circumstances; unable to tolerate due to back pain; too unwell to travel. Six patients missed the 10-week scan – due to deterioration in condition; frailty and shortness of breath. [1] Includes 5 patients who had cancer other than metastatic colorectal cancer.

In the patients with more advanced disease, more scans were missed due to patient factors, however the majority were able to comply with the schedule. One prior concern about the role of perfusion CT measurements in patients receiving SIRT was the impact of coil artefact. Of the 14 patients who received SIRT in first-line CRC, embolisation coils were visible on several scan slices, however this only interfered with analysis of two scans in total (Figure 3.2).

Recruitment was high at 93% with only four patients that were approached declining to participate. The number of scans participants received in PERFORM within the FOXFIRE study was high. The total number of scans available for analysis was significantly lower due to the inability to transfer from another platform from two sites, absence of portal vein, inadequate motion correction, and coil artefacts. Five of the patients' images who had been performed from two sites were unable to be imported into the GE Perfusion 4D software. However, four other patients who had scans on other vendor platforms were successfully imported and analysed. The patient baseline characteristics are described in Table 3.2. The tumour radiology data at baseline for each patient are presented in 2.

Table 3.2. Baseline characteristics of the patients in the PERFORM study.

Characteristic[1]		All registered patients (n=58)	Metastatic colorectal cancer patients (n=53)
Age at registration (years)[2]		58: 59.28 (32.30 – 83.23)	53: 59.28 (32.30 – 83.23)
Time from primary tumour diagnosis to registration (months)[3]		54: 9.07 (1.22 – 20.01)	50: 6.09 (1.15 – 20.86)
Time from liver metastases diagnosis to registration (months)[3]		54: 1.92 (1.02 – 17.05)	50: 1.84 (0.92 – 20.01)
Patient cohort	FOXFIRE	29 (50%)	29 (55%)
	Non-FOXFIRE	29 (50%)	24 (45%)
Cancer type	Metastatic colorectal	53 (91%)	53 (100%)
	ICC	4 (7%)	-
	Uveal melanoma	1 (2%)	-
Treatment type	OxMdG	14 (24%)	14 (26%)
	SIRT ± OxMdG	44 (76%)	39 (74%)
Gender	Male	38 (66%)	36 (68%)
	Female	20 (34%)	17 (32%)
Site of primary colon tumour	Left	32 (55%)	32 (60%)
	Right	13 (22%)	13 (25%)
	Not available	13 (22%)	8 (15%)
KRAS status	Mutation	19 (33%)	19 (36%)
	Wild type	21 (36%)	21 (40%)
	Unknown	18 (31%)	13 (25%)
Liver metastases at primary tumour diagnosis[4]	Synchronous	46 (79%)	42 (79%)
	Metachronous	8 (14%)	8 (15%)
	Unknown	4 (7%)	3 (6%)

[1] n (%) for categorical variables; n: median (range) or n: median (IQR) for continuous variables
[2] n: median (range)[3] n: median (IQR)[4] The disease is considered synchronous if the primary tumour and liver metastases were diagnosed within 8 weeks of each

With regard to the primary objective of the study, the results demonstrated multi-parametric imaging is feasible in patients with advanced hepatic malignancies at multiple time-points (Table 3.3 and 1). Ninety-two (49/53) percent of patients with mCRC (53 patients in total) were able to

participate in pCT across the FOXFIRE and non-FOXFIRE patients. Of the non-FOXFIRE patients with refractory disease only 19/24 (79%) underwent DCE MRI (2). Nine pCT parameters were derived from the artery, portal vein, tumour, and background (tumour-free part of the liver) ROIs in the liver. Three MRI parameters were derived from the tumour and background liver ROIs. All the patients with mCRC who underwent a pCT scan had at least one set of parameters derived from the liver tumour. 84% (16/19) of the mCRC patients who underwent a DCE MRI scan had at least one parameter derived from the liver tumour. From all DCE MRI scans that were performed, maps for K^{trans}, v_e and k_{ep} were generated (Figure 3.5). PK modelling was unable to be completed in a high number of scans (17/45) of scans: 3 at baseline, 6 at four-weeks post-SIRT, and 8 at ten-weeks post-SIRT.

Table 3.3. Number of perfusion CT scans performed at each time-point among patients registered in the PERFORM study

Timepoint	Scan type	
	pCT	DCE MRI[2]
Baseline	47	18
2nd OxMdG cycle[1]	26	
3rd OxMdG cycle[1]	26	
4 weeks post-SIRT	14	14
5th OxMdG cycle[1]	22	
10 weeks post-SIRT	17	13
Total number of scans	152	45

[1]Time-point applies to FOXFIRE patients only
[2]Non-FOXFIRE patients only

Perfusion parameters

For the pCT and DCE MRI scans that were performed but had no perfusion modelling acquired, reasons included the inability to motion correct, lack of inclusion of portal vein, incompatibility with software, and new coding required when MRI was moved from 1.5T to 3T for the introduction of oxygen-enhanced MRI.

Each baseline perfusion parameter is described as the mean with standard deviation (sd) and median interquartile range (IQR) for tumour and background liver regions in Table 3.4. At a descriptive level, of the pCT parameters, the median BV at baseline appeared lower for tumour regions compared to background liver regions. Additionally, of the DCE MRI parameters, the median k_{ep} appeared lower for tumour regions compared to background liver regions, but higher for the v_e parameter. Wilcoxon sign-rank tests for matched observations were used to compare the distribution of each baseline pCT and DCE MRI parameter between tumour and background liver

regions. With the exception of pCT parameters HAF and PS and the DCE MRI parameter K^{trans}, there was a statistically significant difference in the distribution of each baseline pCT and DCE MRI parameter between tumour and background liver regions (all Wilcoxon sign-rank p<0.05).

Table 3.4. Baseline perfusion parameters. Mean (sd) and median (IQR) of baseline perfusion CT and MRI parameters between tumour and background liver regions

Parameter (units)		Region in liver		Wilcoxon sign-rank p-value
		Tumour	Background	
pCT				
BF (mL/min/100g)	N	47	47	0.012
	Mean (sd)	104.02 (62.59)	120.42 (54.15)	
	Median (IQR)	90.71 (76.47, 105.20)	110.80 (81.65, 140.70)	
BV (mL/100g)	N	47	47	<0.001
	Mean (sd)	13.73 (10.01)	24.68 (15.33)	
	Median (IQR)	10.93 (8.83, 15.39)	20.85 (17.22, 25.12)	
HAF (none)	N	47	47	0.216
	Mean (sd)	0.38 (0.16)	0.43 (0.24)	
	Median (IQR)	0.37 (0.26, 0.47)	0.38 (0.24, 0.64)	
MSI (HU/s)	N	43	43	<0.001
	Mean (sd)	1.18 (1.21)	1.56 (1.14)	
	Median (IQR)	0.95 (0.71, 1.24)	1.28 (1.00, 1.80)	
MTT (s)	N	47	47	<0.001
	Mean (sd)	11.89 (3.31)	15.53 (5.45)	
	Median (IQR)	11.72 (9.44, 14.50)	14.63 (11.64, 19.60)	
PEI (none)	N	47	47	<0.001
	Mean (sd)	0.23 (0.51)	0.31 (0.68)	
	Median (IQR)	0.11 (0.07, 0.16)	0.16 (0.11, 0.24)	
PS (mL/min/100g)	N	47	47	0.330
	Mean (sd)	17.57 (17.98)	16.17 (18.68)	
	Median (IQR)	11.59 (7.97, 18.05)	9.93 (4.18, 24.57)	
TTP (s)	N	47	47	<0.001
	Mean (sd)	30.39 (12.91)	33.23 (15.91)	
	Median (IQR)	32.76 (30.08, 34.21)	35.58 (30.86, 37.33)	
Tmax (s)	N	47	47	<0.001
	Mean (sd)	8.71 (2.00)	11.60 (6.05)	
	Median (IQR)	8.46 (7.57, 9.60)	10.12 (8.24, 13.31)	
DCE MRI				
K^{trans} (min^{1})	N	16	16	0.959
	Mean (sd)	0.61 (0.36)	0.60 (0.32)	
	Median (IQR)	0.57 (0.32, 0.86)	0.50 (0.35, 0.90)	
v_e	N	16	16	<0.001
	Mean (sd)	0.88 (0.35)	0.50 (0.18)	
	Median (IQR)	0.87 (0.55, 1.18)	0.46 (0.39, 0.54)	
k_{ep} (min^{1})	N	16	16	<0.001
	Mean (sd)	0.69 (0.28)	1.29 (0.75)	
	Median (IQR)	0.66 (0.58, 0.76)	1.21 (0.64, 1.88)	

[1] Responders are those with a complete or partial response; otherwise non-responders

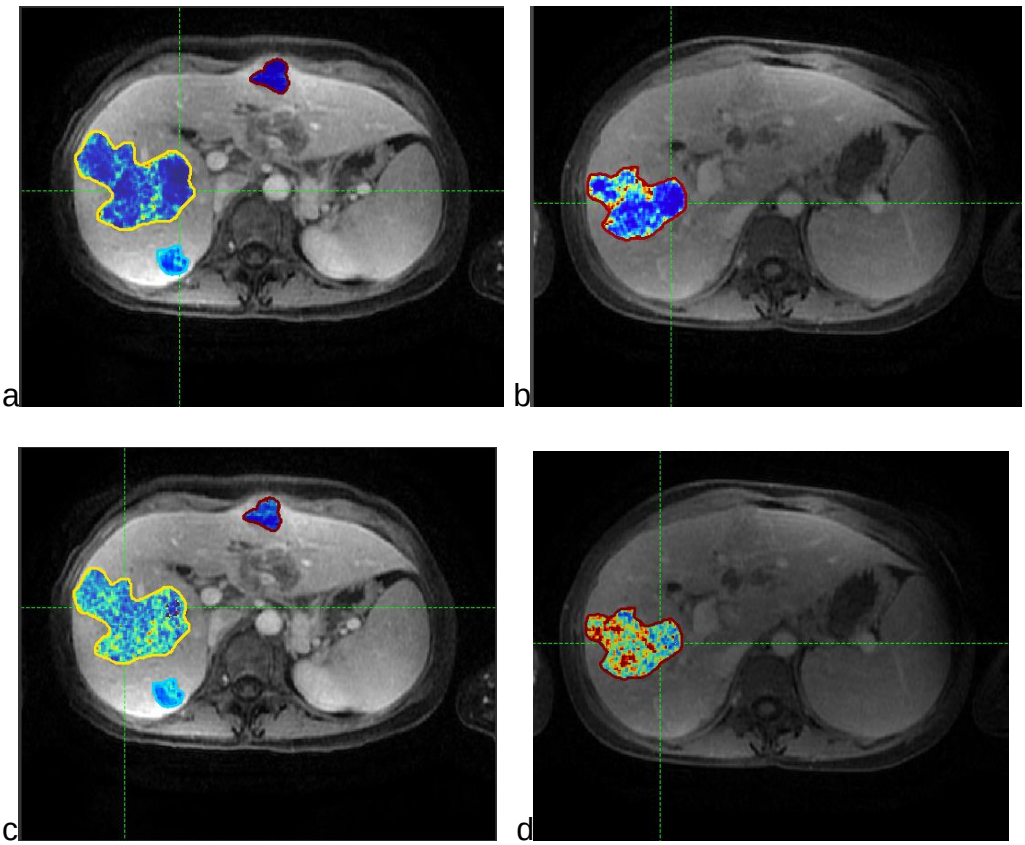

Figure 3.5. DCE MRI parameter maps of sample patient with multiple liver metastases from colorectal cancer. (A) K^{trans} at baseline and (B) ten-weeks following SIRT. (A and C) Baseline Three liver metastases are outlined in yellow, red and blue demonstrating inter-tumour heterogeneity in K^{trans}. (A) Baseline K^{trans} map and (B) at 10 weeks after SIRT. The tumour K^{trans} maps demonstrated small changes between (A) baseline with a mean of K^{trans} = 0.43/min and (B) 10 weeks at K^{trans} = 0.40/min. (C and D) Tumour v_e maps demonstrated intra-tumoural changes between (C) baseline and (D) 10 weeks after SIRT in a responding CRC liver metastases.

The change in parameters was evaluated as the difference between baseline and follow-up overall and in hepatic responders versus non-responders. Analysis considered only the 36 of 53 mCRC patients who received SIRT and had available pCT or DCE MRI data. Two FOXFIRE patients did not have available baseline pCT scan data and were therefore excluded from the analyses. Additionally, one patient did not have available baseline pCT data and excluded, though this patient was still included in the analysis of DCE MRI data. Therefore, 33 patients were included in the analysis of pCT data. There were six non-FOXFIRE patients who did not have available baseline DCE MRI scan data but were still included in the analysis with available pCT data. Therefore, there were 16 patients included in the analysis of DCE MRI data. Of the patients included in the pCT and DCE MRI analysis, 36% (12/33) and 56% (9/16) respectively achieved an objective radiological hepatic response according to RECIST 1.0 (Table 3.5).

Table 3.5. Number (proportion) of SIRT-receiving mCRC patients with hepatic response.

		Participants receiving SIRT number (%)	
		pCT (n=33)	DCE MRI (n=16)
Objective response	Objective response (CR + PR)	12 (36%)	9 (56%)
RECIST 1.0 response	Complete response (CR)	0	0
	Partial response (PR)	12 (36%)	9 (56%)
	Stable disease (SD)	3 (9%)	1 (6%)
	Progressive Disease (PD)	7 (21%)	4 (25%)
	NA	11 (33%) *	2 (13%)
*33% of patients' response assessment not available as not linked at peripheral site CR- complete response, PR – partial response, SD Stable disease, PD-progressive disease, NA not available.			

At a descriptive level, the median pCT and DCE MRI parameters at baseline did not appear to vary considerably between overall responders and non-responders and between hepatic responders and non-responders. The baseline pCT parameters for hepatic responders and hepatic non-responders are described in Table 3.6 as means (sd) and medians (IQR). Wilcoxon rank-sum tests were used to compare the distribution of each baseline pCT parameter between hepatic responders and non-responders. There was no statistically significant difference in the distribution of each baseline pCT parameter between hepatic responders and non-responders (all Wilcoxon rank-sum p-values ≥ 0.05). The baseline DCE MRI parameters for overall and hepatic responders and non-responders are also described in Table 3.6.

Table 3.6. Baseline perfusion parameters from patients aprticipating in PERFORM. Mean (standard deviationsd) and median (Inter quartile range IQR) of baseline pCT and DCE MRI parameters between overall and hepatic SIRT-receiving responders and non-responders. Wilcoxon rank sum compared the hepatic progressors from the non-progressors.

Parameter (units)		Hepatic response		Wilcoxon rank-sum p-value
		Responders[1]	Non-Responders[1]	
Perfusion CT				
BF (mL/min/100g)	n Mean (sd) Median (IQR)	12 112.42 (55.15) 92.21 (80.25, 122.47)	21 84.69 (31.49) 86.51 (67.02, 94.91)	0.116
BV (mL/100g)	n Mean (sd) Median (IQR)	12 16.26 (14.31) 11.04 (9.94, 16.57)	21 12.59 (6.59) 10.54 (7.77, 15.60)	0.331
HAF	n Mean (sd) Median (IQR)	12 0.46 (0.12) 0.43 (0.40, 0.53)	21 0.36 (0.14) 0.36 (0.26, 0.47)	0.061
MSI	n Mean (sd) Median (IQR)	11 1.21 (0.45) 1.13 (0.83, 1.47)	18 1.31 (1.80) 0.94 (0.71, 1.19)	0.132
MTT (sec)	n Mean (sd) Median (IQR)	12 11.85 (3.17) 12.21 (8.82, 14.68)	21 12.46 (3.61) 12.02 (10.49, 13.81)	0.736
PEI	n Mean (sd) Median (IQR)	12 0.13 (0.05) 0.14 (0.09, 0.16)	21 0.34 (0.76) 0.09 (0.07, 0.15)	0.262
PS (mL/min/100g)	n Mean (sd) Median (IQR)	12 20.25 (22.74) 11.63 (9.15, 20.35)	21 17.77 (19.40) 9.63 (7.94, 16.49)	0.636
TTP (sec)	n Mean (sd) Median (IQR)	12 29.48 (9.95) 32.70 (29.66, 34.13)	21 27.76 (16.98) 32.25 (28.99, 33.35)	0.465
Tmax (sec)	n Mean (sd) Median (IQR)	12 8.28 (1.39) 8.69 (6.98, 9.31)	21 9.01 (1.92) 8.52 (8.24, 9.60)	0.454
MRI				
K^{trans} (min^{1})	n Mean (sd) Median (IQR)	9 0.66 (0.39) 0.61 (0.32, 0.79)	7 0.54 (0.32) 0.35 (0.27, 0.93)	
V_e	n Mean (sd) Median (IQR)	9 0.96 (0.32) 0.86 (0.78, 1.27)	7 0.78 (0.38) 0.88 (0.45, 0.91)	
k_{ep} (min^{1})	n Mean (sd) Median (IQR)	9 0.70 (0.31) 0.66 (0.64, 0.69)	7 0.68 (0.24) 0.64 (0.51, 0.86)	
[1] Responders are those with a complete or partial response otherwise non-responders				

At a descriptive level, the change from baseline to follow-up in pCT parameters did not appear to vary considerably between overall responders and non-responders and between hepatic responders and non-responders. The difference from baseline to follow-up for each parameter is described with means (sd) and medians (IQR) for hepatic responders and non-responders in Table 3.7.

Table 3.7. Change of perfusion parameters from baseline to follow-up. Mean (sd) and median (IQR) of change from baseline to follow-up in perfusion CT and MRI parameters for overall and hepatic SIRT-receiving responders and non-responders.

Parameter (units)		Overall response		Hepatic response	
		Responders[1]	Non-Responders[1]	Responders[1]	Non-Responders[1]
Perfusion CT					
BF (mL/min/100g)	n	5	20	10	15
	Mean (sd)	-3.86 (76.02)	0.43 (35.85)	-3.10 (60.40)	1.35 (32.35)
	Median (IQR)	9.52 (-40.61, 49.53)	-0.82 (-16.32, 21.38)	11.21 (-46.93, 42.38)	-1.96 (-9.87, 17.94)
BV (mL/100g)	n	5	20	10	15
	Mean (sd)	-10.83 (21.16)	-0.48 (5.75)	-4.70 (15.77)	-1.12 (6.17)
	Median (IQR)	-6.67 (-8.22, 3.54)	0.11 (-3.13, 2.61)	-0.44 (-6.67, 3.54)	0.17 (-4.21, 3.08)
HAF	n	5	20	10	15
	Mean (sd)	-0.14 (0.10)	-0.04 (0.17)	-0.07 (0.15)	-0.05 (0.18)
	Median (IQR)	-0.09 (-0.17, -0.07)	-0.03 (-0.11, 0.05)	-0.07 (-0.17, 0.06)	-0.03 (-0.12, 0.01)
MSI (?)	n	4	17	8	13
	Mean (sd)	0.18 (0.53)	-0.10 (0.29)	-0.00 (0.50)	-0.08 (0.24)
	Median (IQR)	0.12 (-0.22, 0.58)	-0.04 (-0.19, 0.04)	0.02 (-0.29, 0.24)	-0.04 (-0.19, 0.02)
MTT (s)	N	5	20	10	15
	Mean (sd)	-2.27 (2.54)	0.67 (3.90)	-0.92 (3.92)	0.75 (3.73)
	Median (IQR)	-1.91 (-4.15, -1.01)	0.50 (-2.53, 2.54)	-1.46 (-4.15, 1.06)	1.51 (-2.56, 2.53)
PEI	n	5	20	10	15
	Mean (sd)	0.01 (0.07)	-0.22 (0.82)	0.07 (0.28)	-0.34 (0.90)
	Median (IQR)	-0.00 (-0.03, 0.02)	-0.02 (-0.06, -0.00)	-0.01 (-0.05, 0.02)	-0.02 (-0.07, 0.00)
PS (mL/min/100g)	n	5	20	10	15
	Mean (sd)	-9.16 (34.09)	-4.48 (17.94)	-3.08 (25.03)	-6.97 (19.13)
	Median (IQR)	-3.84 (-8.59, 4.36)	-2.57 (-7.36, 1.34)	-1.64 (-7.84, 4.36)	-3.47 (-8.85, 0.96)
TTP (s)	n	5	20	10	15
	Mean (sd)	7.41 (14.97)	2.35 (12.23)	1.17 (15.64)	4.82 (10.55)
	Median (IQR)	2.78 (2.62, 4.50)	0.61 (-0.66, 4.17)	2.70 (-2.56, 4.50)	0.63 (-0.53, 4.11)
Tmax (s)	n	5	20	10	15
	Mean (sd)	-0.37 (1.47)	0.78 (1.73)	-0.10 (1.38)	0.99 (1.83)
	Median (IQR)	-0.64 (-1.02, -0.43)	0.32 (-0.44, 2.06)	-0.36 (-1.02, 0.33)	0.63 (-0.49, 2.17)
MRI					
K^{trans} (min^{1})	n	3	10	8	5
	Mean (sd)	-0.11 (0.21)	-0.12 (0.30)	-0.07 (0.32)	-0.18 (0.19)
	Median (IQR)	-0.07 (-0.33, 0.08)	-0.08 (-0.45, -0.01)	-0.05 (-0.39, 0.20)	-0.10 (-0.24, -0.06)
v_e	n	3	10	8	5
	Mean (sd)	-0.10 (0.23)	-0.12 (0.38)	-0.07 (0.39)	-0.18 (0.27)
	Median (IQR)	-0.15 (-0.29, 0.15)	-0.12 (-0.48, 0.07)	-0.13 (-0.38, 0.22)	-0.13 (-0.26, 0.02)
k_{ep} (min^{1})	n	3	10	8	5
	Mean (sd)	-0.14 (0.12)	-0.10 (0.28)	-0.07 (0.31)	-0.17 (0.12)
	Median (IQR)	-0.20 (-0.22, -0.01)	-0.14 (-0.22, 0.01)	-0.10 (-0.22, 0.03)	-0.19 (-0.19, -0.08)

[1] Responders are those with a complete or partial response; otherwise non-responders

Table 3.8 describes the baseline perfusion parameters between patients having first-line treatment for mCRC versus patients who were heavily pre-treated and chemotherapy-refractory receiving SIRT in the 3rd line and beyond. MSI was statistically significantly different and may represent biological changes in tumour perfusion over time when mCRC develops resistance to standard chemotherapies.

Table 3.**8**. Mean (sd) and median (IQR) of baseline perfusion CT parameters for FOXFIRE and non-FOXFIRE patients. Participants in FOXFIRE were treated in first-line. The non-FOXFIRE had refractory cancer and were more heavily pre-treated.

Parameter (units)		Patient cohort		Wilcoxon rank-sum p-value
		FOXFIRE	Non-FOXFIRE	
BF (mL/min/100g)	n Mean (sd) Median (IQR)	26 110.10 (74.34) 91.15 (77.34, 116.78)	21 96.49 (44.67) 90.71 (67.02, 99.70)	0.507
BV (mL/100g)	n Mean (sd) Median (IQR)	26 14.72 (12.62) 10.44 (8.83, 14.74)	21 12.49 (5.35) 11.04 (9.31, 15.39)	0.700
HAF	n Mean (sd) Median (IQR)	26 0.35 (0.17) 0.33 (0.23, 0.44)	21 0.42 (0.14) 0.42 (0.33, 0.47)	0.069
MSI	n Mean (sd) Median (IQR)	23 0.93 (0.46) 0.85 (0.63, 1.07)	20 1.48 (1.68) 1.10 (0.79, 1.39)	0.040
MTT (sec)	n Mean (sd) Median (IQR)	26 12.09 (3.58) 11.70 (9.57, 14.72)	21 11.64 (3.01) 12.02 (9.25, 14.41)	0.898
PEI	n Mean (sd) Median (IQR)	26 0.30 (0.68) 0.10 (0.08, 0.14)	21 0.13 (0.06) 0.14 (0.07, 0.16)	0.346
PS (mL/min/100g)	n Mean (sd) Median (IQR)	26 19.78 (22.18) 12.05 (7.94, 18.05)	21 14.84 (10.68) 10.11 (8.18, 16.49)	0.732
TTP (sec)	n Mean (sd) Median (IQR)	26 31.95 (14.90) 32.93 (31.63, 34.94)	21 28.46 (9.95) 31.56 (28.99, 33.49)	0.146
Tmax (sec)	n Mean (sd) Median (IQR)	26 8.88 (2.39) 8.32 (7.68, 9.73)	21 8.49 (1.42) 8.73 (7.19, 9.53)	0.898

3.4 Discussion

This study has demonstrated the feasibility of integrating a perfusion imaging study within a large prospective multi-centre, controlled clinical trial to examine the perfusion characteristics of patients receiving liver-directed therapy in addition to chemotherapy. We have shown the acquisition of perfusion imaging parameters from pCT and DCE MRI is feasible in patients with metastatic disease including patients with mCRC refractory to chemotherapy. DCE MRI, a T1-weighted sequence, usually involving the injection of a low molecular weight gadolinium-chelate contrast agent can be incorporated into normal liver MRI imaging. DCE MRI has become the mostly commonly adopted perfusion technique in cancer patients (O'Connor et al., 2012). DCE MRI has been proposed as a tool to assess vascular physiology of lesions with anatomical detail. The quantitative measurement of these vascular parameters may act as an indirect measure of angiogenesis (Prezzi & Goh). DCE MRI uses tracer kinetic modelling, which allows quantitative characterisations of changes in parenchyma and tumour microcirculation. Coinciding with the development of the anti-angiogenic agents, there has been an increase in studies looking at the parameters measured by DCE MRI as a potential biomarker for antiangiogenic therapy (Miller, 2005). This study confirms that functional parameters can be generated from pCT and DCE MRI. Our data suggest that perfusion imaging parameters may not represent a predictive biomarker for response to SIRT. Although this study did not find any statistical correlation with baseline perfusion parameters and prediction for RECIST 1.0 response, liver tumours with higher BF and MTT may tend towards an increased likelihood to respond to SIRT.

Work from pre-clinical modelling of tumour perfusion heterogeneity with texture analysis is ongoing. The heterogeneity demonstrated in perfusion and vascularity of tumours from texture analysis is worthy of more study and may provide more information on challenges for arterially delivered therapies to large heterogeneous lesions (Winter et al., 2018). Other work from preclinical perfusion modelling was used to analyse patients from this group and found perfusion measure may be more complex and relate to vessel radius and tortuosity (Kannan et al., 2018). Further prospective studies on patient selection and stratification to arterially delivered therapies is worthy of more research.

Subsequent work on dosimetry has explored the absorbed dose and the correlation with response (Abbott et al., 2018). Analysis of 10 patients with mCRC from PERFORM, found that as each unit of BF to the tumour increases, an extra 0.056 Gy was deposited. Likewise, for each additional second it takes for the contrast agent to pass through a tumour, the average dose uptake to the tumour is expected to decrease by 2.8 Gy. These correlations indicate that dose uptake may be assessed

prospectively from pCT parameters such that higher rates of perfusion through tumour tissue achieved higher dose depositions (Unpublished).

All pCT perfusion parameters assessed as change at 3 months follow-up against dose were statistically significant, while none of the DCE MRI parameters was. Potential explanations for this discrepancy include poorer resolution of DCE MRI, nature of in-house methods rather than the mature clinically-deployed workflow from which pCT benefitted, and data limited to 10 patients with 53 individual tumours.

While no baseline perfusion parameters were associated with RECIST 1.0 hepatic or overall response, several baseline perfusion parameters did correlate with either dose or volumetric response. These findings suggest that there may be some prognostic utility for perfusion imaging of ^{90}Y SIRT. As doses deposited were higher and therapeutic effect was expected to be greater, perfusion parameter change was observed. These results are a promising indication that perfusion imaging, in particular pCT metrics, may be associated with the deposition of ^{90}Y SIRT microspheres and tumour response. Further investigations are needed in more patients to confirm these findings, including studies of the effects of perfusion non-uniformity throughout a tissue. Future areas of research may examine the ability for texture analysis and to describe the global distribution of parameters allowing a map of perfusion heterogeneity within tumours. Exploratory work with the quantification of the tumour perfusion heterogeneity used K^{trans} maps as the texture feature maps (Winter et al., 2018).

Determining a relationship between perfusion and revascularisation would be particularly useful as this usually suggests the liver metastases are aggressive and associated with poorer patient outcomes.

Chapter 4: T1 mapping in the Non-Invasive and Comprehensive Liver Assessment (NICOLA) study: results from a prospective imaging study of native T1 mapping and oxygen enhanced MRI in patients with hepatic malignancy

There is a clinical need to develop reliable, non-invasive methods to characterise hepatic lesions. Liver biopsy, the current gold standard, is invasive and limited by sampling variability, operator-expertise, complication risks and potential for biopsy-related seeding of malignant lesions (Chen et al., 2016). The risk of these complications has led to the development of novel magnetic resonance protocols to characterise benign liver tissue. T1 mapping has already demonstrated a high diagnostic accuracy for the assessment of benign liver fibrosis (Banerjee et al., 2014).

A prospective study examining quantitative T1 mapping prior to definitive hepatic resection was developed. The T1 mapping quantitative data reported was generated using shMOLLI. Unselected adult patients referred for liver resection as part of standard of care were recruited after discussion at the hepato-biliary MDT. Scans performed prior to liver resection were analysed prior to the histology results. The associations between magnetic resonance and histology variables were assessed.

Paired magnetic resonance and resection specimens were examined in ten patients. T1 mapping was also quantified during the inhalation of high flow oxygen. The aim was to assess T1 shortening within lesions after high flow oxygen as a non-injectable contrast agent.

Quantitative T1 mapping detected CRCLM and differentiated these lesions from benign cysts. However, T1 mapping was unable to differentiate lower grade NET from benign lesions. T1 values were shortened in malignant lesions with high flow oxygen. Histological assessment of hepatic resection specimens confirmed the nature of the lesions and the effects after neoadjuvant chemotherapy in those with CRCLM. Analysis following chemotherapy demonstrated fibrosis, cholesterol clefts and steatosis in resection specimens.

Native T1 and OE T1 mapping study demonstrated a proof of concept in patients prior to liver resection. The findings of changes in T1 values with O_2 and the novel scanning method described here are worthy of a larger prospective study with patients having pre- and post-neoadjuvant chemotherapy scans, prior to liver resection. The ability of the imaging technique to look at background liver fibrosis, steatosis and haemosiderosis could assist in assessing patients prior to liver-directed therapy. Although T1 mapping is gaining traction in benign liver disease, further work is required to confirm reliability in characterising suspected malignant lesions and differentiation. The specific changes seen with the apparent shortening of T1 with O_2 in some malignant lesions warrant further investigation for an association with chemotherapy response.

4.1 Overview

The Non-Invasive and Comprehensive Liver Assessment (NICOLA) study was designed as a prospective non-invasive, single-centred hepatic imaging study. The primary objective of the whole study was the determination of the role of non-invasive MRI to measure liver fibrosis, fat and iron deposition. However, this report focuses on the exploration of T1 mapping as a quantitative imaging tool, in the assessment of patients with suspected malignant hepatic lesions. T1 mapping has been shown to correlate with tissue composition in benign liver disease and is replacing the need for invasive liver biopsy in assessment of liver fibrosis. The NICOLA trial tested the hypothesis that a non-contrast magnetic resonance imaging T1 mapping sequence, using shortened modified look locker inversion recovery (shMOLLI), was able to identify tumours from background liver without contrast agent. This approach was to determine if a non-invasive approach was feasible in the assessment of hepatic lesions. The study also explored the effect of oxygen enhancement on T1 values and examined the shortening of T1 in hepatic lesions with high flow oxygen administration. Patients with hepatic lesions, were imaged with the sequence, before and during high flow oxygen. Subsequent surgical resection of hepatic lesions supported the correlation of T1 values with the histology of the lesion and the pathological response to chemotherapy, when given. The results of T1 mapping from the cohort of patients with suspected hepatic malignancy are presented.

The hypotheses of this study were:

1) Quantitative T1 mapping of tumours will differ from background liver.
2) T1 mapping detects malignant lesions and differentiates malignant from benign lesions, without the need for IV contrast.
3) Quantitative T1 mapping detects changes in background liver including steatohepatitis and fibrosis in pre-treated patients.
4) Oxygen enhancement, using inhalation of high flow oxygen, will result in T1 shortening in more vascular, aggressive malignant tumours or tumours that have had a poor response to chemotherapy.

4.2 Research Design and Method

4.2.1 Study design and population

The Non-Invasive and Comprehensive Liver Assessment (NICOLA) study (Ethics approval number 13/SC/0243) was a prospective, non-randomised study of a new diagnostic MRI method to evaluate hepatic lesions. The criteria for patient eligibility included RECIST measurable disease together with suitability for resection. All patients were considered at the Oxford University Hospitals Hepatic multi-disciplinary team meeting. Patients were scanned on the 3 T Siemens MRI at the Oxford Centre for Clinical Magnetic Resonance Research (OCMR) at the John Radcliffe Hospital, before definitive surgery.

Hepatic surgery was performed at the Churchill Hospital. The reference standard was histological assessment of resection specimen.

From Jan 2015- March 2017 patients referred for hepatic resection were invited to participate, except those with a contraindication to MRI. Eligible patients included those with indeterminate hepatic lesions, prior colorectal cancer and patients receiving neo-adjuvant chemotherapy for confirmed CRCLM. All had been deemed suitable candidates for recruitment following the multidisciplinary team meeting where hepatic resection was proposed. Sixteen patients were approached and three declined to participate. Thirteen patients gave written informed consent to participate. Two patients withdrew - one patient was unable to undergo MRI due to the logistics of attending imaging at a separate location to surgical appointments, one was unable to attend before scheduled surgery. One patient was recruited prior to the addition of OE MRI. The addition of supplemental O_2 was to investigate this as a non-injectable arterial contrast agent in MRI of hepatic lesions. Therefore, 11 patients are included in the final analysis (Baseline characteristics in Table 4.1). Native and oxygen-enhanced T1 mapping was performed in ten patients who had both scans, however only nine patients proceeded to hepatic resection.

4.2.2 MRI protocol

All MRI scans were performed with the patient in supine position in a 3 Tesla (3T) system (Tim Trio, Siemens Healthcare, Germany). Prior to the non-contrast T1 mapping, patients fasted for 4 hours. The total duration of the multi-parametric MRI protocol was 25 minutes which extended to 45 minutes with the addition of oxygen-enhanced scanning. The protocol acquired MRI data during expiratory breath-hold, with ECG-gating to minimise motion artefacts from respiration and the cardiac cycle.

All subjects were advised to repeatedly hold their breath (to improve the signal to noise ratio) and lie still for 12 - 14 seconds, which was comfortably managed by all participants. These are standard techniques for cardiac data acquisition (Rial, Robson, Neubauer, & Schneider, 2011). The scanning protocol included T1 mapping, T2* and proton spectroscopy that are examine for fibrosis, iron and steatosis respectively. The T1 relaxation time mapping was acquired using the shortened Modified Look Locker Inversion (shMOLLI) recovery sequence (see Chapter 2.4 Background to T1 mapping and oxygen enhanced MRI in patients receiving hepatic resection).

The patient was initially scanned under normoxic conditions, i.e. at 21% O_2. Then, using a standard clinical oxygen mask, 100% O_2 was supplied at 15l/min to introduce hyperoxic conditions. The scan was repeated after a 3 minute delay to allow for complete wash-in of oxygen. End tidal oxygen levels were monitored during this time. T1 quantification was embedded in a full protocol of morphological MRI sequences.

4.2.3 Histological analysis of liver resection specimens

Hepatic resection samples were prepared as per standard pathological clinical practice. All resection specimens were included in the final analysis. Histological review of the hepatic resection samples confirmed pathological diagnosis - underlying benign hepatic lesion, malignant CRCLM, neuroendocrine (NET) or hepatocellular carcinoma (HCC). Histological assessment of the samples included background liver parenchyma, an assessment of chemotherapy exposure and response and CD31 staining of vessels. The histological diagnosis was made by pathologist (LW) as per a standard clinical pathology framework. Analysis of the stained sections was undertaken by the author with pathologist oversight. The resections specimens were analysed for fibrosis, changes related to neo-adjuvant chemotherapy and vascularity. Tumour grading, response to chemotherapy were measured on Haematoxylin and Eosin (H&E) including steatosis, presence of cholesterol clefts, fibrosis and necrosis.

Table 4.1. Baseline characteristics of the 11 patients in the NICOLA study.

	Number
Age, years	
Mean	59.8
Range	50-69
Gender	
Female	6
Male	5
Tumour type	
Colorectal	7
Hepatocellular	1
Pancreatic NET	1
Indeterminate lesions	2

4.3 Results

4.3.1 T1 mapping of malignant lesions within the liver

T1 mapping was quantified in background liver and malignant lesions. Mean T1 values were significantly longer in all lesions from the patients with malignancy than the background liver and patients with benign lesions. The median T1 value at baseline of confirmed malignant lesions was 1485 msec (range 1161 – 2294 msec, standard deviation 344) and compared to the median T1 of background liver 814 msec (range 649 – 960 msec, standard deviation 120). Figures 4.1 and 4.2 demonstrate the quantitative T1 values in two patients with histologically confirmed hepatic malignancies. Increased T1 values are demonstrated within the hepatic malignancy compared to background liver parenchyma. The images in Figure 4.3 compare the images acquired with T1 mapping using shMOLLI and the standard MRI sequence. Two metastatic deposits are seen on the coloured shMOLLI acquired images and the standard MRI.

Figure 4.1. T1 mapping and correlation of hepatic resection specimen (macroscopic). Figure 4.1a. Quantitative T1 mapping with shMOLLI allows identification of a liver metastasis from background liver. Images from a 69 year-old male with rectal cancer (fasted), awaiting hepatic resection. Differential T1 mapping of the metastasis (indicated by the thin black arrow) quantified a T1 of 1182 msec from the hepatic metastasis and T1 of 651 msec from the background liver parenchyma (thick black arrow).

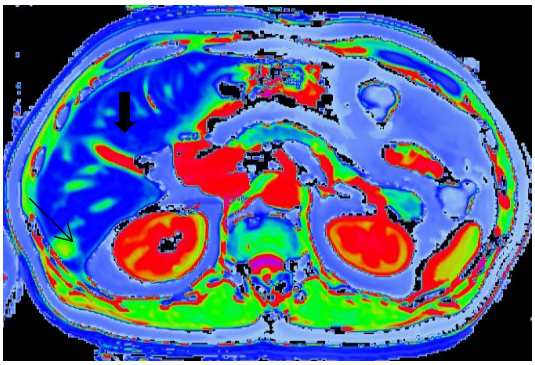

Figure 4.1b. Correlation of imaging slice indicating lesion with increased T1 (shown in Fig.4.1a) with the macroscopic appearance of the hepatic resection specimen (the white peripheral lesion seen on the right of the specimen below represents the metastasis). The cm rule is shown at the bottom.

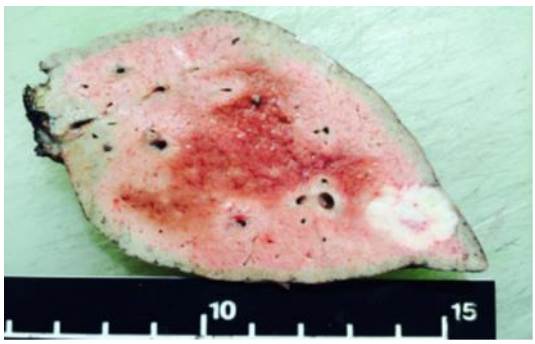

Figure 4.2. Native T1 mapping and correlation with macroscopic appearance of corresponding hepatic metastatic deposit. Figure 4.2a. T1 mapping scan with shMOLLI of a malignant lesion. The malignant lesion had a long T1 value of 1175 msec indicated with thin black arrow, from a female patient with histologically confirmed fully resected metastatic CRCLM. T1 of background liver parenchyma (thick black arrow) measured 640 msec.

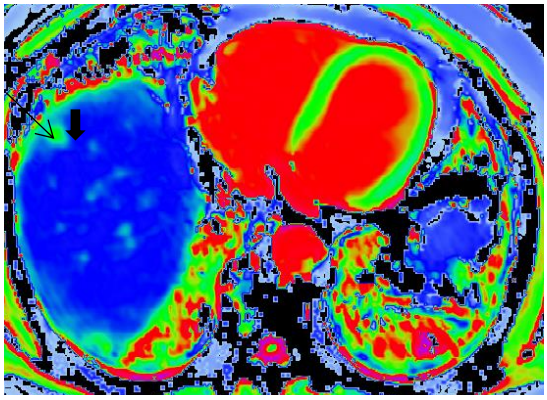

Figure 4.2b. Correlation of imaging shown in Fig.4.2a, with the macroscopic appearance of the hepatic resection specimen (the thin black arrow indicates the corresponding resected metastasis).

Figure 4.3. Comparison of T1 mapping acquired with shMOLLI and standard MRI. Figure 4.3a and 4.3c show the T1mapping acquired with a shMOLLI scans and Figures 4.3b and 4.3d show conventional T1 fat saturation scan, also acquired without intravenous contrast. White arrows indicate metastases.

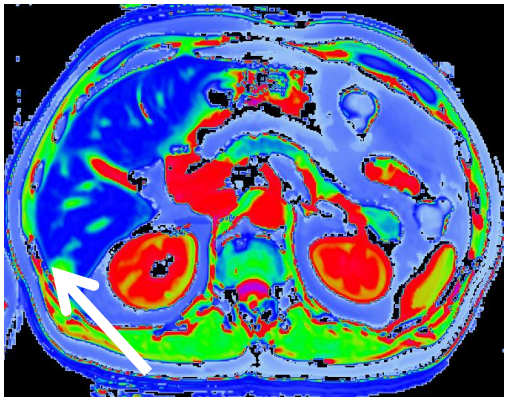

Figure 4.3a

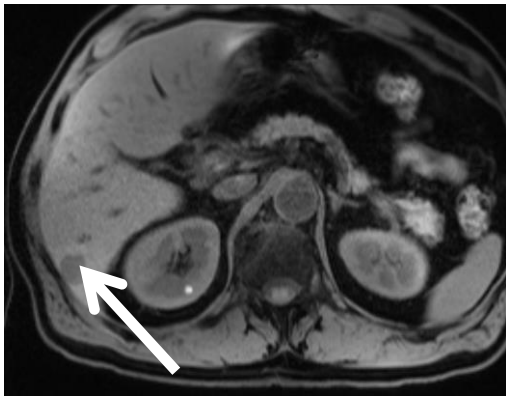

Figure 4.3b

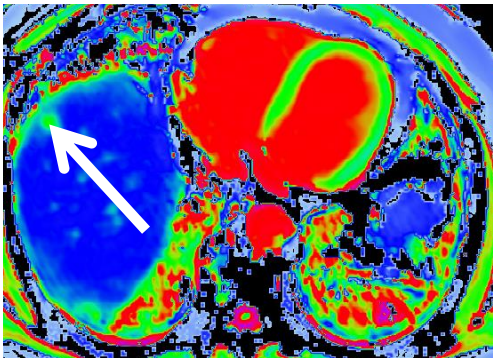

Figure 4.3c

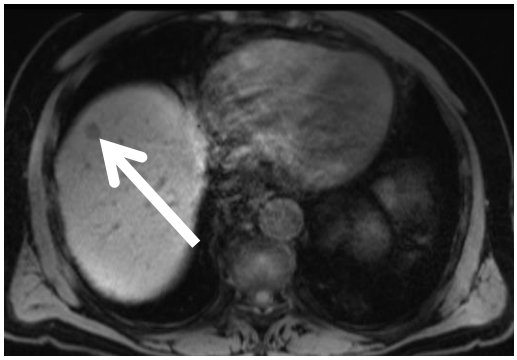

Figure 4.3d

4.3.2 Sub-region analysis of T1 mapping within tumours and normal liver.

Sub-regional was performed to see if T1 mapping detected differences between regions of the malignant lesion including tumour core and at the outer periphery and normal liver. An example of this is displayed in Figure 4.4. The location of the regions of interest (ROI) demonstrate differences in T1 measurement. The regions indicated are: Tumour core (ROI 4); inner tumour periphery 1 (ROI 3), outer periphery 2 (ROI 2) and the immediately adjacent liver (ROI 5).

The tumour displays a gradient of T1, with the longest values in the core and 3 other distinct areas. In Figure 4.4 the central core gives the longest T1 values, compared to the two surrounding peripheral areas. There was a significant difference between T1 values of the tumour core (ROI 4) when compared to the adjacent normal liver (ROI 5) and between T1 at the inner tumour periphery 1 (ROI 3) when compared to adjacent liver (ROI 5).

Figure 4.4. Quantitative T1 in sub-regions of liver tumour and normal liver. Figure 4.4a identifies the Regions of Interest (ROI) across the tumour core and periphery. Figure 4.5a This graph demonstrates a significant difference between T1 values of the tumour core (ROI 4) when compared to the adjacent normal (ROI 5) and between T1 at the inner tumour periphery 1 (ROI 3), when compared to adjacent liver (ROI 5).

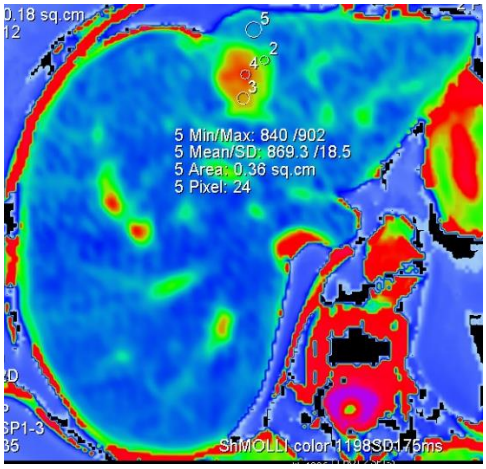

Figure 4.4a

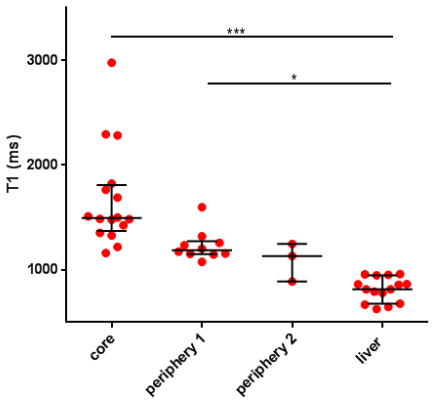

Figure 4.4b

4.3.3 Oxygen-enhanced T 1 mapping

In pre- and post- oxygen scans, patients with residual malignancy evidenced the most significant drop in T1 values when provided high flow oxygen. The steady-state readings for oxygen after high flow oxygen inspiration ranged from 73-98%.

Quantitative T_1 is shortened in hepatic malignancies when measured with inhaled high flow O_2. Figure 4.5 shows T1 mapping from a patient with confirmed hepatic malignancy and demonstrates shortening of T1

(msec) with inhalation of high flow oxygen. Similar, but more pronounced shortening is well described within the oxygenated blood within the left ventricle of the heart when compared to the right ventricle.

Figure 4.5 Oxygen-enhanced T1 mapping of liver metastasis pre- (Figure 4.5a) and post-high flow oxygen (Figure 4.5b). T1 (room air) in the liver metastasis (thick black arrows) measures 1605 msec compared to a shortened value of T1 of 1508 msec on 85% inspired oxygen in liver metastasis on the right (thick black arrow). There is no significant change in the T1 of the background liver (thin black arrows) pre and post-high flow oxygen. T1 822 msec (room air) compared to 815 msec (100% inspired oxygen).

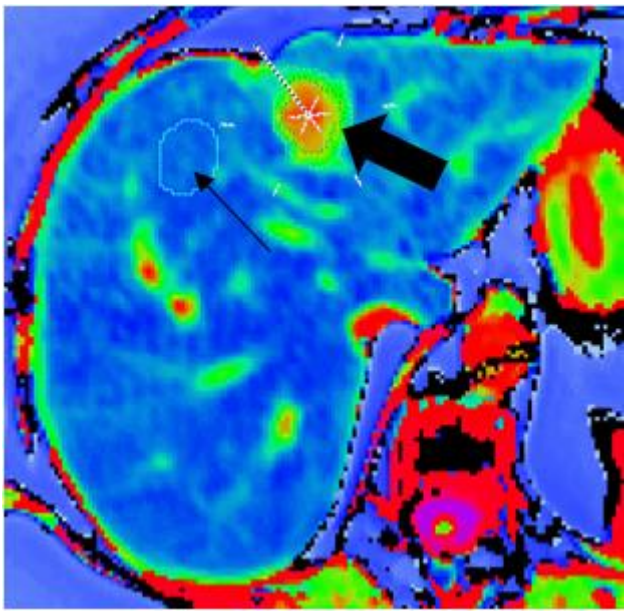

Figure 4.5a T1 1605 msec in metastasis indicated by thick black arrow at room air

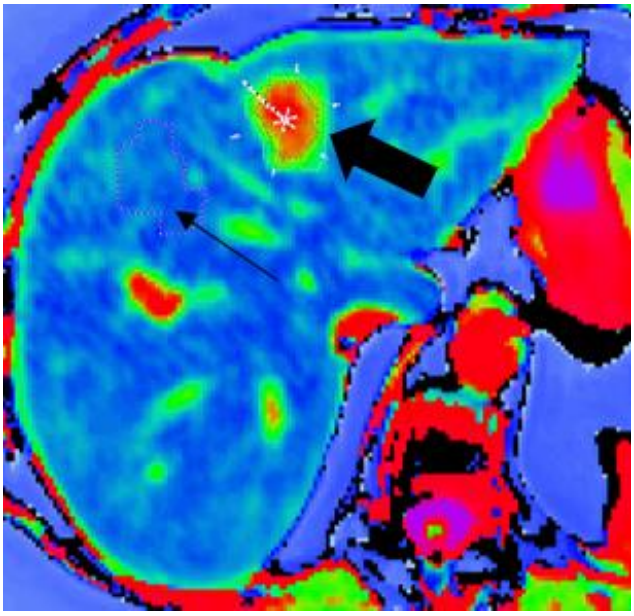

Figure 4.5b T1 1508 msec in metastasis indicated by black thick arrow with high flow inspired O_2

Table 4.2. T1 mapping pre- and post- high flow O2 enhancement. The oxygenation of blood in the left ventricle (LV) when high flow oxygen is inhaled shows a comparison of the shortening of T1 from baseline (on room air) of 1883 msec which is shortened to 1609 msec with high flow oxygen. This compares to T1 values in the right ventricle (RV) which are not shortened when high flow oxygen is inhaled. Similar degree of shortening is seen within the spleen and tumour core. There is no shortening of the background liver seen when T 1 is measured on room air when compared to T1 on high flow oxygen.

(msec)	Baseline (room air)	Standard Deviation	Inhaled O_2	Standard Deviation
LV blood	1883	41	1609	24
RV blood	1849	32	1909	29
Spleen	1541	20	1447	21
Liver parenchyma	822	30	815	17
Cancer periphery	1221	98	1179	98
Cancer core	1605	112	1508	105

Results from the T1 mapping from patients with five colorectal metastases and one hepatocellular carcinoma demonstrated shortened T1 with oxygen enhancement. Establishing this differential response of quantitative T1 with oxygen enhancement supports the hypothesis that oxygen may act as a non-invasive contrast agent that adds to the ability to differentiate hepatic malignancy from benign or background liver. In Figure 4.6a the results from five CRCLM are show in red and one hepatocellular lesion in blue. In Figure 4.6b on the right, two liver cysts are shown in red and the hepatic neuroendocrine lesions are shown in blue – these tend to be lower grade, less vascular lesions.

Figure 4.6. Results from thirteen lesions in the ten patients who received OE MRI. The change in T1 from baseline (patients on room air) with high flow oxygen in different hepatic lesions is seen. In Figure 4.6a the shortening of T1 is seen in a CRCLM and an HCC lesion when patient changes from breathing room air to high low oxygen. This compares to Figure 4.6b where there is no change in T1 with five neuroendocrine lesions and cystic lesions pre or during high flow inhaled oxygen.

Figure 4.6a

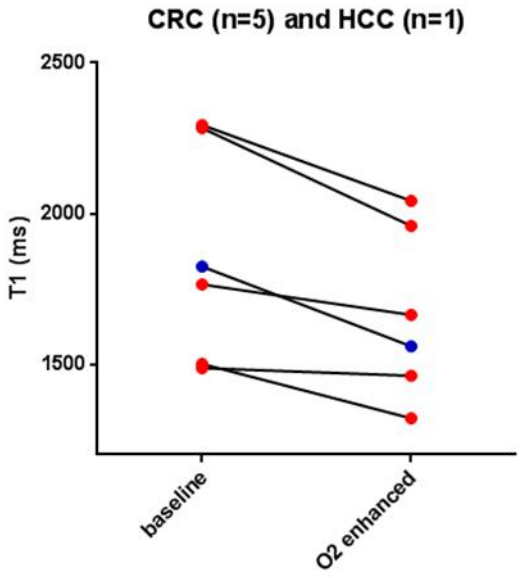

4.1.6b

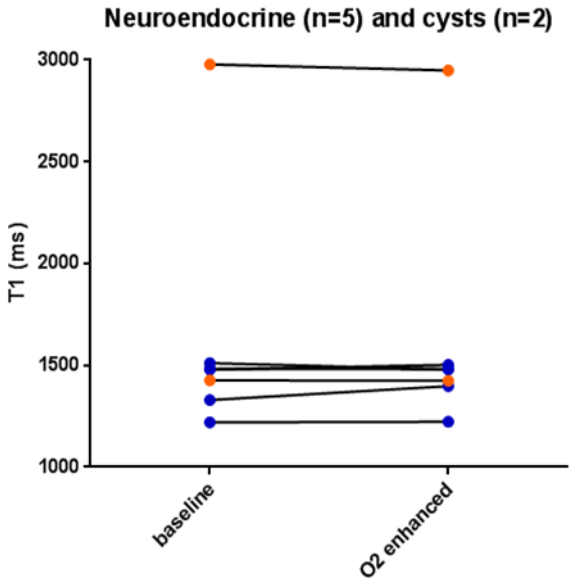

4.3.4 T1 mapping and exploratory analysis with histological response to neo-adjuvant chemotherapy

Correlation of histology and imaging is considered for three patients, each who had received neo-adjuvant chemotherapy and exhibited markedly differing responses.

Figure 4.7 presents the results from Patient 5. The examination of the resection specimen confirmed a complete pathological response. Fatty change and vascular congestion are observed with evidence of veno-occlusive sinusoidal obstructive syndrome (VOD SOS). An absence of tumour cells was reported although a tumour mass effect was evident indicating a response to the chemotherapy. The CD31 staining shown in Figure 4.7b indicates mucin pooling, however there is no dense stroma, no microvasculature and very little residual angiogenesis. The tumour T1 value of 1690 millisecond and background liver T1 value of 669 milliseconds on room air were both found to be elevated for Patient 5. Unfortunately, the scan on oxygen was not suitable for T1 value calculation.

Figure 4.7. T1 mapping and correlation with histology from hepatic resection (microscopic). In Figure 4.7a T1 mapping of the lesion is demonstrated. On room air the background liver had a T1 value of 669 msec and the T1 of the tumour was 1690 msec. This patient was scanned on oxygen however the scan was not of good enough quality to have T 1 mapping quantified. In Figure 4.7b below the hepatic resection specimen is shown. The image below shows the CD31 immunohistochemistry staining in patient with resected CRCLM with a complete pathological response to chemotherapy. The scale rule represents 300 µm, 100 x magnification.

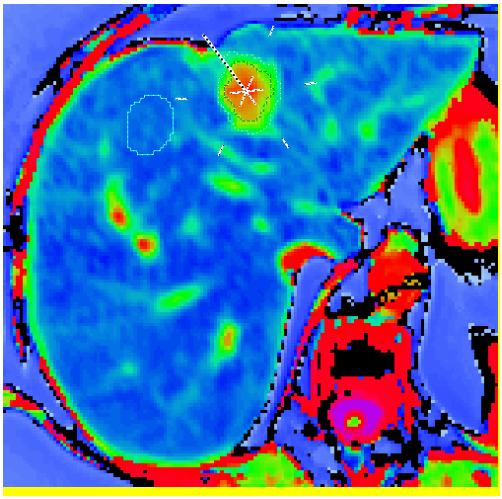

a

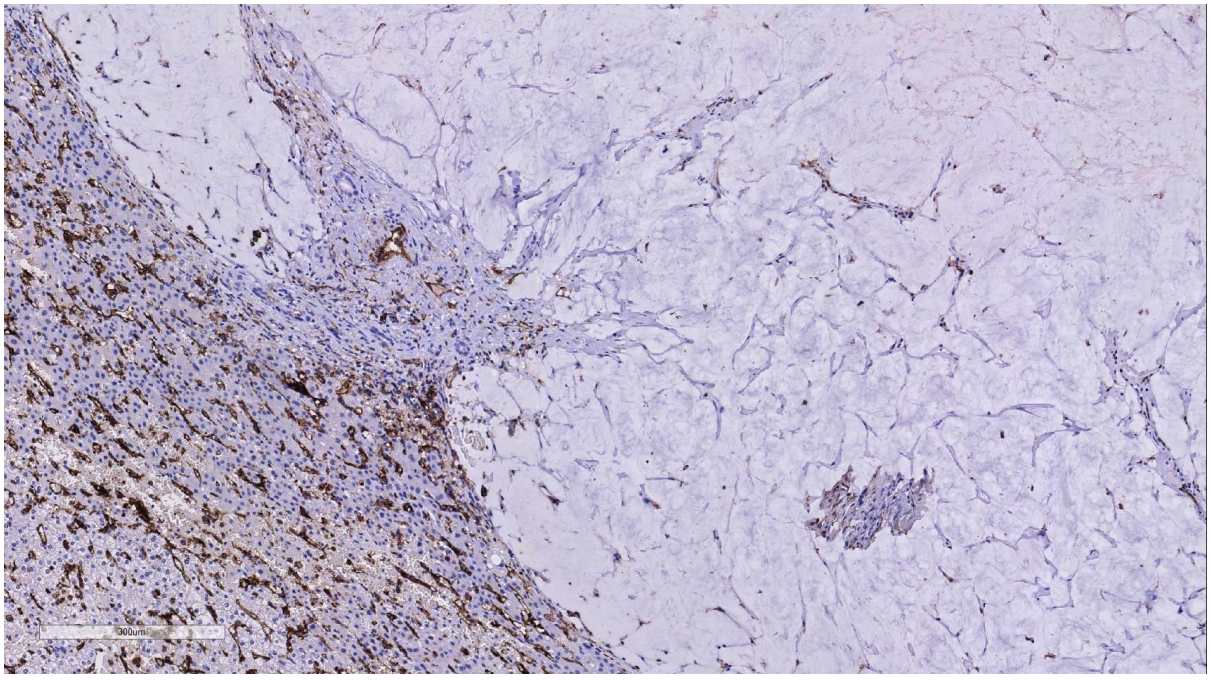

b

In Figure 4.8, a patient with a poor pathological response to chemotherapy is demonstrated. T1 mapping quantification was measured pre- and post-oxygen of patient 8 with a subsequent poor response to neoadjuvant chemotherapy seen from histology at hepatic resection. T1 background liver on room air: 814 msec compared to T1 background liver on high flow O2: 759 msec (7% decrease). The T1 value of this

tumour on room air was 2294 msec which shortened to a T1 value for the tumour on high flow O2 of 2042 msec (11% decrease).On the H & E slide stromal changes can be observed together with elastotic change and fibrosis (Figure 4.8a). There are cholesterol clefts - which represent foreign bodies with giant cell reaction. There is more of a reaction at the edge of the liver interface. Post chemotherapy changes are seen with multi-nucleated giant cells, histiocytes and foamy macrophages. Beany nuclei within these macrophages appear with a cleft, fusing to form giant cells. Within the normal liver, there is evidence of glycogenic sponge or cheese-like change which may suggest some effect from chemotherapy.

Within the tumour round, cribriform central necrosis is evident. Garland necrosis seen is an important feature to confirm the site of origin as colorectal cancer. The dirty garland necrosis seen is almost pathognomonic of colorectal cancer. Tumour glands are seen with lobular and ductal spread. Vessels are seen within the sinusoids. There is tumour mass effect adjacent to the lesion with apparent sinusoidal dilatation and congestion. There is increased CD31 staining suggestive of extensive neoangiogenesis.

T1 mapping pre-and post- oxygen confirm a significant drop in T1 with oxygen enhancement compared to the T1 values on room air. Findings of the significant shortening in T1 with oxygen and residual vascular tumour together with CD31 proving neo-angiogenesis suggest it may be worthwhile to explore the hypothesis that highly vascular tumours will have an increased reduction in T1 mapping using shMOLLI with high flow O_2 inhalation.

Figure 4.8. Resection specimen from a patient who had a poor response to neoadjuvant chemotherapy for CRCLM.

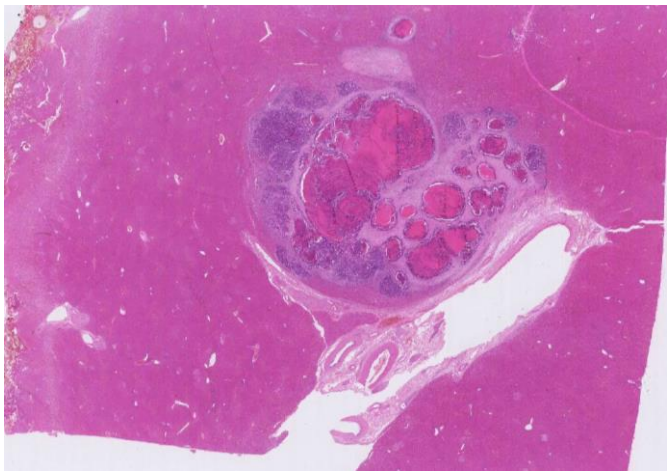

Figure 4.8a. Haematoxylin and Eosin confirms a well-circumscribed residual tumour with garland necrosis and persistence of tumour glands. Stromal changes can be observed together with elastotic change and fibrosis. Cholesterol clefts - which represent foreign bodies with giant cell reaction - are also seen.

Figure 4.8b. CD31 immunohistochemistry staining. Scale represents 200 µm, 100 x magnification.

(below) This shows there is increased CD31 staining suggestive of extensive neoangiogenesis in a non-responder to chemotherapy.

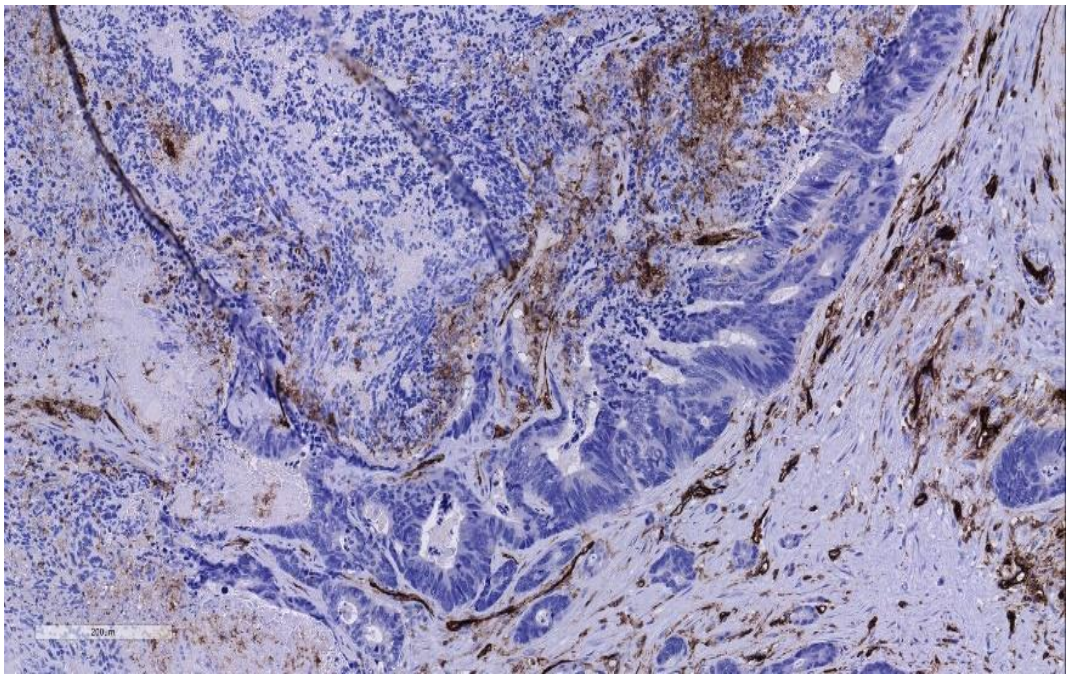

Figure 4.9 shows the results from patient 9 that was subsequently found to have an intermediary response to neo-adjuvant chemotherapy. Patient 9 was a partial responder and there results showed minimal change from T1 mapping on air to T1 mapping with high flow oxygen. T1 background liver on room air: 863 msec; T1 background liver on 100% O2: 836 msec (3% drop). T1 tumour on room air: 1487 msec; T1

tumour on 100% O2: 1462 msec (1.6% drop). Changes observed revealed evidence of a moderate response to chemotherapy, with some evidence of an intrabiliary ductal spread, tumour within the bile duct and areas of hyalinised stroma with residual mucin. Non-specific calcification was also suggestive of a response to chemotherapy as were observed mucin change, hyalinization and fibrosis. Elastotic changes and cholesterol clefts were also present. Although there was residual tumour present the patient has had a partial tumour regression. The residual tumour has mucinous differentiation.

On CD 31 staining there is only a small area of normal vasculature apparent (Figure 4.9b). More vascular changes were seen by the use of Haematoxylin and Eosin, veno-occlusive disease, sinusoidal obstruction syndrome and haemorrhagic change and each apparent. The intervening stroma evidences vessels with a microvessel density. Little angiogenesis is demonstrated.

Figure 4.9. CD31 immunohistochemistry staining of patient 9 who had an intermediary response to systemic therapy. Scale represents 300 µm, 100 x magnification. Patient 9 had pathological changes suggestive of a response to neoadjuvant chemotherapy prior to hepatic resection. CD31 staining showed only a normal area of vasculature with little angiogenesis.

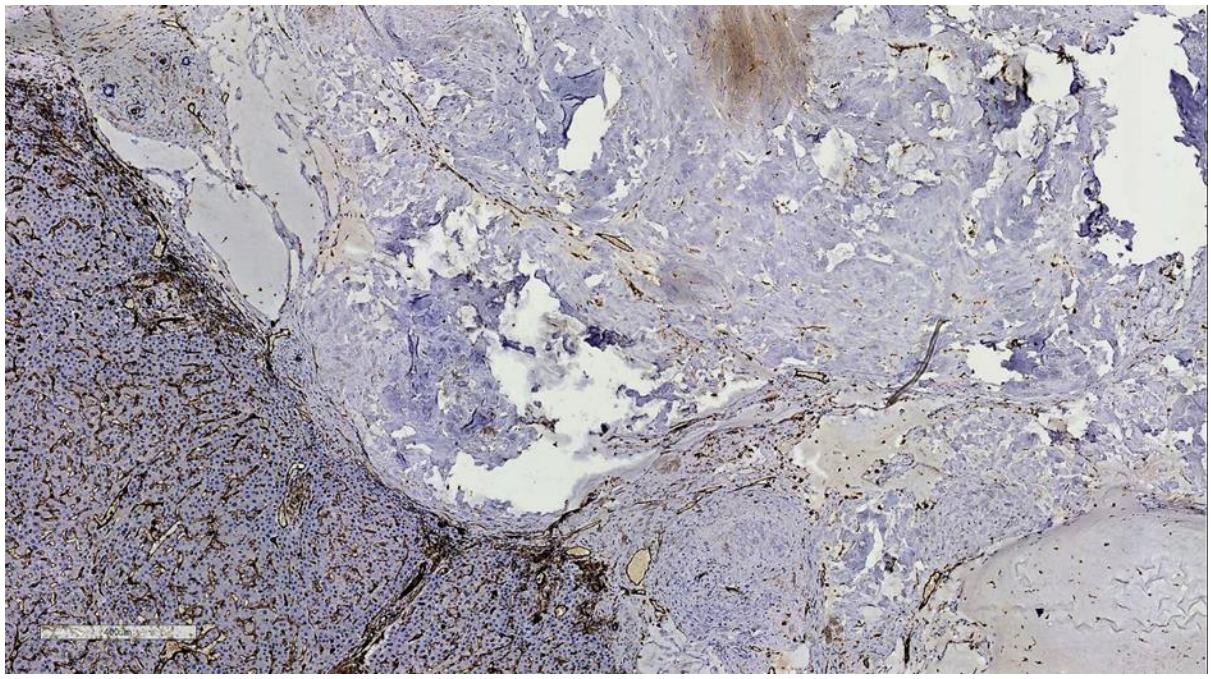

4.4 Summary of Results

The results from the NICOLA study demonstrate quantitative T1 mapping, with shMOLLI, in the liver is feasible through use of the described method. T1 mapping with shMOLLI assisted in the characterisation of liver lesions. The key findings were:

1. The feasibility of quantitative of native T1 mapping and T1 mapping with oxygen-enhancement in patients, with resectable liver metastases, is demonstrated.

2. Quantitative T1 mapping of tumours differed to background liver. Increased T1 values were quantifiable and T1 differed in CRCLM compared to background liver parenchyma.
3. T1 mapping detects malignant lesions and differentiates some malignant from benign lesions, without need for IV contrast.
4. Changes of T1 values with inhaled oxygen were seen in some malignant lesions (CRCLM and one HCC), and less commonly observed in background liver, benign and neuroendocrine lesions.

In summary, non-contrast T1 observed values were longer in malignant hepatic lesions than the background liver. T1 mapping with and without oxygen is feasible in patients with advanced cancer and prior to hepatic surgery. Histological correlation with underlying response to chemotherapy and residual malignancy was observed although warrants further investigation. The observation of an apparent difference of the reduction in T1 and response to chemotherapy for malignant lesions is hypothesis generating. The use of the inhalation of high flow oxygen, may result in T1 shortening in more vascular, aggressive malignant tumours or tumours that have had a poor response to chemotherapy and is worthy of further study.

Future analysis may include quantitative T1 mapping as a tool to detect changes in surrounding liver parenchyma including detecting steatohepatitis and fibrosis after chemotherapy and liver-directed therapies. Further prospective study of quantitative T1 mapping to assess liver parenchyma and hepatic lesions and the role of high flow oxygen as a non-injectable contrast agent are indicated.

Chapter 5: Hepatic resection following Selective Internal Radiation Therapy for Colorectal Cancer Liver Metastases: Safety and microsphere distribution

5.1 Overview

The FOXFIRE trial randomised patients to receive chemotherapy with OxMdG (oxaliplatin, 5-fluouracil and folinic acid) alone (Arm A) versus combined chemotherapy with SIRT using yttrium-90 resin spheres (Arm B). This was in the first line management of patients with liver-dominant, unresectable metastatic CRC. Although the combination failed to demonstrate an improvement in overall survival (Wasan et al., 2017) the outcomes, in terms of the type of hepatic resection, the rate of hepatic resection and complications from the patients that subsequently received hepatic resections are reported here and compared to the patients randomised to the chemotherapy alone arm. The safety of hepatic resection after this novel combination, the outcomes after hepatic resection and an exploratory analysis of the histopathology of the resected hepatic specimens are examined. This analysis included the distribution of microspheres and pathological features seen in the hepatic tissues after SIRT.

5.2 Methods

Trial participants

Ethical approval was granted from the Berkshire Research Ethics Committee (Ethics number 09/H0505/1). The trial registration number was ISRTCTN83867919. The trial was conducted in accordance with Good Clinical Practice, Declaration of Helsinki and ISO14155. All participants gave written informed consent to participate in FOXFIRE and an additional consent for analysis of the pathology of surgical specimens. Patients were required to be eligible for systemic chemotherapy for metastatic CRC and performance status 0-1. Inclusion criteria included histologically confirmed CRC, liver-dominant or liver only metastases, unresectable disease at time of study entry (as determined by liver surgical MDT), life expectancy of greater than 3 months. Exclusion criteria included the presence of ascites, cirrhosis, main portal vein thrombosis and portal hypertension.

Treatments

The treatment with OXMDG was planned for 12 cycles given two weekly. The doses were 85 mg/m2 oxaliplatin infusion over 2 hours, l-folinic acid 350 mg infusion over 2 hours, 400 mg/m2 bolus 5-FU followed by continuous 46 hour infusion of 2400 mg/m2 5-FU. For patients receiving SIRT, the dose of oxaliplatin was modified to 60 mg/m2 for 3 cycles around the procedure, based on early phase date (R. A. Sharma et al., 2007). Hepatic arteriogram and nuclear medicine scans formed the work-up and planning imaging pre-SIRT delivery. The patient's body surface area, liver volume and magnitude of liver- lung shunt were used to determine the dose delivered in GBq. The delivery of Y90-resin microspheres was scheduled for day 3-4 of cycle 2.

Hepatic surgery

All patients were reassessed at hepatic MDTs, following treatment for possible resection. Liver surgery was offered across 16 sites. The analysis of the surgery uses the descriptions from the Brisbane 2000 classification (Strasberg et al., 2000). Complications from surgery were recorded and classified in keeping with standard hepatic surgery complication grading (Dindo, Demartines, & Clavien, 2004).

Histopathology and Immunohistochemistry

Sections of formalin fixed paraffin embedded tissue (liver in 27 cases, and gall bladder in 18 cases) were scanned using the Aperio AT Turbo digital scanner (Leica Microsystems, Milton Keynes, UK) and used for the assessment of tumour viability and regression, associated fibrosis and microsphere distribution. The sections were stained with Haematoxylin and Eosin and Sirius Red to assess fibrosis. An assessment of vascular pathology and fatty change away from the tumour was also performed.

The density and distribution of microspheres was determined using zonal analysis using Aperio ImageScope (Leica Microsystems, Milton Keynes, UK). An estimation of the spheres density in Non-Neoplastic Tissue (NNT) was calculated using a mean average of the density in two 3 mm X 3 mm – 5 mm X 5 mm areas of tissue for each case (3 mm X 3 mm regions were used in cases where limited NNT was present). A microsphere density for the tumour centre was also calculated; the tumour centre was defined as the area 2mm proximal to the tumour border. Sphere densities within the 1mm and 2mm zones of the tumour border and the tumour centre were expressed as a ratio of the sphere density calculated for the NNT (Supplementary Figure 1).

Immunohistochemical staining for CD68 (with mouse clone PGM1, Dako M087601-2), smooth muscle actin (ABCAM and CD31 (ab7817, DAKO M0823) was performed on the Leica Bond III automated immunostaining platform using Leica Bond Polymer Refine detection with DAB chromogen (Leica, DS9800). Dewaxing and peroxidase blocking were performed on-board as per kit, according to the manufacturer's instructions. Antibody was applied for 15 minutes at room temperature, following on-board heat-induced epitope retrieval (HIER) for 30 minutes at 99C with Leica Epitope Retrieval 1 solution (pH 6, Leica, AR9961).

Statistical analysis

The hepatic resection rate was defined as the number of patients receiving resection in each arm divided by the total number assigned to that group. Time-to-event analysis was performed for each subgroup of patients who received hepatic resection. The time of the first surgery was taken in the time-to-event analysis for patients receiving more than one resection. The time from randomisation to resection was calculated in months from date of randomisation to date of first hepatic resection surgery. The time from hepatic surgery to death was calculated from the date of surgery to death by any cause. Any patients not recorded as deceased were censored at the last recorded alive date.

The proportion of patients receiving hepatic resection in each group was compared using the chi-squared test. The comparison of time-to-event analysis included Kaplan-Meier curves, Cox Proportional hazards

models and log-rank tests. The Mann-Whitney U test was used to compare tumour characteristics between groups. A two-sided 5 % significance level was used for all tests. The analysis was performed on STAT 15 and GraphPad Prism version 6.0 (GraphPad Software La Jolla, California, USA).

5.3 Results

Patient characteristics

The FOXFIRE study recruited 364 patents from 13 November 2009 to 31 October 2014. The randomisation resulted in 182 patients allocated into each arm. The full characteristics of the trial participants have been reported (Wasan et al., 2017). Of the 364 patients, 71 (20%) were subsequently offered hepatic resection following first-line therapy with chemotherapy alone or chemotherapy combined with SIRT. Demographics are shown in Table 5.1.

Forty-seven (66 %) male patients and 24 (34 %) female patients proceeded to surgery. Twelve (17 %) patients had extrahepatic disease. In terms of the volume of hepatic metastases the majority of patients 57 (79 %) had 25 % or less involvement of the liver by metastases. Fifteen (21 %) patients had greater than 25 % involvement of the liver by tumour. Of the 71 patients 33 (46 %)) were in Arm A and 38 (54 %) were in Arm B. The median follow-up for these 71 patients was 42.7 months.

The addition of a biological therapy was given concomitantly in 15 (45 %) patients receiving chemotherapy-alone. Eight received bevacizumab and 7 received cetuximab). In the combination Arm B, 6 (15 %) patients received a biological agent concomitantly with chemotherapy (4 received bevacizumab and 2 received cetuximab). The study flow chart is shown in Figure 5.1.

Table 5.1. Characteristics of the study participants who had hepatic resection during the FOXFIRE clinical trial. n is the number of participants (%) for categorical variables; median (min-max) for continuous variables.

Characteristic at baseline		OxMdG (n=33)	OxMdG+SIRT (n=38)	Total (n=71)
Age at randomisation (years)		62 (42-78)	61 (30-83)	61 (30-83)
Extra-hepatic metastases status	No	28 (85%)	31 (82%)	59 (83%)
	Yes	5 (15%)	7 (18%)	12 (17%)
Degree of liver involvement	<=25%	27 (82%)	29 (76%)	56 (79%)
	>25%	6 (18%)	9 (24%)	15 (21%)
Gender	Male	22 (67%)	25 (66%)	47 (66%)
	Female	11 (33%)	13 (34%)	24 (34%)
Ethnicity	Caucasian	32 (97%)	33 (89%)	65 (93%)
	Asian	0 (0%)	2 (5%)	2 (3%)
	Black/African American	0 (0%)	1 (3%)	1 (1%)
	Other	1 (3%)	1 (3%)	2 (3%)
WHO performance status	0	29 (88%)	24 (65%)	53 (76%)
	1	4 (12%)	13 (35%)	17 (24%)
Metastases present at initial diagnosis	No - Metachronous	8 (24%)	5 (14%)	13 (19%)
	Yes - Synchronous	25 (76%)	32 (86%)	57 (81%)
Primary tumour site	Left-sided primary	25 (86%)	31 (82%)	56 (84%)
	Right-sided primary	4 (14%)	7 (18%)	11 (16%)
Primary tumour in situ	No	14 (42%)	16 (42%)	30 (42%)
	Yes	19 (58%)	22 (58%)	41 (58%)
KRAS	Unknown	12 (36%)	10 (26%)	22 (31%)
	Wild Type	15 (45%)	23 (61%)	38 (54%)
	Mutation	6 (18%)	5 (13%)	11 (15%)
Chemotherapy with biological therapy		15 (45%)	6 (16%)	21 (30%)
Prior adjuvant chemotherapy	No	31 (94%)	37 (97%)	68 (96%)
	Yes	2 (6%)	1 (3%)	3 (4%)

Figure 5.1. Study flow chart. FOXFIRE participants that were considered for hepatic resection after OxMdG: oxaliplatin, 5-fluorouracil and folic acid chemotherapy alone or OxMdG combined with SIRT: selective internal radiotherapy. One patient in the OxMdG + SIRT group who underwent a hepatic resection had started OxMdG chemotherapy but did not receive SIRT.

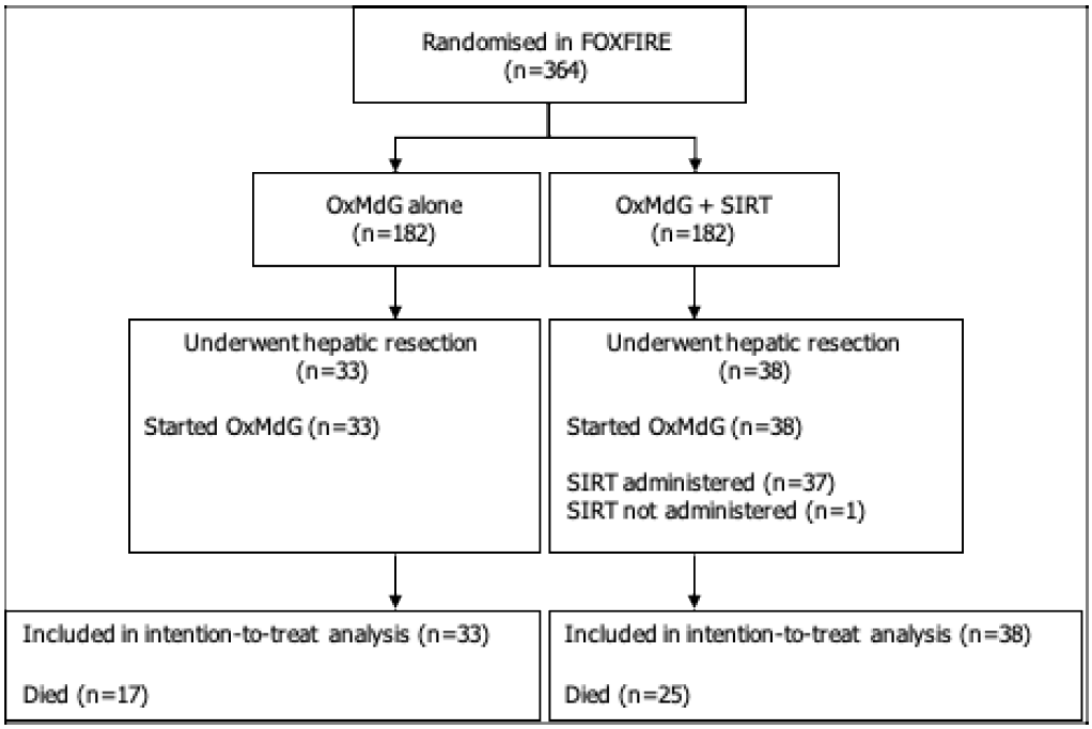

Surgical outcomes

There were 82 surgical episodes among the 71 patients. Nine (13 %) patients had two operations, and one patient had three surgeries. The liver surgery was performed across 16 sites, however 3 hospitals performed the majority of the surgery. The operations performed within FOXFIRE, described by the Brisbane classification are shown in Table 5.2. Overall, the proportion of FOXFIRE patients proceeding to surgery was not statistically significantly different. Thirty-three (18 %) of the chemotherapy-alone compared to 38 (21 %) of the combination group. The commonest surgical procedure was a right hepatectomy (n= 22 (31 %). Other surgeries include 12 (17 %) segmentectomies and 9 (13%) left hepatectomies. Of the 15 patients who had more than 25 % liver involvement at baseline, four (27 %) required a two-stage resection. Four patients were open-and-closed and did not have a resection.

Table 5.2. Types of surgery for hepatic resection after SIRT and / or chemotherapy. Based on the Brisbane 2000 classification. ns - Not specified. ALPPS - Associated Liver Partition and Portal vein ligation for Staged hepatectomy.

Type of surgery	Incidence of Surgery	Additional procedures
Right hepatectomy	22	Two patients had sub-segmentectomies (segments IVa, V; II, III)
Left hepatectomy	9	One patient had IVC resection. One patient had subsegmentectomies (ns)
Segmentectomies	12	Segmentectomies: Two patients: II, III; One patient each: III, VI, VII; III, IV, VII; IVb, V, VI; IV, V, VI (and subsegmentectomy and ablation); I, II, III; IV and ablation; IVa, VIII. One patient each with one segmentectomy: Vi; IV; II (subsegmentectomy III).
Extended right hemihepatectomy	7	Three with subsegmentectomies (I; III; ns)
Extended left hemihepatectomy	1	
Left lateral hepatectomy	2	Atypical
Subsegmentectomies	9	Three patients: ns. Two patients: segment II only. One patient each: III; IVa, IVb, II; V, VI, VII (ablation II, IV);
No hepatic surgery report available	14	Details of cholecystectomy specimen only received.
Open and close and / or biopsy	4	
Other	2	First part ALPPS. Right post sectionectomy (VI, VII).

Twenty-six (37%) of patients had a complication after resection, the majority (20 patients) had grade I and II complications. Four patients (3 from the OxMdG + SIRT, 1 from OxMdG group) had grade III complications requiring surgical or radiological intervention. This included one patient who developed a pneumothorax; on resection of part of the diaphragm subsequently, microspheres were present on part of the resected diaphragm. One post-hepatectomy liver failure was documented and one patient in the chemotherapy-alone group required readmission. Two patients in the combination arm reported severe complications. One patient developed grade IVa endocarditis which occurred five months after SIRT. This patient had a prolonged hospital admission of 52 days after surgery. Another patient developed a grade IVb complication with the development of a pulmonary embolus, myocardial infarction and sepsis. However, this patient was discharged home after 15 days in hospital. There were no reported deaths within 90 days from hepatic resection. Full complications are described in Table **5.3**

Table 5.3. Classification and grading of surgical complications in chemotherapy-alone (OxMdG) and in the combination group (OxMdG + SIRT).

Grade	OxMdG	OxMdG + SIRT	Total
I	4	5	9
II	7	4	11
III	1	3	4
IVa	0	1	1
IVb	0	1	1
V	0	0	0

Time-to-event analysis

Time from randomisation to death

Overall survival is presented as the time of randomisation to the time of death for the patients in the each of the two treatment groups. Forty-two of the 71 (59 %) of patients who had a resection had died at the time of the analysis. Twenty-nine (41 %) patients remained alive. Seventeen out of the 33 (52 %) patients in the chemotherapy-alone group and 25 out of 38 (66%) in the combination group had died (Table 5.4).

The median overall survival for the chemotherapy-alone (OxMdG) group was 37.3 months (95% CI = 28.9 - not estimated) and in the chemotherapy with SIRT (OxMdG + SIRT) group was 33.2 months (95% CI = 28.4 - 41.5). A log-rank test offered no support to a difference between the OxMdG and OxMdG + SIRT survival functions (chi-squared=1.71; p=0.191). Cox models were used to compare the rate of death between treatment groups. There was no statistically significant difference in overall survival between the two groups (HR = 1.55; 95 % CI = 0.83 – 2.89). The Kaplan-Meier curve of time from randomisation to death for each treatment group during the FOXFIRE study duration is shown in Figure 5.2.

Table 5.4. The number (N) and percentage (%) of deaths per treatment group after a median follow up of 42.7 months (n=71). Of the 42 patients who had died at time of the analysis, 25 were in the combination group (OxMdG and SIRT) and 17 in chemotherapy-alone (OxMdG). N is the frequency with (%).

	Treatment arm		
	OxMdG N (%)	OxMdG+SIRT N (%)	Total N (%)
Alive	16 (48.5)	13 (34.2)	29 (40.9)
Dead	17 (51.5)	25 (65.8)	42 (59.1)
Total	33 (100)	38 (100)	71 (100)

Figure 5.2. Kaplan-Meier curve of time from randomisation to death for each treatment group during the FOXFIRE study duration. There was no difference in overall survival between the two groups from time of randomisation to death.

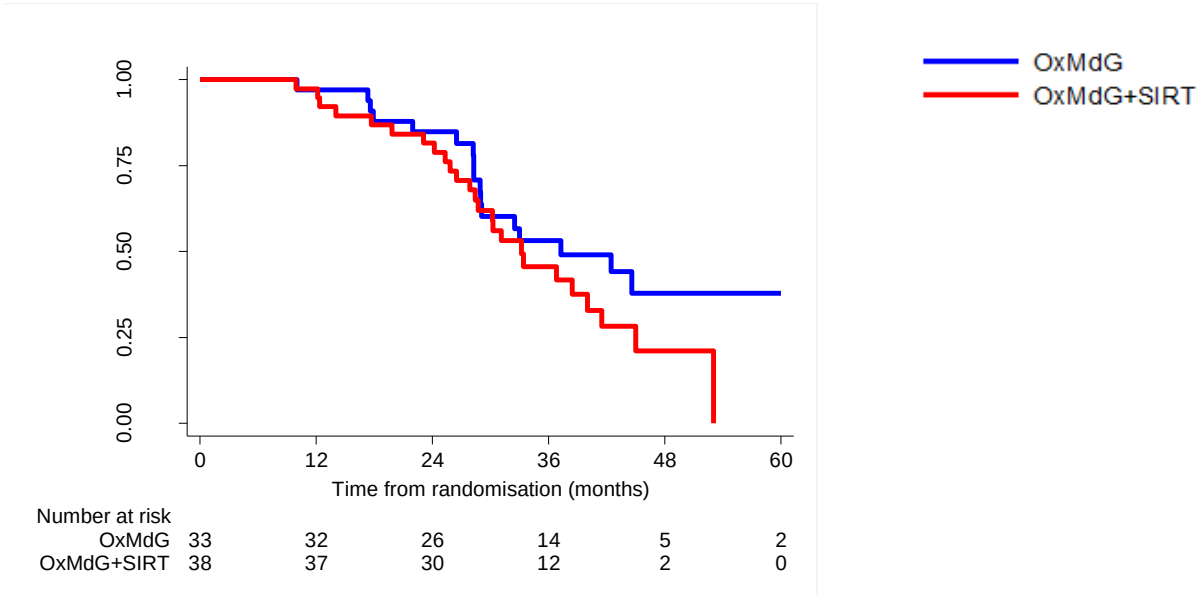

Time from randomisation to resection

The median time to resection in the chemotherapy-alone group was 7.8 months (95% CI = 6.5 - 8.5) and in the chemotherapy with SIRT group was 8.3 months (95% CI = 7.4 - 9.9). A log-rank test demonstrated there was no statistical difference in the time to resection for each treatment group (chi-squared=0.06; p=0.810). A Kaplan-Meier curve of time from randomisation to hepatic resection is shown in Figure 5.3.

Cox models were used to compare the rate of hepatic resection between the treatment groups. There was no statistically significant difference. (HR=0.94; 95% CI=0.58-1.52).

Figure 5.3. Kaplan-Meier curve of time from randomisation to hepatic resection for each treatment group during the FOXFIRE study duration.

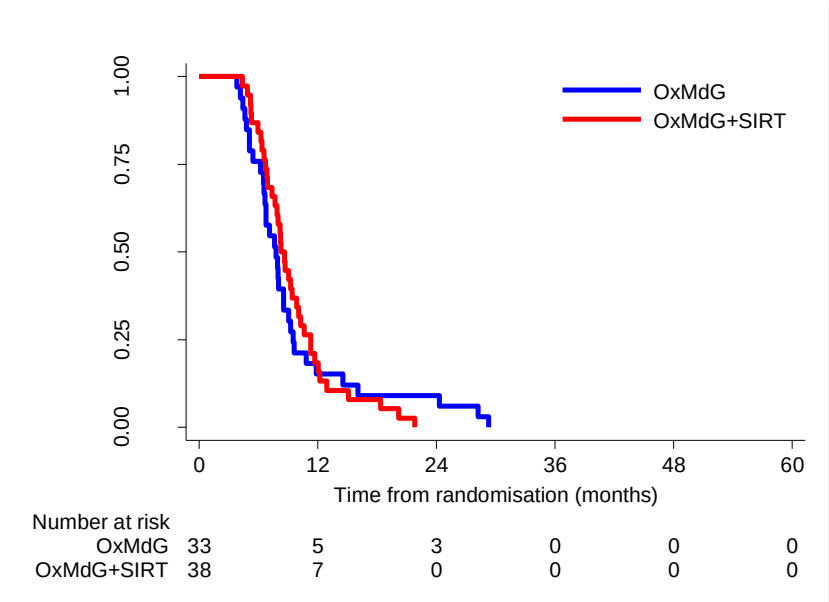

The median time from resection to death in the chemotherapy-alone group (OxMdG) was 25.2 months (95% CI = 21.0 - Not estimated) compared to 21.9 months (95% CI = 19.0 - 35.7) in the combination group (OxMdG + SIRT). A log-rank test demonstrated no groups of time from resection to death (chi-squared=1.94; p=0.164). Note: for patients who underwent multiple hepatic resections, the first occurrence was used in the time-to-event analyses.

Histopathology findings

Forty-five from a total of seventy-one resection samples were both located and available. Reasons for the unavailability of twenty-six samples included being their return to a primary treating site for further molecular testing and no optional informed consent for analysis.

Microspheres were found in the resection specimens from all patients who had received SIRT. The microspheres were typically clustered around small vessels within tumour vasculature, associated with macrophages. The analysis was from the twenty-seven patients who had provided optional informed consent for tissue analysis. This was sixteen from Arm A and eleven from B. The histological analysis looked at treatment effects within the tumour and background liver. The percentage of viable tumour in the patients treated with SIRT (Arm B) and chemotherapy (Arm A) both ranged from 0 – 80%. However, the Arm B patients had less viable tumour in the analysis with more fibrosis and inflammatory changes seen.

Sirius red staining highlighted extensive hepatic fibrosis (Figure 5.4). Sample tissue from both arms of the trial demonstrated mild vascular changes in the adjacent background liver. However, in two patients who received SIRT severe vascular changes in the adjacent tissue were seen. Both arms had cases of fatty infiltration and there did not appear to be a significant difference in this respect between groups.

Figure 5.4. Histological images of tumour and adjacent liver parenchyma from patients post hepatic resection after receiving chemotherapy and SIRT. 5.4A: Complete tumour necrosis. Necrotic tissue seen in central tumour (Haematoxylin and Eosin stain). 5.4B: Extensive tumour fibrosis within tumour; collagen stained red (Sirius Red stain).

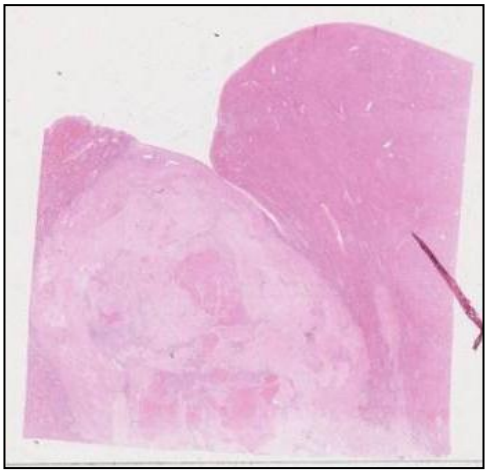

(A)

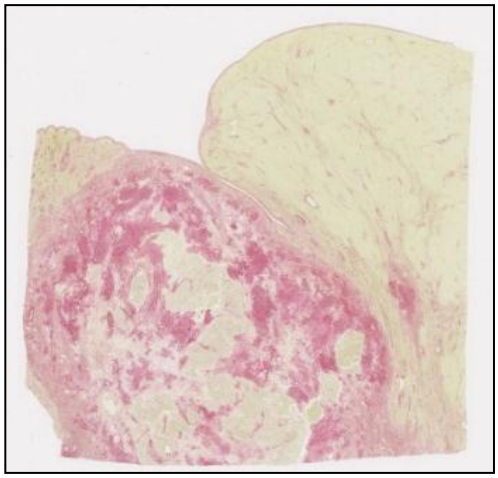

(B)

Distribution of microspheres within tumour and adjacent tissue

The distribution of microspheres was measured in microspheres (mm^2). Zones from the tumour margin were demarcated at distances of 0-1 mm and 1-2 mm. These zones may be described as intra-tumoural and extra-tumoural respectively. Zones at this distance were characterised by the presence of microspheres outside the tumour margin or within the tumour margin as illustrated in Supplementary Figure 1.

The highest density of microspheres was found within the 0-1 mm zone followed by the 1-2 mm zone still within the tumour margin, the next highest density was seen at 0-1 mm outside the tumour margin. Mean tumour density did not vary between the zones at 1-2 mm zone outside of the tumour margin and that seen in the tumour centre. Low microsphere density was also seen in the adjacent background liver of resection specimens (Supplementary Figure 1).

Distribution of microspheres in relation to blood vessels

Microspheres have a relatively small diameter of 30 μm in comparison to the diameter of medium (30-100 μm) and large blood vessels (> 100 μm). This would suggest that microspheres would not lodge in the larger blood vessels a priori. This premise of the distribution was confirmed through α-smooth muscle actin (α-sma) staining. Only two cases out of 11 (18%) evidenced microspheres in the larger vessels and only one case showed microspheres present in a vessel with a diameter > 100 μm. The results from the distribution of microspheres in relation to blood vessels are shown in Figure 5.5.

Evidence of the presence of microspheres within small vessels is presented in Figure 5.5 C & D. Most patients showed no microspheres trapped within the endothelium. This raises the likelihood of endothelium destruction. CD31 staining of endothelial cells revealed that some microspheres are not trapped within these smaller vessels. A clustering of microspheres outside the endothelium suggests possible destruction of these cells leading to extravasation of the microspheres at the tumour vasculature (Figure 5.5 E).

A likely interpretation of the low concentration of microspheres within smaller blood vessels is that spheres are initially trapped, leading to a loss of integrity of the cell membrane and destruction of the cell. Microspheres then extravasate and cluster externally to the damaged vessel.

Figure 5.5. Histological images of microspheres within hepatic resection specimens from patients receiving chemotherapy plus SIRT. 5.5A and B Microspheres present in arterioles. These are identified by the smooth muscle in their walls using immunohistochemical staining for α-smooth muscle actin staining are displayed. Medium sized vessels have a diameter of 30-100 μm and large-sized arteries which have a diameter of >100 μm. The microspheres, diameter ≅ 30 μm have passed through the larger vessels. The dark circular spots indicated by the arrow represent microspheres present in a medium sized vessel. The microsphere trapped within a tumour blood vessel is indicated with the arrow in Figure 5B. 5.5 C & D. Distribution of microspheres within small vessels using immunohistochemical staining CD31, an endothelial marker. 5.5E. Clustering of microspheres outside of the endothelium suggest extravasation through a destroyed endothelium.

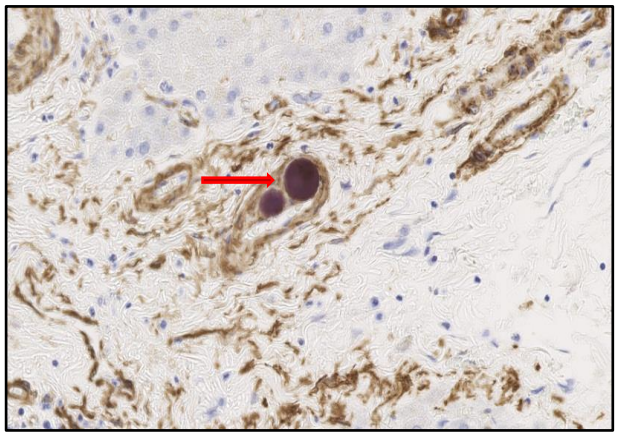

(A)

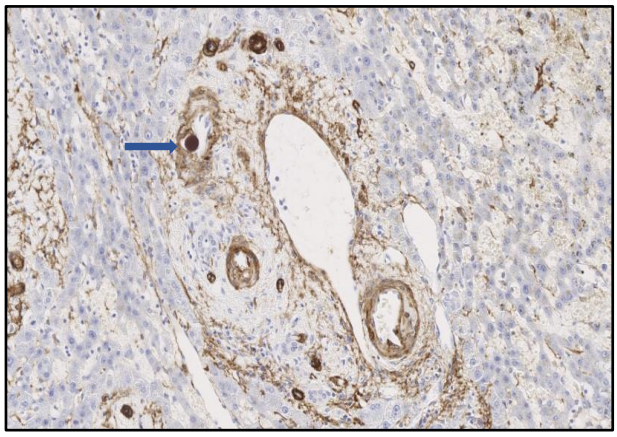

(B)

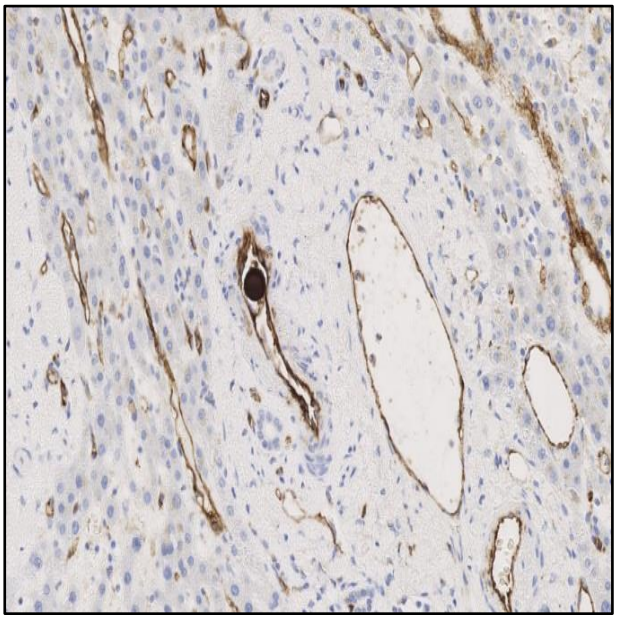

(C)

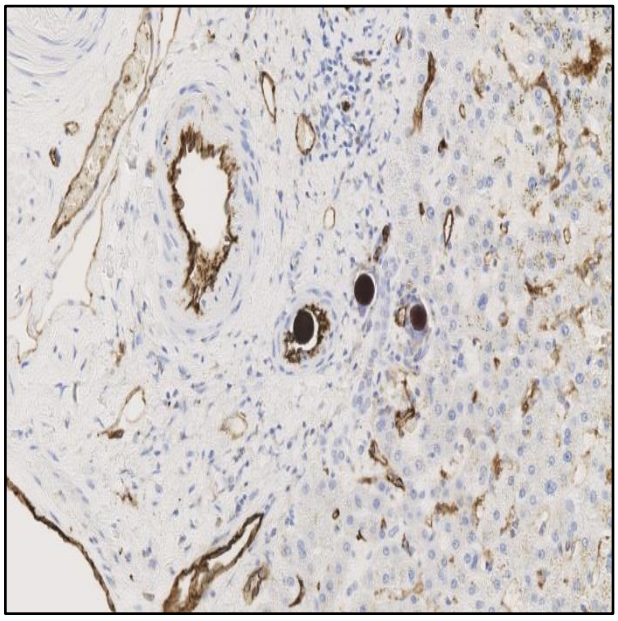

(D)

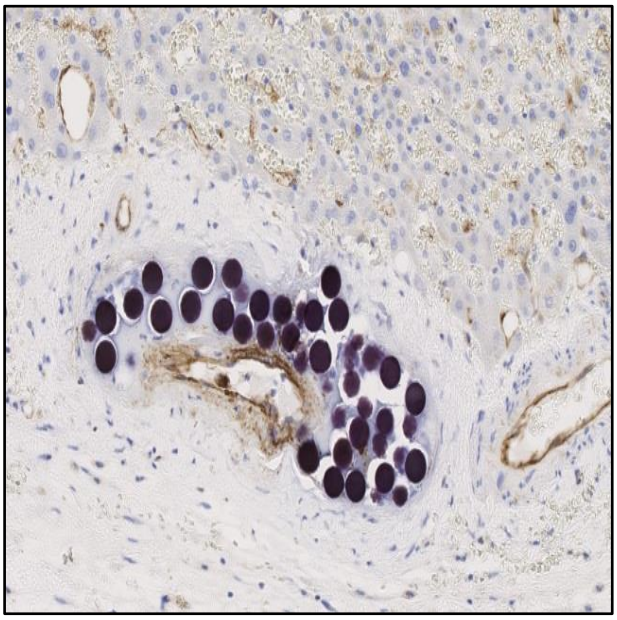

(E)

Figure 5.5E shows a section stained for the macrophage marker, CD68. This highlights the macrophage reaction to the microspheres. Macrophage clustering and localised macrophage reaction was associated with microspheres. CD68 staining also detected the foreign body giant cell, composed of macrophages and representative of a typical cellular response to a foreign implant. The activated macrophages had become fused to form a giant cell. Eight out of eleven cases showed localised macrophage reaction. However, up to 65 % of the microspheres are found clustered within the macrophagic reaction or within macrophages, and within the tumour (Figure 5.6).

Figure 5.6A depicts Haematoxylin and Eosin staining of microspheres and clearly evidences the trapping of microspheres and a high degree of macrophage clustering. Figures 5.6 B&C show CD68 staining and the foreign body giant cell reaction from macrophages. Although frequently seen as a reaction to implantation of foreign material the tumour-associated macrophage may have a more important role in tumour growth regulation. Up to 65% of the microspheres were found within macrophages.

Figure 5.6. Macrophage clustering around microspheres. 5.6A: Haemotoxylin and Eosin staining of hepatic resection after SIRT. There is a trapping of microspheres and a high degree of macrophage clustering. 5.6B&C: Section stained for the macrophage marker, CD68, to highlight the macrophage reaction to the microspheres and the foreign body giant cell reaction from macrophages.

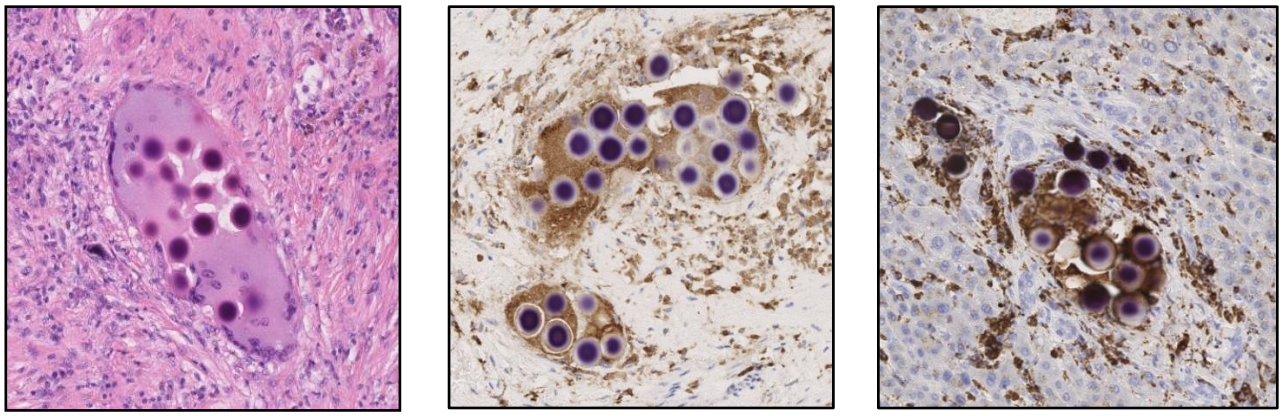

(A) (B) (C)

5.4 Discussion

This is the first detailed report of a large series of patients who have undergone hepatic resection after receiving chemotherapy and SIRT in a prospective randomised clinical trial. The results from the 71 patients with the hepatic resections were after a long follow-up period, median 42.7 months. The results demonstrated that 71 out of 364 (19.5 %) of the randomised patients were referred for hepatic resection. Of these patients there was no statistical difference between those referred in the chemotherapy-alone group versus the combination group.

The majority of patients receiving hepatic resection had 25 % or less of liver involvement with tumour. Of the 15 (21%) patients with more than 25 % of liver involvement; 4 required a two-stage resection.

Although FOXFIRE was a multi-centre study, with surgery carried out across 14 sites, three hepatic units performed the majority of all the surgeries: Oxford (17 patients), Imperial (16 patients) and Nottingham (11 patients). This may highlight the limited expertise and decision-making of multi-disciplinary teams outside of these centres. The commonest resections were right hepatectomy, segmentectomies and left hepatectomy.

These results focus on the participants in the FOXFIRE study who received hepatic resection. The aims of this series of surgical cases were to describe the hepatic resection rate, detail the surgery and complication rates following chemotherapy or the combination of SIRT and chemotherapy. These results from the surgical outcomes of patients receiving hepatic resection from both arms of the FOXFIRE trial have demonstrated the rate of surgical complications and safety following the addition of SIRT is comparable to chemotherapy alone. These results are consistent with the SIRFLOX study. In SIRFLOX, a trial with the same design, also reported no significant difference in conversion rates to surgery in the patients receiving chemotherapy alone and those randomised to receive chemotherapy plus SIRT: 13.7 % (36 patients) compared with 14.2 % (38 patients) (p= 0.857) (van Hazel et al., 2016). The numbers of resected patients are comparable, however, there was no detailed information on the surgery, complications or histopathological analysis after surgery in the SIRFLOX study.

In the FOXFIRE study, there was a low incidence of grade III or IV complications after surgery. There was only one incidence of post-hepatectomy liver failure. This confirms the findings of a retrospective series by other investigators suggesting that surgery is safe after chemotherapy plus SIRT for CRCLM (Pardo et al., 2017). The P4S study retrospectively analysed the safety of hepatic resection or liver transplantation in 100 patients with various primary or secondary liver cancers following treatment with SIRT. It concluded that the mortality, complication and liver failure rates were similar in these patients to rates expected in patients who had not received SIRT prior to resection or transplantation. Consideration of these studies provide supportive data for hepatic multi-disciplinary teams when they are considering SIRT to downstage tumours prior to resection.

The distribution of microspheres within hepatic metastases, the proximity to tumour vasculature and the association of macrophages is demonstrated. The finding that most microsphere are distributed within medium – small vessels.

Changes in liver parenchyma after chemotherapy have been well described and include steatohepatitis and sinusoidal obstruction syndrome (Aloia et al., 2006; Khan, Morris-Stiff, & Makuuchi, 2009; Maor & Malnick, 2013; Ryan et al., 2010). In a neoadjuvant study of oxaliplatin-based-chemotherapy in patients with CRCLM, 44 out of 87 patients (51%) had sinusoidal dilatation and haemorrhage, with disruption of the sinusoidal barrier compared to none without prior chemotherapy (Rubbia-Brandt et al., 2004). Nearly half of these patients developed perisinusoidal and veno-occlusive fibrosis. Vascular complications from chemotherapy alone have been described previously: sinusoidal vasodilatation, congestion, haemorrhagic centrilobular necrosis and regenerative nodular hyperplasia (Aloia et al., 2006).

There are limited published data on histopathological changes in specimens from hepatic resections post-SIRT. Histology from a small number of studies have described features following SIRT including microsphere distribution, tumour response and changes to background liver. In one paper, significant histological features were described (Wang et al., 2013). Macrophages associated with a giant cell reaction and radiation changes were described, and the absence of a cellular inflammatory response supported the theory that SIRT caused direct radiation injury to cancer cells (Wang et al., 2013). Our study reported here demonstrates clusters of microspheres associated with aggregations of macrophages. This may have some relevance to the mechanism by which the microspheres act on tumour tissue. Chew describes the significant effect that microspheres have on the immune cells and the tumour microenvironment in hepatocellular carcinoma (Chew et al., 2018). Further work is required to decipher the effect that SIRT has on the immune cells in the tumour microenvironment in patients with colorectal liver metastases.

Following resection, it is known that the microspheres are localised within tumour vasculature and that the non-tumour bearing liver can show evidence of portal triaditis with portal and periportal fibrosis. The largest published cohort to date confirmed resin microspheres within the vascular bed of the tumour and portal fibrosis on the adjacent normal liver (Justinger et al., 2015). Although previous case reports have described microspheres in the gall bladder, we report microspheres present in the gall bladder in seven patients following SIRT. Fortunately, these patients did not report any significant clinical symptoms from the presence of microspheres in the gall bladder, but our findings suggest that persistent upper abdominal pain in patients who have received SIRT should be considered as possibly related to radiation cholecystitis until an alternative clinical cause for the pain is found.

Due to the ethical requirement for separate voluntary consent to analyse histopathology specimens from surgical resection, there were limited numbers of patients for detailed histological analysis. Despite this limitation, we performed an exploratory comparison of histopathological changes in cases treated with chemotherapy alone, versus those treated with chemotherapy plus SIRT. Interestingly, the SIRT cases had

a lower percentage of viable tumour than those treated with chemotherapy alone (p=0.034) and tumour necrosis occurred at a higher rate in cases treated with chemotherapy alone (p=0.054). Additionally, the novel methodology we developed for zonal analysis of metastases demonstrated that the cases, which displayed the highest percentage of viable tumour within the SIRT group, had the lowest microsphere densities within the cohort (Supplementary Figure 1 and Supplementary Table 3). This is preliminary evidence in favour of the hypothesis that microsphere density is inversely related to the percentage of viable tumour post-treatment. The high microsphere density we observed at the tumour periphery is consistent with dosimetric studies published over a decade ago (A. S. Kennedy, Nutting, Coldwell, Gaiser, & Drachenberg, 2004).

The results demonstrate an acceptable safety profile and the feasibility of patients proceeding to surgery after a combination of chemotherapy with SIRT. There was no statistically significant difference in the timing of the resection in the two treatment groups. Specifically there was no significant delay in receiving resection in patients who received the combination regimen.

The association of macrophages and giant cell reactions is of interest and provides further evidence for investigation of the tumour microenvironment as a potential drug target in combination with localised radiotherapy techniques and or immune modulation.

Chapter 6 Results from circulating biomarkers

6.1 ctDNA in patients receiving SIRT with CRC - Aims

The exploratory ctDNA study investigated the inclusion of circulating biomarkers within the PERFORM imaging biomarker study. Methods were developed to quantify and sequence ctDNA at serial time-points in patients with refractory CRCLM and ICC receiving SIRT. This study was developed to address the following aims:

- To examine the feasibility of detecting somatic mutations from ctDNA in patients with refractory hepatic malignancy receiving SIRT and participating in an imaging study.
- To explore the additional information ctDNA may provide to complement imaging.
- To investigate the clinical utility of ctDNA in patients with refractory hepatic- dominant malignancy and a high burden of liver malignant disease
- To determine the ability to detect and quantify ctDNA in these patients at three time-points: baseline, one month, ten weeks and compare to imaging response.
- To determine the concordance of *KRAS* status detected in ctDNA when compared to historical *KRAS* status from formalin paraffin embedded (FFPE) in the same patients.
- To investigate the ability of ctDNA to detect mutations in patients with ICC and correlate circulating metabolites with *IDH I* mutation status in patients with ICC.

6.2 Methods and Patients

All patients approached provided written informed consent to participate in the optional circulating biomarker study. All patients had liver predominant malignancy. Berkshire Research Ethics Committee trial number: 10 H0505 95. Twenty-nine patients gave written informed consent. One patient withdrew as deteriorated before able to provide blood test after consent. Table 6.1 summarises the clinical characteristics of 28 patients recruited to PERFORM who provided blood for analysis for ctDNA.

Sample processing and extraction of ctDNA and germline (g) DNA

To minimise lymphocyte lysis, blood samples were centrifuged at 2060 x g (3000 rpm in Beckman GS-6R centrifuge) for 10 minutes at room temperature without brake within 6 hours of collection (Page et al., 2013). Plasma was transferred to a new tube, mixed, and aliquots were pipetted into microfuge tubes. After 10 min in the centrifuge at 7000 rpm, the supernatants were transferred to new microfuge tubes and stored at -80 °C until DNA extraction. ctDNA was isolated using Qiagen QIAamp Circulating Nucleic Acid kit according to the manufacturer's protocol (QIAGEN Ltd., Manchester, UK). Matching gDNA was extracted from whole blood using Qiagen QIAamp DSP DNA Blood mini kit. DNA quantity was determined using Qubit dsDNA High Sensitivity assay kit on a Qubit 2.0 Fluorometer (ThermoFisher, Paisley, UK).

Targeted Sequencing Using 50 Cancer gene panel

An Ion AmpliSeq™ Cancer Hotspot Panel v2 (50 cancer gene panel) was used to detect potentially actionable somatic mutations, using a collection of primers designed to interrogate hotspot regions in 50 genes (207 amplicons) commonly mutated in cancer (ThermoFisher Scientific, Waltham, MA USA). Libraries were generated according to the manufacturer's protocol. Briefly, multiplex PCR was performed with the Ion Ampliseq library kit 2.0 using approximately 10 ng DNA and the panel primer pool. Following PCR, the amplicons were partially digested and IonXpress-barcoded adapters were attached by ligation. The libraries were purified using Agencourt AMPure XP magnetic beads (Beckman Coulter Ltd, High Wycombe, UK) and amplified using adapter primers. The amplified libraries were purified again, and quantified on an Agilent 2100 Bioanalyzer using the High Sensitivity DNA kit (Agilent Technologies, Stockport, UK). Library templates for sequencing were prepared by emulsion PCR on the One Touch 2 instrument and loaded onto 318 semiconductor chips and the Ion Torrent PGM™ sequencer (Merriman & Rothberg, 2012). Sequence analysis was performed using Torrent Variant Caller (TVC) v4.4.5 and Ion Reporter v5.0.

Table 6.1. Summary of clinical characteristics of 28 patients recruited to PERFORM ctDNA study.

	Parameter value
Age, years	
Mean (range)	58.8 (32-83)
Gender n (%)	
Female	11 (36.4)
Male	17 (63.6)
Tumour type n (%)	
Colorectal	22 (79)
ICC	4 (14)
Small bowel	1 (3.5)
Uveal melanoma	1 (3.5)
Lines of previous systemic therapy for advanced disease n (%)	
0	0
1	4 (14)
2+	24 (86)
Patients receiving SIRT n (%)	24 (86)
Patients not proceeding with treatment	4 (14)

Concurrent chemotherapy with SIRT n (%)	12 (50)

Figure 6.1. Enrolment of participants in the ctDNA exploratory circulating component of PERFORM. Of the 29 enrolled patients 4 were unable to proceed to SIRT (due to deterioration in performance status, liver function, rapidly progressive disease and one patient was unable to tolerate procedure). The patient with rapidly progressive disease withdrew. Only patients with CRC had KRAS mutation testing on FFPE. N number; PFS progression-free survival; OS overall survival; DNA did not attend.

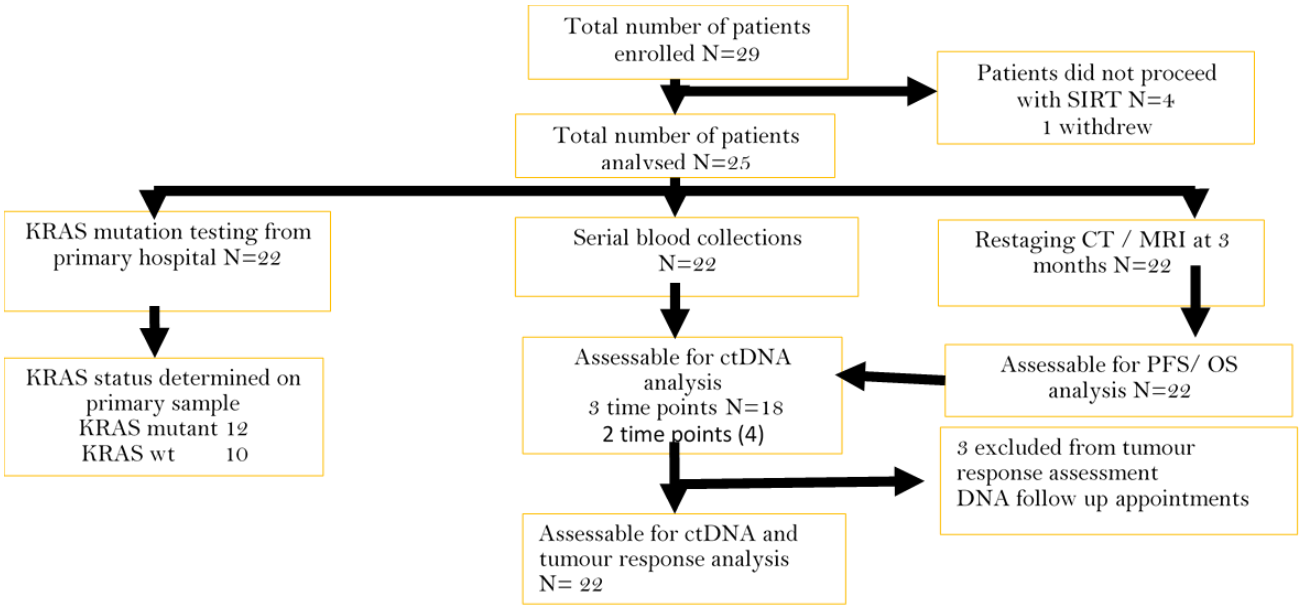

6.3 The feasibility of the sampling of ctDNA in patients receiving SIRT

Of the 29 patients who gave informed consent four patients were unable to proceed with SIRT. One patient had rapidly deteriorating performance status, another patient had abnormal liver function tests that were a contraindication to receiving SIRT, one patient was unable to tolerate the SIRT procedure and a patient with rapidly progressive disease withdrew. The feasibility of the prospective collection of ctDNA in patient receiving SIRT with advanced malignancies was demonstrated with no patients declining to participate in the optional circulating biomarker study and sampling times performed within the recommended windows. All patients that were participating in the amended PERFORM imaging study gave written informed consent to participate in the optional circulating biomarker study. These additional 30 mL blood samples were taken when patients attended for clinical or trial procedures at baseline and at four and 10 weeks.

The mean time from the blood sample being taken to the time it arrived in the lab was 2 hours and 12 minutes. The mean time for preparing the plasma and subsequent DNA extraction was 47 minutes. All samples were immediately transferred to a -80 °C freezer. The average time for buffy coat extraction (for germline analysis) to commence was within 50 minutes. This was well within the recommended limit of 48 hours for buffy coat preparation after refrigeration following collection.

The quantification of ctDNA (in ng/mL of plasma) for each patient at each time point is shown in Table 6.2. Three of the patients (1501, 1507 and 1510) who did not receive SIRT all died in less than 150 days.

Table 6.2. The quantification of ctDNA (ng/mL plasma) for each time-point (baseline, 4 weeks and 10 weeks after SIRT) collected and patient radiological response in the liver as defined by RECIST 1.0.

Patient id	Overall survival (days)	ctDNA baseline (ng/mL)	ctDNA 4 weeks (ng/mL)	ctDNA 10weeks (ng/mL)	Patient outcome (liver) PD = progressive disease; SD = Stable disease; PR = partial response
1501	147	178.5	none	none	no scan
1502	642	312.0	138.4	100.0	PR
1503	387	17.6	26.8	39.3	PR
1504	630	94.5	43.8	185.3	PR
1505	614	19.4	33.4	17.5	PD
1506	600	49.4	85.8	none	PD
1507	45	898.7	none	none	no scan
1508	617	29.8	none	none	no scan
1509	607	109.3	160.4	none	PD
1510	57	none	none	none	Withdrew - no scan
1511	558	97.0	38.4	50.0	PR
1512	568	48.1	27.1	none	PD
1513	467	none	none	none	no scan
1514	286	159.6	176.8	282.3	PD
1515	99	377.2	89.1	122.5	PD
1516	537	9.2	35.6	15.1	SD
1517	295	61.9	none	43.5	PD
1518	544	149.9	none	50.6	PR
1519	533	26.8	102.9	118.0	PD
1520	523	282.1	81.0	98.0	PR
1521	518	498.2	33.1	105.2	PR
1522	488	42.5	50.8	23.9	SD
1523	481	61.7	74.6	60.6	PR
1524	481	53.5	116.3	35.0	SD
1525	483	41.0	90.7	38.3	PR
1526	41	76.1	112.2	none	PD
1527	399	16.0	21.6	26.5	PR
1528	505	58.0	51.6	33.1	SD
1529	77	675.5	none	none	SD

There was no statistical significant correlation between baseline ctDNA quantification and survival in days from baseline. There was no statistical significant difference in patients who had a decrease in ctDNA and patients who had an increase in quantity from baseline to 10 weeks and overall survival. One patient who had the highest baseline of ctDNA 898.7 ng/mL only survived 45 days. One patient who was reported to have stable disease died within 77 days and had a very high baseline ctDNA of 675.5 ng/mL.

Sixteen patients (16/28, 58%) were able to give all three samples.

6.4 The detection of specific mutations in ctDNA in patients with mCRC

The ability to detect somatic mutations in these patients with a high burden of hepatic disease was demonstrated. Concordance of *KRAS* mutational status in ctDNA and tissues was supported by the standard testing in historical tissue FFPE samples of the patients with CRC (see section 6.5).

The panel also detected other somatic mutations on the ctDNA (Table 6.3). In 12 out of 22 (55%) CRC patients multiple mutations were detected. In patient 1501 the mutations *KRAS G12D*, *APC* and *TP53* were detected. In another patient (1505) low levels of *BRAFv600*, *AKT1* and *GNAS* were seen. In patient 1529 high levels of *KRAS*, *APC* and *TP53* were found. This patent had been KRAS wt on FFPE when tested 596 days earlier. This patient only survived 77 days from baseline testing of ctDNA.

Table 6.3. The number (percentage) of patients with a specific somatic mutation detected in ctDNA from patients with CRC.

Mutation	Number out of 22 total patients with CRC with ctDNA (%)	Population based prevalence from literature
KRASG12/13	14 (64%)	25%
KRAS Q61	1 (5%)	
NRAS Q61	1 (5%)	
APC	6 (27%)	
TP53	13 (60%)	50%
PIK3CA	3 (14%)	15-30% 7-30%
BRAF V600	1*	10% poor prognosis 2.3%
AKT1	**1***	
GNAS	**1***	

*denotes all mutations found in same patient

The patient with the *NRAS q61* mutation had a rectal tumour, which had been diagnosed only 279 days earlier. From the literature *NRAS* are found in approximately three percent of patients with CRC and associated with left-sided tumours and a poorer prognosis as in this case (Cercek et al., 2017).

The one patient with a *BRAF v600* mutation had *AKT1* and a *GNAS* but no *KRAS*. This fits with the literature that *BRAF* and *KRAS* are mutually exclusive. The three patients with a *PIK3CA* all had an associated *KRAS* mutation. This supports the literature that shows the association of *PIK3CA* with *KRAS* and the loss of

MGMT (o6-methylguanine-DNA methyltransferase) expression. These findings support the known PIK/AKT/mTOR signalling axis and its significant role in the development and progression of CRC.

There was a high prevalence of *TP53* mutations detected which were found predominantly in tumours of the rectum and left-side of the colon as described in the literature (Loree et al., 2018). Of the thirteen patients with *TP53* mutations detected in ctDNA, five had rectal primaries; three had sigmoid tumours, one had a splenic flexure cancer, two had a transverse colon cancers, one patient had a caecal tumour and one patient had a small bowel tumour.

6.5 Concordance of *KRAS* mutations from ctDNA with historical archived histology samples FFPE *KRAS* from pyrosequencing

Fourteen of the 22 patients with CRC had *KRAS* mutations detected in ctDNA. Eleven out of these 14 (79%) had the matching *KRAS* mutation on historical FFPE testing. The three remaining patients who had a *KRAS* mutation detected on ctDNA were *KRAS* wt on historical FFPE samples. Of the 12 patients who had *KRAS* mutations on FFPE, all patients had the same mutation detected in ctDNA except one patient who was *KRAS wt* on ctDNA. Overall *KRAS* status was concordant in 18 out of 22 (82%) patients and discordance in 4 out of 22 (18%). Any patients who may have switched *KRAS* status between the timing of the FFPE and ctDNA sampling may have received incorrect management if based only on the FFPE result.

This high rate of concordance supports findings from other studies. However, most of these previous studies have shown concordance when the sampling times were done very close together –i.e. the timing of the ctDNA was taken at the same time point as the mutation testing in the primary tissue. With the patients in PERFORM, who were receiving treatment in the refractory setting the ctDNA sampling was taken at a mean of 670 days after the original FFPE testing on the tissue samples (range 58-1547 days). The patient who had ctDNA taken at 1547 days after *KRAS* wt was found on FFPE, had a *KRAS G12V* mutation detected in ctDNA. However two patients had the same *KRAS G12D* mutation detected in ctDNA at 1127 and 385 days after the same mutation was detected on their primary tissues. Another patient had the same *KRAS G13D* mutation detected in ctDNA 610 days after it was first detected in the tissue sample (Table 6.4). Overall there was a high concordance of *KRAS* status demonstrated with identical *KRAS* mutations detected in sampling from ctDNA and the FFPE samples. Five different *KRAS* mutations were detected across the group in ctDNA (*G12D* (4 patients); *G12V* (4 patients); *G13D* (4 patients); *G12A* (one patient); *G12C* (one patient). Of these 14 patients who were *KRAS* mutant on ctDNA, 10 patients had other mutations detected; 4 patients had *KRAS* mutations alone. Of the eight remaining ctDNA *KRAS* wt patients, one patient had no other mutations detected, the other seven patients had at least one mutation detected.

The changes in the variant allele frequency (VAF) with treatment are demonstrated in Table 6.5. VAF changes are detectable after SIRT treatment. The serial ctDNA samples were analysed for VAF (%) at baseline, four weeks and 10 weeks.

Table 6.4 Detection of specific *KRAS* mutations from ctDNA in patients on PERFORM study compared to the historical NHS pyrosequencing from fixed formalin paraffin embedded (FFPE) tumour tissue. Other mutations detected in ctDNA from both *KRAS* wt and *KRAS* mutant patients. 18/22 (82%) *KRAS* status concordance.

Patient ID	FFPE	ctDNA	FFPE & ctDNA concordant (Y or N)	Time from FFPE & ctDNA (days)	KRAS G12/G13	KRAS Q61	NRAS Q61	APC	TP53	PIK3CA	BRAF V600	AKT1	GNAS
1501	KRAS G12D	KRAS G12D plus APC & TP53	Y	385	31.5%			41.5%	38.7%				
1502	KRAS G12V	KRAS wt in ctDNA plus APC	N	814	wt			12.3%					
1503	KRAS G12C	KRAS G12C	Y		22.3%								
1504	KRAS wt	KRAS wt plus TP53	Y	734	wt				35.3%				
1505	KRAS wt	KRAS wt plus BRAF AKT1 & GNAS	Y	824	wt						4.8%	8.8%	12.3%
1507	KRAS G12V	KRAS G12V plus TP53 & PIK3CA	Y	504	22.3%				47.0%	36.9%			
1509	KRAS G12V	KRAS G12V plus TP53	Y	875	6.3%				4.7%				
1510	KRAS G12D	KRAS G12D	Y	1127	done at JR								
1511	KRAS G12V	KRAS G12V	Y	315	35.7%								
1512	KRAS G13D	KRAS G13D plus PIK3CA & TP53	Y	785	4.9%				4.9%	4.1%			
1514	KRAS G13D	KRAS G13D plus APC & TP53	Y	610	14.4%			14.6%	32.1%				
1517	KRAS G12D	KRAS G12D plus PIK3CA	Y	58 (liver)	37.4%					30.4%			
1518	KRAS G13D	KRAS G13D plus TP53	Y	635	63.7%				69.9%				
1519	KRAS wt	KRAS wt plus NRAS & TP53	Y	916			22.0%		29.8%				
1520	KRAS, NRAS wt	KRAS wt NRAS wt plus TP53	Y		wt		wt		45.5%				
1521	KRAS wt	KRAS G12A** plus KRAS Q61 & TP53	N	508	1.2%	9.3%			65.7%				
1523	KRAS, BRAF, PIK3CA wt	KRAS, BRAF, PIK3CA wt plus TP53	Y		wt				48.9%	wt	wt		
1524	KRAS, NRAS wt	KRAS & NRAS wt	Y	324									
1525	KRAS G12D	KRAS G12D plus APC & TP53	Y		23.7%			8.4%	13.5%				
1527	KRAS wt	KRAS wt, plus APC	Y	490	wt			0.9%					
1528	KRAS wt	KRAS G12V	N	1547	15.80%								
1529	KRAS, NRAS wt	KRAS G13D plus APC & TP53	N	596	48.9%			61.0%	49.9%				

Table 6.5 Changes of percentage of variant allele frequency of specific somatic mutations detected in ctDNA over time with SIRT treatment. The serial ctDNA samples were analysed for variant allele frequency (%) at baseline, 4 weeks and 10 weeks.

Patient	Survival	Timepoint	KRAS G12/G13	KRAS Q61	NRAS Q61	APC	TP53	PIK3CA	KDR	BRAF V600	AKT1	GNAS
id1503	387d	Baseline	22.3%									
		4w post-SIRT	1.5%									
		10w post-SIRT	0.0%									
id1521	371d	Baseline	1.2%	9.3%	0.0%							
		4w post-SIRT	0.0%	2.6%	0.0%							
		10w post-SIRT	2.5%	6.3%	2.2%							
id1511	239d	Baseline	35.7%									
		4w post-SIRT	0.0%									
		10w post-SIRT	14.5%									
id1512	385d	Baseline	4.9%				4.9%	4.1%				
		4w post-SIRT	7.6%				14.3%	12.0%				
		10w post-SIRT	Not done				Not done	Not done				
id1518	259d	Baseline	63.7%				69.9%					
		4w post-SIRT	2.0%				4.5%					
		10w post-SIRT	Not done				Not done					
id1525	306d	Baseline	23.7%			8.4%	13.5%					
		4w post-SIRT	0.0%			1.0%	0.0%					
		10w post-SIRT	3.7%			1.5%	3.5%					
id1523	464d	Baseline		0.0%			48.9%					
		4w post-SIRT		0.0%			1.8%					
		10w post-SIRT		0.7%			42.4%					
id1520	108d	Baseline					45.5%					
		4w post-SIRT					21.2%					
		10w post-SIRT					41.9%					
id1502	438d	Baseline				12.3%			1.2%			
		4w post-SIRT				0.0%			4.9%			
		10w post-SIRT				0.0%			6.4%			
id1523	464d	Baseline		0.0%			48.9%					
		4w post-SIRT		0.0%			1.8%					
		10w post-SIRT		0.7%			42.4%					
id1509	642d	Baseline	6.3%				4.7%					
	(alive)	4w post-SIRT	0.0%				0.0%					
		10w post-SIRT	Not done				Not done					
id1505	614d	Baseline								4.8%	8.8%	12.3%
		4w post-SIRT								0.0%	0.0%	0.0%
		10w post-SIRT								0.0%	0.0%	0.8%

6.6 ctDNA in ICC

Molecular profiling of ICC from ctDNA was performed on four patients who were due to receive SIRT under CTE. The mutations detected from the 4 patients with ICC are presented. WGS was also carried out and is presented in the Supplementary figure.

CtDNA was extracted from four patients with ICC at baseline, 4 weeks and 10 weeks after SIRT. Targeted sequencing using the 50 cancer gene hotspot panel as described above, identified two somatic mutations. Three of the four patients were found to have the same mutation in *NRAS Q61R* and one patient also had an *IDH1 R132C* mutation (Table 6.6).

Table 6.6. Hotspot mutations detected in ctDNA from 4 patients with ICC,
SNV single nucleotide variants, VAF variant allele frequency.

Patient	Baseline quantity ctDNA (ng/µl)	Mutation (single nucleotide variants (SNV))	VAF (%) Baseline	VAF (%) 4 weeks post-SIRT	VAF (%) 10 weeks post-SIRT
1	1.71	*NRAS*, NM_002524.5: c.182A > G; p.Q61R	0.6 (T = 5168, C = 31)	na	nd
2	18	*NRAS*, NM_002524.5: c.182A > G; p.Q61R	46 (T = 4408, C = 3773)	28 (T = 6375, C = 2518)	32 (T = 4254, C = 2000)
3	2.98	*NRAS*, NM_002524.5: c.182A > G; p.Q61R	21 (T = 7509, C = 2014)	8 (T = 7819, C = 680)	na
		IDH1, NM_005896.3: c.394C > T; p.R132C	12 (G = 8490, A = 1109)	5 (G = 9369, A = 480)	na
4	1.19	None	nd	na	na

VAF—% variant allele fraction with allele counts in brackets. A detection threshold of 0.5% variant allele fraction was applied. na—not available, as Patient 3 deceased and Patient 4 was lost to follow up (Patient 4 did not receive SIRT); nd—variant not detected according to filtering criteria.

As an *IDH1* mutation was identified in patient 3, the levels of 2-hydroxyglurate (2-HG) and other metabolites were determined using metabolomics analysis of plasma using anion-exchange chromatography coupled with tandem mass spectrometry. The results of the relative elevated levels of 2-HG are shown in Figure 6.2. The patient with the IDH1 mutation had far higher levels than controls without cancer and the three patients with ICC who had no *IDH1* mutation. The other finding from the metabolite analysis was the finding of elevated levels of orotate.

Figure 6.2. Normalised relative abundance of 2-hydroxyglutarate (2-HG) levels in plasma samples comparing ICC patients and controls. 2-HG was elevated at multiple time points, in patient 3 with the *IDH1* mutation. Patients 1, 2 and 4 had no *IDH1* mutation and showed similar levels of 2-HG to those of controls. Error bars show standard deviation from the mean.

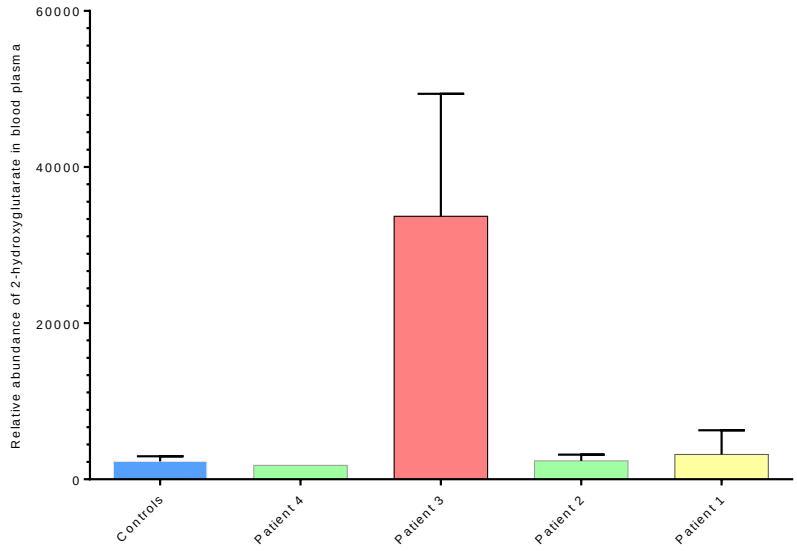

Discussion

6.7 Discussion on the inclusion of ctDNA within the imaging study PERFORM.

Cancer genomics and the potential role of the liquid biopsy as a predictive biomarker are key areas of focus across many cancer treatments. Much of the work carried out has included patients with CRC due to the high mutational load. In the era of precision medicine, the combination of investigating genomic data within an imaging biomarker study reflects the climate of the field of cancer genomics, tumour evolution and heterogeneity as an integral component to patient selection and stratification with new therapies.

The decision to include ctDNA analysis in PERFORM reflects this worldwide approach. The exploration to investigate ctDNA as a potential biomarker for the early response in patients continues. This includes patients who are receiving treatment for many advanced cancers, including mCRC. The addition of complementary genomic data to PERFORM supports an ongoing recognition of a multi-pronged approach to biomarkers. The collection of this data also explored ctDNA changes specifically with SIRT, in the rapidly evolving field of ctDNA in patients with CRC receiving systemic therapy and surgical treatments.

Although it remains unlikely that ctDNA will replace imaging assessments, key advantages of this approach permit more regular assessments and in the future may be performed at the bedside. The potential for ctDNA to outperform and replace biopsies for histological analysis in some settings exists. The non-invasive nature of ctDNA challenges the role for higher-risk, low-yield tissue biopsies. The approach offers a more comprehensive measure of tumour heterogeneity, as well as the ability to quantify tumour mutational burden and to detect clonal evolution (Fisher, Larkin, & Swanton, 2011). Although yet to be validated in CRC, data suggests that early variations may be predictive of subsequent imaging restaging at two months (J. Tie et al., 2015). It was recently recommended that larger studies are needed on the clinical utility of ctDNA combined with radiological imaging (Siravegna et al., 2019).

The decision to combine the parallel acquisition of novel imaging biomarkers and circulating biomarkers is therefore an adaptive response to these changing times. In the future, patient selection may be based on a combination of radiomics, genomics and other data such as proteomics and metabolomics.

6.8 Discussion on the choice of ctDNA in monitoring response to SIRT

The feasibility of the detection of ctDNA from the patients with mCRC supported the choice of ctDNA rather than CTC as the circulating biomarker of choice. A major limitation on CTC analysis is the requirement for an enrichment step due to the frequent observation of small numbers of CTC from some cancers, even when high levels of ctDNA are isolated. The isolation for CTCs was considered more technically challenging and not feasible in the inclusion in PERFORM. There was also more emerging data on the role of ctDNA in the monitoring of CRC.

Although PERFORM has demonstrated the feasibility of quantifying and sequencing ctDNA in patients receiving SIRT, its exact role has not been determined. This fits with a small study of patients with mCRC patients treated in first-line with chemotherapy. In one study significant reductions in ctDNA were seen after the first cycle of chemotherapy but the PFS of patients with a greater than tenfold decrease in ctDNA from baseline, was not statistically significantly better than patients who did not have the same decrease (Tie et al., 2015).

The ideal time-points for monitoring response to disease has yet to be determined as the half-life is estimated from 15 minutes through to several hours, prior to renal and hepatic clearance. Although some forms may survive longer than others. The exact timing may be dependent on the therapy under assessment. Sampling with earlier time points e.g. 48 hours and at two weeks after radiation may be of value. This was not feasible in PERFORM due to the distances patients travelled for their treatment.

The finding of the three patients who had very high baseline values of ctDNA and very short survival in PERFORM has been reported in other work. Patients with metastatic disease and high levels of ctDNA may have worse survival time overall (Fan et al., 2017).

6.9 Discussion on ctDNA to detect resistance genes to therapy including SIRT and for future treatment selection.

There is limited prospective data of the role of ctDNA in measuring resistance genes to radiation therapy, in particular in patients with advanced CRC. This study was not developed to detect the emergence of resistance genes to radiation, but the results support future research in ctDNA to monitor the evolution of tumour mutations in response to radiation therapy.

In this study, specific mutations were detected in actionable targets, including *KRAS* mutations that reflect anti-EGFR resistance. Cetuximab and panitumumab (anti-EGFR monoclonal antibodies, used to treat patients with mCRC) are ineffective in tumours with mutations in the *RAS* pathway (*EGFR-RAS-RAF-MEK*

signalling cascade). There was discordance in 18 % of patients of *KRAS* status, this may reflect true changes or may be related to initial sampling errors. However, this means up to 1 in 5 patients may not receive the appropriate treatment for this target. The role of ctDNA for *RAS* mutational status may help identify non-responders to targeted therapy or monitor patients who have developed resistance to anti-EGFR antibodies. The detection of mutations in *KRAS* from ctDNA has been found in patients with acquired resistance to *EGFR* (Misale et al., 2012; Mohan et al., 2014; Montagut et al., 2018). A study on the efficacy of Sym004, using a combination of two anti-EGFR monoclonal antibodies, found patients with acquired resistance to anti-EGFR therapy had changes in *EGFR* detected in ctDNA (Montagut et al., 2018) .

In PERFORM, two patients who were *KRAS* wt on FFPE, who then progressed after systemic therapies, were subsequently found to have *KRAS* mutations on ctDNA at 1547 and 506 days after *KRAS* wt status measured on FFPE. This has been found in other studies, where mutations in *KRAS* and *MET* have been detected from ctDNA in a cohort of patients who developed resistance to anti-EGFR therapy (Mohan et al., 2014). In another study of patients who developed resistance to anti-EGFR therapy, there was an emergence of *KRAS* amplification or other *KRAS* mutations in 60% of cases. In one patient the presence of the *KRAS* mutation was detected in ctDNA 10 months before radiographic disease progression (Misale et al., 2012). However, as most of the evidence comes from small studies it remains unclear whether mutational status detected from ctDNA will lead to improved outcomes.

Further evaluation in prospective studies is needed to establish the benefits of using ctDNA to guide patient treatment decisions, including the role of anti-EGFR therapy and other novel therapies including arterially-delivered radiation. In future, imaging biomarker studies such as those explored in PERFORM e.g. identifying predictive perfusion parameters, the role of genomics and the complementary information from circulating biomarkers may add value. Improved imaging biomarkers of early response are likely to be of increasing importance in the era of immunotherapy and cellular therapies where imaging assessments may not conform to standard criteria assessment with RECIST.

6.10 Discussion on concordance findings

The high correlation of *KRAS* mutations shown in the PERFORM participants is consistent with the literature. Specifically, the concordance between plasma ctDNA and tumour FFPE *KRAS* mutational status was 82 % in PERFORM. This compares to 70- 90 % for patients with colorectal liver metastases (Bettegowda et al., 2014; Mouliere et al., 2013; Schmiegel et al., 2017). This has been validated in a larger study with over 1000 patients (Strickler et al., 2018). *KRAS* mutation analysis of matched primary tumour and ctDNA has also shown there is a higher detection rate of *KRAS* sequence variations in plasma (Kuo, Chen, Fan, Li, & Chan, 2014) .

In PERFORM the *KRAS* mutational status concordance was confirmed over a significant time difference between *KRAS* status testing in the FFPE and in ctDNA. As the patients were heavily pre-treated and *KRAS* testing on FFPE samples was completed as standard of care early in diagnosis, the time between this and ctDNA sampling was up to 1127 days apart. This may be supported by prior mathematical modelling on

serial ctDNA mutational allele analysis that demonstrated *KRAS* mutations most likely pre-exist as a clonal subpopulation rather than occurring *de novo* (Diaz et al., 2012).

One of the limitations in the PERFORM study was that only *KRAS* status was tested in the FFPE samples, and therefore there was no concordance of the other mutations detected in ctDNA. This is because NHS pathology departments only test *KRAS* on FFPE samples as a standard of care. In future studies, funding and ethics approval should be sought for both tissue and plasma testing for all panel mutations. However, in PERFORM the *KRAS* concordance was found to be high despite significant time intervals between initial tissue *KRAS* testing and subsequent testing in ctDNA. This is an unusual finding as most studies report concordance of tissue and circulating samples at synchronous time points.

6.11 Discussion on ctDNA in PERFORM

This exploratory study has demonstrated the feasibility of collecting and analysing ctDNA from patients with refractory liver-predominant malignancy. Hotspot mutational analysis detected many of the mutations involved in CRC carcinogenesis and potential actionable targets such as *AKT* and *BRAF*. A high concordance of *KRAS* status was found, despite a long time frame between FFPE and ctDNA testing.

However, ctDNA has not yet demonstrated its utility as a biomarker for the assessment of an early response to SIRT. Earlier time points of ctDNA at 48 hours and at two weeks to investigate the presence of an early peak that may signify increased cell death may be important to explore in the future. The ability to detect evolving somatic mutations (clonal evolution) after SIRT has not previously been investigated, but no new mutations associated with radiation resistance were detected. There is little in the literature about ctDNA as a tool to detect mutations after radiation therapy (Corradetti et al., 2019). However, the ability to reproducibly measure somatic mutations in ctDNA demonstrated in PERFORM suggests a future focus for research on the role of ctDNA as a biomarker of clonal evolution and in the identification of somatic mutations arising during therapy, including those associated with tumour resistance for some therapies (Bettegowda et al., 2014; Diaz, Jr., Sausen, Fisher, & Velculescu, 2013; Diaz et al., 2012; Murtaza et al., 2013).The integration of ctDNA assays into clinical practice requires ongoing reliability of the method and validation of the clinical significance. The additional measurement of circulating microRNAs and exosomes may also provide information on cancer progression.

6.12 Discussion on *IDH1* mutation detection and circulating 2-hydroxyglutarate finding

The sequencing of ctDNA in patients with ICC has rarely been reported, and then usually as isolated cases in multi-tumour site cohorts. The sequencing of ctDNA coupled with circulating metabolites in patients with ICC has not previously been reported. Although few in number, the inclusion of these patients with ICC who had refractory disease and were receiving SIRT indicates the potential for ctDNA and circulating metabolites as potential biomarkers, including as predictive tools for targeted drug therapies.

The finding of an *IDH1* mutation detected by the 50 cancer gene panel in one of the four patients is in good accordance with the reported range of *IDH* mutations in ICC of up to 20% (Borger et al., 2012). Recent trial data show safety and efficacy of the *IDH* mutation inhibitor Ivosidenib (Abou-Alfa et al., 2019). This drug

recently received FDA approval for *IDH* mutant AML. In PERFORM the detection of an *IDH1* mutation in ctDNA from a patient with ICC correlated with the measurement of high levels of circulating 2-HG, the functional metabolite of this mutated gene. Further prospective validation of circulating *IDH1* mutational status coupled with metabolites is planned in a larger cohort.

Chapter 7 Discussion on key findings and conclusions

7.1 Summary of thesis and key findings

The delivery of SIRT to patients with advanced CRCLM is unlikely to be curative. However, improved patient selection based on biomarkers may identify a subgroup of patients who may achieve longer hepatic progression-free survival, whilst avoiding this treatment in patients unlikely to benefit. The hypothesis that patients with favourable tumour perfusion as identified from perfusion parameters detected from imaging with pCT and or DCE MRI may be more likely to respond has been examined.

A predictive biomarker that may indicate a high likelihood of microsphere delivery and thus delivered radiation dose leading to a response would offer a more targeted approach to arterially delivered brachytherapy. However, a validated single imaging biomarker that predicts for response leading to improved survival has not been identified.

Imaging and or circulating biomarkers that detect patients with an early relapse after SIRT who have not responded may result in improved outcomes if earlier identification leads to a therapeutic intervention sooner. The detection of somatic mutations from ctDNA may subsequently lead to more personalised therapies, and this analysis of imaging findings coupled with information of tumour genomics from circulating biomarkers may provide complimentary information in the identification of tumours which may develop a different mutational profile for example – with the detection of an emerging resistance mechanism.

The findings described provide an insight into the feasibility, method development and the generation of predictive perfusion biomarkers whilst highlighting the ongoing steps for biomarker validation. The PERFORM study also examines the complimentary addition of circulating biomarkers.

T1 mapping with shMOLLI in the imaging of suspected hepatic malignancy may represent a non-invasive technique that discriminates liver tumours from background liver. It has shown promise in differentiating benign and low-grade tumour from higher grade tumours. However, this has not yet demonstrated that it replaces the need for histological assessment and resection in hepatic lesions.

OE MRI has shown promise as a non-contrast agent in liver lesion characterisation. It is feasible and changes in T1 pre- and during oxygen enhancement in hepatic malignancies may help characterise lesions.

The shortening of T1 during high-flow oxygen inhalation from patients with malignant hepatic lesions, prior to resection was demonstrated. The assessment of T1 mapping with oxygen enhancement initially on Siemens and then transferring to GE MRI was challenging. This confirms the ongoing challenges of finding IB that may be generalizable to the real-world where patients may be scanned on different vendor scanners within the same hospital complex.

The FOXFIRE analysis of hepatic resection after SIRT confirms the safety, complications and survival following treatment with ^{90}Y microspheres. The findings of the histological analysis demonstrate the

location of the microspheres carried in the vasculature secondary to hepatic perfusion and confirm the necrosis caused by SIRT.

The addition of a complimentary circulating biomarker, ctDNA show that the genomic information from this may complement the imaging assessments and offer an insight into the additional benefit of a combined approach with imaging and genomics. The additional analysis of metabolites in patients with ICC and correlation of 2-HG with *IDH1* mutation status was a novel finding.

7.2 SIRT in CRCLM

The aim of delivering tumouricidal doses of radiation to the tumour, with sparing of normal liver parenchyma exploits the high arterial blood supply to hepatic metastases. The SIRFLOX study showed a 7.9 month hepatic progression-free survival (van Hazel et al., 2016).

The patients in the amended PERFORM protocol accessed SIRT through CTE – a national programme for SIRT for patients with CRCLM. The results from this prospective single-arm observation study confirmed a median overall survival of 7.6 months (95% confidence interval 6.9-8.3) (J. White et al., 2019). The ability to stratify patients based on background liver, tumour perfusion, genomic profile of the tumour and metabolomics properties may improve patient selection in the future. A strategy for improved selection and the validation of predictive biomarkers is still needed to determine whether SIRT offers an overall survival advantage for selected patients. Patient characteristics such as no extra-hepatic disease, fewer than 6 tumours and less than 25% ratio of tumour-to-liver volume may be more likely to benefit (Wasan et al., 2017). This selection by patient and tumour characteristics may also be aided by combining radiation with novel systemic therapies. These patient characteristics and the potential to stimulate an increased immune response may be as important as tumour perfusion characteristics in conferring an overall survival advantage.

7.3 Summary and conclusions from pCT and DCE MRI

Perfusion imaging with pCT and DCE MRI is feasible in patients with a high burden on hepatic malignancy at serial time-points, when receiving liver-directed therapy. Clinical feasibility was demonstrated in the PERFORM study with the majority of patients able to participate and have perfusion CT and subsequently pCT and DCE MRI whilst receiving SIRT. Studies with patients with refractory malignancy are limited by progression and changes in performance status and frailty that may make those with progressive disease unable to complete the full schedule of scans. This may be ameliorated by reducing need for long breath-holds and reducing scans for example when investigating the role of oxygen-enhancement and time required for steady-state to be achieved. However, the feasibility of combining an imaging sub-study, PERFORM, as part of a large multi-centre randomised-controlled trial FOXFIRE was demonstrated.

Ongoing research on developing perfusion parameters and reproducing findings from the few other small studies on SIRT that have described specific predictive biomarkers (Morsbach et al., 2014). Technically the

feasibility of the generation of quantitative perfusion parameters was feasible in pCT. The main issues in pCT analysis was the technical challenge of importing pCT from other vendor platforms into GE software v4.

However, for DCE MRI there were some issues with the generation of parameter maps with many of the scans not supporting analysis due to technical challenges of PK modelling.

Both pCT and DCE MRI did generate perfusion data from patients with a high burden of hepatic malignancy at serial time-points, receiving liver-directed therapy.

These scans provided important data for comparison with pre-clinical data (Kannan et al., 2018). Pre-clinical modelling has provided more insights into the accurate determination of tumour vascularity and the impact of vessel tortuosity. Analysis of the vascular and functional parameters within lesions demonstrated complex relationship when compared to pre-clinical data. Structural variants included vessel volume, radius and tortuosity (Kannan et al., 2018).

The data also supported dosimetry data analysis (Abbott et al., 2018). Emerging analysis from preliminary DCE MRI data has been used to explore texture analysis looking at tumour vascular heterogeneity (Winter et al., 2018).

Changes in tumour perfusion may also be important for drug delivery for subsequent therapies. This has implications in the sequencing of treatments. This includes the use of concomitant versus sequential systemic therapy, role of immunotherapy and the timing of arterially delivered therapies that may alter tumour vascularity. The ideal magnitude of perfusion and blood flow for the delivery of SIRT has yet to be determined.

7.4 Conclusions from T1 mapping with shMOLLI and OE MRI in imaging hepatic malignancy

Native T1 mapping and OE MRI provided quantitative data on patients with hepatic lesions receiving surgical resection. The ability to differentiate hepatic malignancies from low grade neuroendocrine tumours and background mapping is a new potential application of T1 mapping. The adaption of shMOLLI from cardiac imaging to hepatic benign malignancy was recently established (Banerjee et al., 2014). The ability to test this technique in patients with hepatic lesions, prior to hepatic resection provided important information in the method development of T1 mapping in imaging malignant liver lesions and providing more data of liver lesions difficult to characterise on standard MRI imaging. These patients had all been discussed at the hepatic MDT and uncertainty remained about many of these lesions. Improved functional imaging and the ability to differentiate benign lesions from malignant lesions may avoid hepatic surgery for some. The ability to differentiate low grade from higher grade lesions may also determine prioritisation for surgery and the role of neoadjuvant approaches. However, the replacement of biopsy or resection from results with T1 mapping in suspected malignancy has yet to be established as it has in liver fibrosis.

OE MRI remains a research tool that offers potential for non-injectable contrast and has few contraindications and risks compared to IV contrast scans.

7.5 Conclusions from FOXFIRE hepatic resections after SIRT

Hepatic resection after the novel combination of systemic OxMdG chemotherapy (oxaliplatin, 5-fluorouracil and folic acid) with SIRT in the first-line management of liver-dominant metastatic colorectal cancer is safe when compared to OxMdG chemotherapy alone. A Multi-Disciplinary Team deemed all patients inoperable before registration. FOXFIRE randomised 182 participants to chemotherapy alone and 182 to chemotherapy with SIRT. There was no statistically significant difference between groups in the rate of liver surgery, nor in survival from time of resection (HR = 1.55; 95% CI = 0.83–2.89).

The exploratory analysis of histopathology confirmed the highest density of microspheres at the tumour periphery. Ectopic microsphere deposition in the gall bladder was an incidental histological finding. Patients treated with SIRT plus chemotherapy displayed lower values of viable tumour in comparison to those treated with chemotherapy alone ($p < 0.05$).

Liver surgery should be considered following the clinical response to SIRT. These findings confirm that when resection is performed after SIRT – microsphere delivery is associated with a radiation reaction, tumour penetration and necrosis with limited damage to surrounding normal liver parenchyma.

7.6 Conclusions on circulating biomarkers in hepatic malignancy

The decision for the addition of a circulating biomarker (ctDNA) was justified by the emerging data on ctDNA in the assessment of early CRC and in mCRC (Tie et al., 2015; Tie et al., 2016). The decision to add the exploratory circulating biomarker as ctDNA rather than CTC was justified by the higher yield rates, and easier detection and analysis techniques. Circulating tumour cells are intact, viable cancer cells with DNA, RNA and protein analysis potential. The advantages this could have offered were functional *in vitro* and *in vivo* assays. However, current detection techniques remain cumbersome and technically challenging. In view of the ability to detect mutations in the ctDNA from these patients with a high burden of disease this decision was justified. For future selection of a complimentary biomarker for patients consideration should be given to acquisition and amount of blood; analysis time; yield and mutation burden from tumour site, and time points. For example – repeating this study I would have recommended an early time-point within 48 hrs to see what happened to initial ctDNA where a steep rise may proceed a decline in responsive tumours (Tie et al., 2015). ctDNA and where available a companion circulating metabolite, remains an area of ongoing research interest for cholangiocarcinoma patients (Winter et al., 2019).

For patients receiving novel new therapies including arterially directed therapies with a high burden of disease and potential changing mutational burden and status. It is proposed that ctDNA remains a potential predictive biomarker. This would include in studies in patients treated with arterially-directed therapies, immunotherapy and targeted radiation where radiological pseudoprogression is a challenge for patients awaiting results of assessments for treatments. ctDNA analysis provides key molecular information and may identify putative resistance mechanisms to therapy.

The role of ctDNA to assess early response to new combinations such as targeted therapies combined with immunotherapy, tumour infiltrating lymphocyte and adaptive cellular therapies remains largely unexplored.

The ability to detect evolving somatic mutations (clonal evolution) after SIRT has not previously been investigated. However more work is needed to detect new mutations following high dose targeted brachytherapy.

7.6.1 ctDNA in patients with heavily pre-treated CRCLM

ctDNA analysis with Ion Torrent Amplicon sequencing in PERFORM patients did detect 9 somatic mutations at baseline including *KRAS* G13D, *KRAS* G12V and a rare *AKT1* E17K mutation in patients with CRC. The concordance with tissue *KRAS* status was high at 82%, up to 1127 days after FFPE testing. This supports other evidence that ctDNA may be used to determine *KRAS* status in mCRC (Mouliere et al., 2013).

Results from patients with colorectal cancer with detectable mutations in ctDNA at baseline demonstrated a change in ctDNA levels from baseline to 4 weeks after SIRT suggesting ctDNA is detectable and reproducible in patients undergoing SIRT. However, this was not validated as a biomarker of response with standard radiological assessment. The timing of assessments may need refinement as an early decrease in ctDNA in mCRC after first line chemotherapy was found to predate radiological response (J. Tie et al., 2015).

In PERFORM, the change in VAF was measured in ctDNA from patients receiving SIRT which has not been previously reported. This study failed to detect evolving somatic mutations after radiation however the ability of ctDNA to detect emerging radiation-resistance genes would be of interest in future radiation studies.

No correlation with survival was found from ctDNA levels. However, this was also limited by incomplete details on subsequent therapies received by these patients after SIRT.

Combining imaging assessments with complimentary circulating biomarkers is advised in new biomarker studies which provide complimentary information of tumour genomic and the tumour mutational burden. The early change in ctDNA may provide an earlier assessment of response that pre-dates radiological assessment and avoids pseudo-progression by radiation effects.

7.6.2 ctDNA and circulating metabolites in ICC

The whole genome sequencing (WGS) data from the four ICC patients demonstrated the additional value of examining copy number variants.

In conclusion, the role of liquid biopsies including ctDNA and plasma metabolites may be particularly useful in hard-to-reach, hard-to-treat cancers such as ICC. By combining circulating genomic and metabolite analysis preliminary data has demonstrated potential for this approach. These results suggest this has potential to identify novel genetic markers and inform diagnosis and/or prognosis in ICC. The scope for a larger cohort study to validate the correlation between circulating metabolites and ICC mutational status, particularly to explore the observation that orotate levels are increased in some patients, potentially as a consequence of genetic variants. This minimally invasive approach for detection of tumour mutations, with complimentary metabolite profiling, may also be useful for early detection and disease monitoring in response to therapy.

7.7 Justification for imaging and circulating biomarkers

Few studies have looked at the complimentary role of ctDNA analysis and functional imaging. A recent study in patients with melanoma looked to assess the role of ctDNA analysis combined with PETCT to monitor tumour burden and genomic heterogeneity. They described that early changes in ctDNA and metabolic disease burden were important components of treatment response (Wong et al., 2017). The role of artificial intelligence and machine learning are also providing opportunities in imaging data acquisition and analysis. The way cancers are imaged and analysed for the provision of radiomic features are also evolving (Khorrami et al., 2019). As machine-learning is developed in radiology the ability to interrogate multi-parametric imaging and large dataset analysis may lead to similar transformative development and integration into research protocols as cancer genomics. This has been used specifically with CT scans from lung cancer patients treated with immunotherapy with responders most likely to show significant textural change. By using machine learning, changes in texture, volume and shape as well as size were detected (Khorrami et al., 2019).

7.8 Impact and Future developments

The clinical imaging techniques from PERFORM were incorporated with pre-clinical modelling of vessel tortuosity and resulted in confirmation of the mechanism (Kannan et al., 2018).

The development of techniques and vendor transfer identified in PERFORM have led to improvements in newer studies of parameter generation. The work from PERFORM was incorporated with dosimetry work and has explored the impact of blood flow and dose delivery (Abbott et al., 2018).

Preliminary analysis of the DCE MRI maps after PK modelling has supported the feasibility, generated from pre-clinical modelling, of tumour perfusion heterogeneity with texture analysis (Winter et al., 2018). The DCE MRI images from some patients with CRC participating in PERFORM have been analysed and quantified for tumour perfusion heterogeneity using 26-point neighbourhoods in 3D K^{trans} maps, to serve

as texture feature maps. Extravascular extracellular space enhancement modelling used pharmacokinetic modelling using the Toft's model and a population-derived AIF. The most dominant local textures were found with K-means clustering on 26-point local neighbourhood features in 3D. Global heterogeneity was then modelled by proportions of local textures across the whole tumour. Preliminary work showed changes in heterogeneity seen in the texture analysis of pre-treatment and post treatment CRCLM may offer some explanation for the differential hepatic response to SIRT which is delivered by the vasculature.

The FOXFIRE surgical and resection outcomes paper also highlighted the importance of TME and the potential for future investigation of macrophage polarisation (Winter et al., 2019).

The combination of ctDNA and metabolomics in a small number of patients with ICC, found a correlation of IDH status and 2-HG levels. The metabolite orotic acid was also a new finding and further large-scale studies are required to demonstrate the significance of this metabolite and its role in ICC or as a potential target for drug development (H. Winter et al., 2019).

7.9 Concluding statements

Personalised medicine aims to identify the right patient for the right intervention at the right time. Improved patient selection based on functional imaging and baseline tumour perfusion parameters may assist in the selection and delivery of arterially delivered novel therapies. However the current evidence has not demonstrated validated predictive imaging biomarkers for SIRT. Work leading from PERFORM has looked at dose delivery in Gy from SIRT microsphere deposition (Abbott et al., 2018). However more work is needed to validate these initial findings. Future foci for research includes the exploration of cellular infiltrates; gene and protein expression and changes in the tumour microenvironment and immune cell niche.

The role of detecting complimentary circulating biomarkers in parallel will strengthen imaging findings against the developing reliance on ctDNA and genomic expression. The identification of radio-sensitising and radio-resistant genes from tissues may indicate the right intervention for patients. Establishing the role for ctDNA or other non-invasive biomarkers for the detection of emerging drug or therapy resistance remains an important approach. The ability to detect an evolving mutational status in the circulation at serial time-points, confirming the current mutational status for a patient may indicate the timing for novel therapies. Coupling tumour genomics and the TME with patient characteristics may further improve patient selection. In the era of stratified medicine, new alternatives and approaches to assessment biomarkers will be important and direct comparisons with emerging approaches such as ctDNA will be essential.

References

Abbott, E., Falzone, N., Winter, H., Greenhalgh, T., Kartsonaki, C., Craig, A., . . . Vallis, K. (2018). Absorbed dose from ^{90}Y selective internal radiotherapy (SIRT) is correlated with individual lesion response in colorectal cancer patients. *European Journal of Surgical Oncology, 44*, S53. doi:10.1016/j.ejso.2018.01.029

Abdalla, E. K., Bauer, T. W., Chun, Y. S., D'Angelica, M., Kooby, D. A., & Jarnagin, W. R. (2013). Locoregional surgical and interventional therapies for advanced colorectal cancer liver metastases: expert consensus statements. *HPB (Oxford), 15*(2), 119-130. doi:10.1111/j.1477-2574.2012.00597.x

Abdalla, E. K., Vauthey, J.-N., Ellis, L. M., Ellis, V., Pollock, R., Broglio, K. R., . . . Curley, S. A. (2004). Recurrence and Outcomes Following Hepatic Resection, Radiofrequency Ablation, and Combined Resection/Ablation for Colorectal Liver Metastases. *Annals of Surgery, 239*(6), 818-827. doi:10.1097/01.sla.0000128305.90650.71

Abou-Alfa, G. K., Macarulla Mercade, T., Javle, M., Kelley, R. K., Lubner, S., Adeva, J., . . . Zhu, A. X. (2019). LBA10_PRClarIDHy: A global, phase III, randomized, double-blind study of ivosidenib (IVO) vs placebo in patients with advanced cholangiocarcinoma (CC) with an isocitrate dehydrogenase 1 (IDH1) mutation. *Annals of Oncology, 30*(Supplement_5). doi:10.1093/annonc/mdz394.027

Adam, R., Delvart, V., Pascal, G., Valeanu, A., Castaing, D., Azoulay, D., . . . Bismuth, H. (2004). Rescue surgery for unresectable colorectal liver metastases downstaged by chemotherapy: a model to predict long-term survival. *Ann Surg, 240*(4), 644-657; discussion 657-648.

Adams, R. A., Meade, A. M., Seymour, M. T., Wilson, R. H., Madi, A., Fisher, D., . . . Maughan, T. S. (2011). Intermittent versus continuous oxaliplatin and fluoropyrimidine combination chemotherapy for first-line treatment of advanced colorectal cancer: results of the randomised phase 3 MRC COIN trial. *The Lancet Oncology, 12*(7), 642-653. doi:http://dx.doi.org/10.1016/S1470-2045(11)70102-4

Aliberti, C., Carandina, R., Sarti, D., Mulazzani, L., Catalano, V., Felicioli, A., . . . Fiorentini, G. (2016). Hepatic Arterial Infusion of Polyethylene Glycol Drug-eluting Beads for Primary and Metastatic Liver Cancer Therapy. *Anticancer Research, 36*(7), 3515-3521.

Aloia, T., Sebagh, M., Plasse, M., Karam, V., Levi, F., Giacchetti, S., . . . Adam, R. (2006). Liver histology and surgical outcomes after preoperative chemotherapy with fluorouracil plus oxaliplatin in colorectal cancer liver metastases. *J Clin Oncol, 24*(31), 4983-4990. doi:10.1200/jco.2006.05.8156

Archer, S. G., & Gray, B. N. (1989). Vascularization of small liver metastases. *Br J Surg, 76*(6), 545-548.

Archetti, M. (2013). Evolutionary game theory of growth factor production: implications for tumour heterogeneity and resistance to therapies. *Br J Cancer, 109*(4), 1056-1062. doi:10.1038/bjc.2013.336

Banerjee, R., Pavlides, M., Tunnicliffe, E. M., Piechnik, S. K., Sarania, N., Philips, R., . . . Neubauer, S. (2014). Multiparametric magnetic resonance for the non-invasive diagnosis of liver disease. *J Hepatol, 60*(1), 69-77. doi:10.1016/j.jhep.2013.09.002

Baudelet, C., & Gallez, B. (2002). How does blood oxygen level-dependent (BOLD) contrast correlate with oxygen partial pressure (pO2) inside tumors? *Magn Reson Med, 48*(6), 980-986. doi:10.1002/mrm.10318

Benson, A., Geschwind, J. F., Mulcahy, M. F., Rilling, W., Siskin, G., Wiseman, G., . . . Salem, R. (2013). Radioembolisation for liver metastases: Results from a prospective 151 patient multi-institutional phase II study. *European Journal of Cancer, 49*(15), 3122-3130. doi:DOI 10.1016/j.ejca.2013.05.012

Bettegowda, C., Sausen, M., Leary, R. J., Kinde, I., Wang, Y., Agrawal, N., . . . Diaz, L. A., Jr. (2014). Detection of circulating tumor DNA in early- and late-stage human malignancies. *Sci Transl Med, 6*(224), 224ra224. doi:10.1126/scitranslmed.3007094

Blockley, N. P., Jiang, L., Gardener, A. G., Ludman, C. N., Francis, S. T., & Gowland, P. A. (2008). Field strength dependence of R1 and R2* relaxivities of human whole blood to ProHance, Vasovist, and deoxyhemoglobin. *Magn Reson Med, 60*(6), 1313-1320. doi:10.1002/mrm.21792

Borger, D. R., Tanabe, K. K., Fan, K. C., Lopez, H. U., Fantin, V. R., Straley, K. S., . . . Iafrate, A. J. (2012). Frequent mutation of isocitrate dehydrogenase (IDH)1 and IDH2 in cholangiocarcinoma identified through broad-based tumor genotyping. *The oncologist, 17*(1), 72-79. doi:10.1634/theoncologist.2011-0386

Bottomley, P. A., Foster, T. H., Argersinger, R. E., & Pfeifer, L. M. (1984). A review of normal tissue hydrogen NMR relaxation times and relaxation mechanisms from 1-100 MHz: dependence on tissue type, NMR frequency, temperature, species, excision, and age. *Med Phys, 11*(4), 425-448. doi:10.1118/1.595535

Breedis, C., & Young, G. (1954). The Blood Supply of Neoplasms in the Liver. *The American Journal of Pathology, 30*(5), 969-985.

Brouquet, A., Abdalla, E. K., Kopetz, S., Garrett, C. R., Overman, M. J., Eng, C., . . . Vauthey, J.-N. (2011). High Survival Rate After Two-Stage Resection of Advanced Colorectal Liver Metastases: Response-Based Selection and Complete Resection Define Outcome. *Journal of Clinical Oncology, 29*(8), 1083-1090. doi:10.1200/JCO.2010.32.6132

Bull, S., White, S. K., Piechnik, S. K., Flett, A. S., Ferreira, V. M., Loudon, M., . . . Myerson, S. G. (2013). Human non-contrast T1 values and correlation with histology in diffuse fibrosis. *Heart, 99*(13), 932-937. doi:10.1136/heartjnl-2012-303052

Cercek, A., Braghiroli, M. I., Chou, J. F., Hechtman, J. F., Kemeny, N., Saltz, L., . . . Yaeger, R. (2017). Clinical Features and Outcomes of Patients with Colorectal Cancers Harboring NRAS Mutations. *Clinical cancer research : an official journal of the American Association for Cancer Research, 23*(16), 4753-4760. doi:10.1158/1078-0432.CCR-17-0400

Chen, I., Lorentzen, T., Linnemann, D., Nolsøe, C. P., Skjoldbye, B., Jensen, B. V., & Nielsen, D. (2016). Seeding after ultrasound-guided percutaneous biopsy of liver metastases in patients with colorectal or breast cancer. *Acta Oncologica, 55*(5), 638-643. doi:10.3109/0284186X.2015.1093657

Chew, V., Lee, Y. H., Pan, L., Nasir, N. J. M., Lim, C. J., Chua, C., . . . Chow, P. K. H. (2018). Immune activation underlies a sustained clinical response to Yttrium-90 radioembolisation in hepatocellular carcinoma. *Gut*. doi:10.1136/gutjnl-2017-315485

Chiandussi, L., Greco, F., Sardi, G., Vaccarino, A., Ferraris, C. M., & Curti, B. (1968). Estimation of hepatic arterial and portal venous blood flow by direct catheterization of the vena porta through the umbilical cord in man. Preliminary results. *Acta Hepatosplenol, 15*(3), 166-171.

Choti, M. A., Sitzmann, J. V., Tiburi, M. F., Sumetchotimetha, W., Rangsin, R., Schulick, R. D., . . . Cameron, J. L. (2002). Trends in long-term survival following liver resection for hepatic colorectal metastases. *Ann Surg, 235*(6), 759-766.

Collins, J. M. (2003). Functional imaging in phase I studies: decorations or decision making? *J. Clin. Oncol., 21*, 2807-2809.

Corradetti, M. N., Torok, J. A., Hatch, A. J., Xanthopoulos, E. P., Lafata, K., Jacobs, C., . . . Nixon, A. B. (2019). Dynamic Changes in Circulating Tumor DNA During Chemoradiation for Locally Advanced Lung Cancer. *Advances in Radiation Oncology, 4*(4), 748-752. doi:10.1016/j.adro.2019.05.004

d'Arcy, J. A., Collins, D. J., Padhani, A. R., Walker-Samuel, S., Suckling, J., & Leach, M. O. (2006). Informatics in Radiology (infoRAD): Magnetic Resonance Imaging Workbench: analysis and visualization of dynamic contrast-enhanced MR imaging data. *Radiographics, 26*(2), 621-632. doi:10.1148/rg.262045187

Dall'Armellina, E., Piechnik, S. K., Ferreira, V. M., Si, Q. L., Robson, M. D., Francis, J. M., . . . Neubauer, S. (2012). Cardiovascular magnetic resonance by non contrast T1-mapping allows assessment of severity of injury in acute myocardial infarction. *J Cardiovasc Magn Reson, 14*, 15. doi:10.1186/1532-429x-14-15

De Roock, W., Claes, B., Bernasconi, D., De Schutter, J., Biesmans, B., Fountzilas, G., . . . Tejpar, S. (2010). Effects of KRAS, BRAF, NRAS, and PIK3CA mutations on the efficacy of cetuximab plus

chemotherapy in chemotherapy-refractory metastatic colorectal cancer: a retrospective consortium analysis. *Lancet Oncology, 11*(8), 753-762. doi:Doi 10.1016/S1470-2045(10)70130-3

Dezső, K., Bugyik, E., Papp, V., László, V., Döme, B., Tóvári, J., . . . Paku, S. (2009). Development of Arterial Blood Supply in Experimental Liver Metastases. *The American Journal of Pathology, 175*(2), 835-843. doi:10.2353/ajpath.2009.090095

Diaz, L. A., Jr., Sausen, M., Fisher, G. A., & Velculescu, V. E. (2013). Insights into therapeutic resistance from whole-genome analyses of circulating tumor DNA. *Oncotarget, 4*(10), 1856-1857.

Diaz, L. A., Williams, R., Wu, J., Kinde, I., Hecht, J. R., Berlin, J., . . . Vogelstein, B. (2012). The molecular evolution of acquired resistance to targeted EGFR blockade in colorectal cancers. *Nature, 486*(7404), 537-540. doi:10.1038/nature11219

Dindo, D., Demartines, N., & Clavien, P.-A. (2004). Classification of Surgical Complications: A New Proposal With Evaluation in a Cohort of 6336 Patients and Results of a Survey. *Annals of Surgery, 240*(2), 205-213. doi:10.1097/01.sla.0000133083.54934.ae

Dowlati, A. (2005). Novel phase I dose de-escalation design trial to determine the biological modulatory dose of the antiangiogenic agent SU5416. *Clin. Cancer Res., 11*, 7938-7944.

Dutton, S. J., Kenealy, N., Love, S. B., Wasan, H. S., & Sharma, R. A. (2014). FOXFIRE protocol: an open-label, randomised, phase III trial of 5-fluorouracil, oxaliplatin and folinic acid (OxMdG) with or without interventional Selective Internal Radiation Therapy (SIRT) as first-line treatment for patients with unresectable liver-only or liver-dominant metastatic colorectal cancer. *BMC Cancer, 14*, 497. doi:10.1186/1471-2407-14-497

Eisenhauer, E. A., Therasse, P., Bogaerts, J., Schwartz, L. H., Sargent, D., Ford, R., . . . Mooney, M. (2009). New response evaluation criteria in solid tumours: revised RECIST guideline (version 1.1). *Eur J Cancer, 45*. doi:10.1016/j.ejca.2008.10.026

Elias, D., Ouellet, J. F., De Baere, T., Lasser, P., & Roche, A. (2002). Preoperative selective portal vein embolization before hepatectomy for liver metastases: long-term results and impact on survival. *Surgery, 131*(3), 294-299.

Evrard, S., Poston, G., Kissmeyer-Nielsen, P., Diallo, A., Desolneux, G., Brouste, V., . . . Fong, Y. (2014). Combined ablation and resection (CARe) as an effective parenchymal sparing treatment for extensive colorectal liver metastases. *PLoS One, 9*(12), e114404. doi:10.1371/journal.pone.0114404

Falcone, A., Ricci, S., Brunetti, I., Pfanner, E., Allegrini, G., Barbara, C., . . . Masi, G. (2007). Phase III trial of infusional fluorouracil, leucovorin, oxaliplatin, and irinotecan (FOLFOXIRI) compared with infusional fluorouracil, leucovorin, and irinotecan (FOLFIRI) as first-line treatment for metastatic colorectal cancer: the Gruppo Oncologico Nord Ovest. *J Clin Oncol, 25*(13), 1670-1676. doi:10.1200/jco.2006.09.0928

Fan, G., Zhang, K., Yang, X., Ding, J., Wang, Z., & Li, J. (2017). Prognostic value of circulating tumor DNA in patients with colon cancer: Systematic review. *PloS one, 12*(2), e0171991-e0171991. doi:10.1371/journal.pone.0171991

Ferlay J, Soerjomataram I, Ervik M, Dikshit R, Eser S, Mathers C, . . . Bray, F. (2013). *Cancer Incidence and Mortality Worldwide: IARC CancerBase No. 11* Retrieved from

Fiorentini, G., Aliberti, C., Mulazzani, L., Coschiera, P., Catalano, V., Rossi, D., . . . Ricci, S. (2014). Chemoembolization in Colorectal Liver Metastases: The Rebirth. *Anticancer Research, 34*(2), 575-584.

Fisher, R., Larkin, J., & Swanton, C. (2011). Delivering preventive, predictive and personalised cancer medicine for renal cell carcinoma: the challenge of tumour heterogeneity. *EPMA J, 3*(1), 1. doi:10.1007/s13167-011-0137-3

Fong, Y., Cohen, A. M., Fortner, J. G., Enker, W. E., Turnbull, A. D., Coit, D. G., . . . Brennan, M. F. (1997). Liver resection for colorectal metastases. *J Clin Oncol, 15*(3), 938-946.

Galbraith, S. M. (2002). Effects of 5,6-dimethylxanthenone-4-acetic acid on human tumor microcirculation assessed by dynamic contrast-enhanced magnetic resonance imaging. *J. Clin. Oncol., 20*, 3826-3840.

Garlipp, B., de Baere, T., Damm, R., Irmscher, R., van Buskirk, M., Stubs, P., . . . Seidensticker, M. (2014). Left-liver hypertrophy after therapeutic right-liver radioembolization is substantial but less than after portal vein embolization. Hepatology, 59(5), 1864-1873. doi:10.1002/hep.26947

Gerlinger, M., Rowan, A. J., Horswell, S., Larkin, J., Endesfelder, D., Gronroos, E., . . . Swanton, C. (2012). Intratumor Heterogeneity and Branched Evolution Revealed by Multiregion Sequencing. *New England Journal of Medicine, 366*(10), 883-892.

Goh, V., Halligan, S., Daley, F., Wellsted, D. M., Guenther, T., & Bartram, C. I. (2008). Colorectal Tumor Vascularity: Quantitative Assessment with Multidetector CT-Do Tumor Perfusion Measurements Reflect Angiogenesis? *Radiology, 249*(2), 510-517. doi:DOI 10.1148/radiol.2492071365

Hurwitz, H., Fehrenbacher, L., Novotny, W., Cartwright, T., Hainsworth, J., Heim, W., . . . Kabbinavar, F. (2004). Bevacizumab plus irinotecan, fluorouracil, and leucovorin for metastatic colorectal cancer. *N Engl J Med, 350*(23), 2335-2342. doi:10.1056/NEJMoa032691

Ippolito, D., Capraro, C., Casiraghi, A., Cestari, C., & Sironi, S. (2012). Quantitative assessment of tumour associated neovascularisation in patients with liver cirrhosis and hepatocellular carcinoma: role of dynamic-CT perfusion imaging. *European Radiology, 22*(4), 803-811. doi:DOI 10.1007/s00330-011-2307-z

Jiang, H. J., Zhang, Z. R., Shen, B. Z., Wan, Y., Guo, H., & Li, J. P. (2009). Quantification of angiogenesis by CT perfusion imaging in liver tumor of rabbit. *Hepatobiliary & Pancreatic Diseases International, 8*(2), 168-173.

Justinger, C., Kouladouros, K., Gartner, D., Tatsch, K., Reimer, P., Rudiger, T., . . . Schon, M. R. (2015). Liver resection after selective internal radiotherapy (SIRT): Proof of concept, initial survival, and safety. *J Surg Oncol, 112*(4), 436-442. doi:10.1002/jso.24000

Kabbinavar, F. F., Hambleton, J., Mass, R. D., Hurwitz, H. I., Bergsland, E., & Sarkar, S. (2005). Combined analysis of efficacy: the addition of bevacizumab to fluorouracil/leucovorin improves survival for patients with metastatic colorectal cancer. *J Clin Oncol, 23*(16), 3706-3712. doi:10.1200/jco.2005.00.232

Kannan, P., Kretzschmar, W. W., Winter, H., Warren, D., Bates, R., Allen, P. D., . . . Kersemans, V. (2018). Functional Parameters Derived from Magnetic Resonance Imaging Reflect Vascular Morphology in Preclinical Tumors and in Human Liver Metastases. *Clinical cancer research : an official journal of the American Association for Cancer Research, 24*(19), 4694-4704. doi:10.1158/1078-0432.CCR-18-0033

Kappadath, S. C., Mikell, J., Balagopal, A., Baladandayuthapani, V., Kaseb, A., & Mahvash, A. (2018). Hepatocellular Carcinoma Tumor Dose Response After ⁹⁰Y-radioembolization With Glass Microspheres Using ⁹⁰Y-SPECT/CT-Based Voxel Dosimetry. *International Journal of Radiation Oncology • Biology • Physics, 102*(2), 451-461. doi:10.1016/j.ijrobp.2018.05.062

Karoui, M., Penna, C., Amin-Hashem, M., Mitry, E., Benoist, S., Franc, B., . . . Nordlinger, B. (2006). Influence of preoperative chemotherapy on the risk of major hepatectomy for colorectal liver metastases. *Ann Surg, 243*(1), 1-7.

Katz, S. C., Burga, R. A., McCormack, E., Wang, L. J., Mooring, W., Point, G. R., . . . Junghans, R. P. (2015). Phase I Hepatic Immunotherapy for Metastases Study of Intra-Arterial Chimeric Antigen Receptor-Modified T-cell Therapy for CEA+ Liver Metastases. *Clin Cancer Res, 21*(14), 3149-3159. doi:10.1158/1078-0432.ccr-14-1421

Kellock, T., Liang, T., Harris, A., Schellenberg, D., Ma, R., Ho, S., & Yap, W. W. (2018). Stereotactic body radiation therapy (SBRT) for hepatocellular carcinoma: imaging evaluation post treatment. *The British journal of radiology, 91*(1085), 20170118. doi:10.1259/bjr.20170118

Kennedy, A., Nag, S., Salem, R., Murthy, R., McEwan, A. J., Nutting, C., . . . Coldwell, D. (2007). Recommendations for radioembolization of hepatic malignancies using yttrium-90 microsphere brachytherapy: a consensus panel report from the radioembolization brachytherapy oncology consortium. *Int J Radiat Oncol Biol Phys, 68*(1), 13-23. doi:10.1016/j.ijrobp.2006.11.060

Kennedy, A. S., Nutting, C., Coldwell, D., Gaiser, J., & Drachenberg, C. (2004). Pathologic response and microdosimetry of (90)Y microspheres in man: review of four explanted whole livers. *Int J Radiat Oncol Biol Phys, 60*(5), 1552-1563. doi:10.1016/j.ijrobp.2004.09.004

Khan, A. Z., Morris-Stiff, G., & Makuuchi, M. (2009). Patterns of chemotherapy-induced hepatic injury and their implications for patients undergoing liver resection for colorectal liver metastases. *J Hepatobiliary Pancreat Surg, 16*(2), 137-144. doi:10.1007/s00534-008-0016-z

Khorrami, M., Prasanna, P., Gupta, A., Patil, P., Velu, P. D., Thawani, R., . . . Madabhushi, A. (2019). Changes in CT Radiomic Features Associated with Lymphocyte Distribution Predict Overall Survival and Response to Immunotherapy in Non–Small Cell Lung Cancer. *Cancer Immunology Research*. doi:10.1158/2326-6066.CIR-19-0476

Kim, S. H., Kamaya, A., & Willmann, J. K. (2014). CT Perfusion of the Liver: Principles and Applications in Oncology. *Radiology, 272*(2), 321-343. doi:DOI 10.1148/radiol.14130091

Kuo, Y. B., Chen, J. S., Fan, C. W., Li, Y. S., & Chan, E. C. (2014). Comparison of KRAS mutation analysis of primary tumors and matched circulating cell-free DNA in plasmas of patients with colorectal cancer. *Clin Chim Acta, 433*, 284-289. doi:10.1016/j.cca.2014.03.024

Lam, V. W., Pang, T., Laurence, J. M., Johnston, E., Hollands, M. J., Pleass, H. C., & Richardson, A. J. (2013). A systematic review of repeat hepatectomy for recurrent colorectal liver metastases. *J Gastrointest Surg, 17*(7), 1312-1321. doi:10.1007/s11605-013-2186-5

Leggett, D. A., Kelley, B. B., Bunce, I. H., & Miles, K. A. (1997). Colorectal cancer: diagnostic potential of CT measurements of hepatic perfusion and implications for contrast enhancement protocols. *Radiology, 205*(3), 716-720. doi:10.1148/radiology.205.3.9393526

Liapi, E., Mahesh, M., & Sahani, D. V. (2015). Is CT Perfusion Ready for Liver Cancer Treatment Evaluation? *Journal of the American College of Radiology, 12*(1), 111-113. doi:DOI 10.1016/j.jacr.2014.10.007

Linnik, I. V., Scott, M. L., Holliday, K. F., Woodhouse, N., Waterton, J. C., O'Connor, J. P., . . . Parker, G. J. (2014). Noninvasive tumor hypoxia measurement using magnetic resonance imaging in murine U87 glioma xenografts and in patients with glioblastoma. *Magn Reson Med, 71*(5), 1854-1862. doi:10.1002/mrm.24826

Liu, Y., & Matsui, O. (2007). Changes of intratumoral microvessels and blood perfusion during establishment of hepatic metastases in mice. *Radiology, 243*(2), 386-395. doi:10.1148/radiol.2432060341

Loree, J. M., Pereira, A. A. L., Lam, M., Willauer, A. N., Raghav, K., Dasari, A., . . . Kopetz, S. (2018). Classifying Colorectal Cancer by Tumor Location Rather than Sidedness Highlights a Continuum in Mutation Profiles and Consensus Molecular Subtypes. *Clinical cancer research : an official journal of the American Association for Cancer Research, 24*(5), 1062-1072. doi:10.1158/1078-0432.CCR-17-2484

Loupakis, F., Cremolini, C., Masi, G., Lonardi, S., Zagonel, V., Salvatore, L., . . . Falcone, A. (2014). Initial therapy with FOLFOXIRI and bevacizumab for metastatic colorectal cancer. *N Engl J Med, 371*(17), 1609-1618. doi:10.1056/NEJMoa1403108

Malafosse, R., Penna, C., Sa Cunha, A., & Nordlinger, B. (2001). Surgical management of hepatic metastases from colorectal malignancies. *Ann Oncol, 12*(7), 887-894.

Maor, Y., & Malnick, S. (2013). Liver Injury Induced by Anticancer Chemotherapy and Radiation Therapy. *International Journal of Hepatology, 2013*, 815105. doi:10.1155/2013/815105

Masi, G., Loupakis, F., Pollina, L., Vasile, E., Cupini, S., Ricci, S., . . . Falcone, A. (2009). Long-term outcome of initially unresectable metastatic colorectal cancer patients treated with 5-fluorouracil/leucovorin, oxaliplatin, and irinotecan (FOLFOXIRI) followed by radical surgery of metastases. *Ann Surg, 249*(3), 420-425. doi:10.1097/SLA.0b013e31819a0486

Massimino, K. P., Kolbeck, K. J., Enestvedt, C. K., Orloff, S., & Billingsley, K. G. (2012). Safety and efficacy of preoperative right portal vein embolization in patients at risk for postoperative liver failure following major right hepatectomy. *HPB : The Official Journal of the International Hepato Pancreato Biliary Association, 14*(1), 14-19. doi:10.1111/j.1477-2574.2011.00402.x

Mattar, R. E., Al-Alem, F., Simoneau, E., & Hassanain, M. (2016). Preoperative selection of patients with colorectal cancer liver metastasis for hepatic resection. *World J Gastroenterol, 22*(2), 567-581. doi:10.3748/wjg.v22.i2.567

Maughan, T. S., Adams, R. A., Smith, C. G., Meade, A. M., Seymour, M. T., Wilson, R. H., . . . on behalf of the, M. R. C. C. T. I. (2011). Addition of cetuximab to oxaliplatin-based first-line combination chemotherapy for treatment of advanced colorectal cancer: results of the randomised phase 3 MRC COIN trial. *Lancet, 377*(9783), 2103-2114. doi:10.1016/S0140-6736(11)60613-2

Meijerink, M. R., van Waesberghe, J. H. T. M., van der Weide, L., van den Tol, P., Meijer, S., Comans, E. F., . . . van Kuijk, C. (2009). Early Detection of Local RFA Site Recurrence Using Total Liver Volume Perfusion CT: Initial Experience. *Acad Radiol, 16*(10), 1215-1222. doi:DOI 10.1016/j.acra.2009.03.023

Merriman, B., & Rothberg, J. M. (2012). Progress in ion torrent semiconductor chip based sequencing. *Electrophoresis, 33*(23), 3397-3417. doi:10.1002/elps.201200424

Mewton, N., Liu, C. Y., Croisille, P., Bluemke, D., & Lima, J. A. (2011). Assessment of myocardial fibrosis with cardiovascular magnetic resonance. *J Am Coll Cardiol, 57*(8), 891-903. doi:10.1016/j.jacc.2010.11.013

Miles, K. A. (1991). Measurement of tissue perfusion by dynamic computed tomography. *Br J Radiol, 64*(761), 409-412. doi:doi:10.1259/0007-1285-64-761-409

Miles, K. A. (2003). Perfusion CT for the assessment of tumour vascularity: which protocol? *Br J Radiol, 76 Spec No 1*, S36-42. doi:10.1259/bjr/18486642

Miles, K. A., Leggett, D. A. C., Kelley, B. B., Hayball, M. P., Sinnatamby, R., & Bunce, I. (1998). In vivo assessment of neovascularization of liver metastases using perfusion CT. *British Journal of Radiology, 71*(843), 276-281.

Miller, K. D. (2005). A multicenter phase II trial of ZD6474, a vascular endothelial growth factor receptor-2 and epidermal growth factor receptor tyrosine kinase inhibitor, in patients with previously treated metastatic breast cancer. *Clin. Cancer Res., 11*, 3369-3376.

Minagawa, M., Makuuchi, M., Torzilli, G., Takayama, T., Kawasaki, S., Kosuge, T., . . . Imamura, H. (2000). Extension of the frontiers of surgical indications in the treatment of liver metastases from colorectal cancer: long-term results. *Ann Surg, 231*(4), 487-499.

Misale, S., Yaeger, R., Hobor, S., Scala, E., Janakiraman, M., Liska, D., . . . Bardelli, A. (2012). Emergence of KRAS mutations and acquired resistance to anti-EGFR therapy in colorectal cancer. *Nature, 486*(7404), 532-536. doi:10.1038/nature11156

Mocellin, S., Pilati, P., Lise, M., & Nitti, D. (2007). Meta-Analysis of Hepatic Arterial Infusion for Unresectable Liver Metastases From Colorectal Cancer: The End of an Era? *Journal of Clinical Oncology, 25*(35), 5649-5654. doi:10.1200/JCO.2007.12.1764

Mohan, S., Heitzer, E., Ulz, P., Lafer, I., Lax, S., Auer, M., . . . Speicher, M. R. (2014). Changes in colorectal carcinoma genomes under anti-EGFR therapy identified by whole-genome plasma DNA sequencing. *PLoS genetics, 10*(3), e1004271-e1004271. doi:10.1371/journal.pgen.1004271

Montagut, C., Argilés, G., Ciardiello, F., Poulsen, T. T., Dienstmann, R., Kragh, M., . . . Tabernero, J. (2018). Efficacy of Sym004 in Patients With Metastatic Colorectal Cancer With Acquired Resistance to Anti-EGFR Therapy and Molecularly Selected by Circulating Tumor DNA Analyses: A Phase 2 Randomized Clinical Trial. *JAMA oncology, 4*(4), e175245-e175245. doi:10.1001/jamaoncol.2017.5245

Morsbach, F., Sah, B. R., Spring, L., Puippe, G., Gordic, S., Seifert, B., . . . Reiner, C. S. (2014). Perfusion CT best predicts outcome after radioembolization of liver metastases: a comparison of radionuclide and CT imaging techniques. *European Radiology, 24*(7), 1455-1465. doi:DOI 10.1007/s00330-014-3180-3

Mouliere, F., El Messaoudi, S., Gongora, C., Guedj, A. S., Robert, B., Del Rio, M., . . . Thierry, A. R. (2013). Circulating Cell-Free DNA from Colorectal Cancer Patients May Reveal High KRAS or BRAF Mutation Load. *Transl Oncol, 6*(3), 319-328.

Murtaza, M., Dawson, S.-J., Tsui, D. W. Y., Gale, D., Forshew, T., Piskorz, A. M., . . . Rosenfeld, N. (2013). Non-invasive analysis of acquired resistance to cancer therapy by sequencing of plasma DNA. *Nature, 497*(7447), 108-112. doi:10.1038/nature12065. http://www.nature.com/nature/journal/v497/n7447/abs/nature12065.html#supplementary-information

Nicolay, N. H., Berry, D. P., & Sharma, R. A. (2009). Liver metastases from colorectal cancer: radioembolization with systemic therapy. *Nat Rev Clin Oncol, 6*(12), 687-697. doi:10.1038/nrclinonc.2009.165

Nordlinger, B., Poston, G. J., & Goldberg, R. M. (2015). Should the results of the new EPOC trial change practice in the management of patients with resectable metastatic colorectal cancer confined to the liver? *J Clin Oncol, 33*(3), 241-243. doi:10.1200/jco.2014.58.3989

Nordlinger, B., Sorbye, H., Glimelius, B., Poston, G. J., Schlag, P. M., Rougier, P., . . . Gruenberger, T. (2008). Perioperative chemotherapy with FOLFOX4 and surgery versus surgery alone for resectable liver metastases from colorectal cancer (EORTC Intergroup trial 40983): a randomised controlled trial. *Lancet, 371*(9617), 1007-1016. doi:10.1016/s0140-6736(08)60455-9

Nordlinger, B., Sorbye, H., Glimelius, B., Poston, G. J., Schlag, P. M., Rougier, P., . . . Gruenberger, T. (2013). Perioperative FOLFOX4 chemotherapy and surgery versus surgery alone for resectable liver metastases from colorectal cancer (EORTC 40983): long-term results of a randomised, controlled, phase 3 trial. *The Lancet Oncology, 14*(12), 1208-1215. doi:http://dx.doi.org/10.1016/S1470-2045(13)70447-9

Normanno, N., Tejpar, S., Morgillo, F., De Luca, A., Van Cutsem, E., & Ciardiello, F. (2009). Implications for KRAS status and EGFR-targeted therapies in metastatic CRC. *Nat Rev Clin Oncol, 6*(9), 519-527. doi:10.1038/nrclinonc.2009.111

O'Connor, J., Jackson, A., Parker, G., Roberts, C., & Jayson, G. (2012). Dynamic contrast-enhanced MRI in clinical trials of antivascular therapies. *Nat Rev Clin Oncol, 9*, 167 - 177.

O'Connor, J. P., Jackson, A., Parker, G. J., & Jayson, G. C. (2007). DCE-MRI biomarkers in the clinical evaluation of antiangiogenic and vascular disrupting agents. *Br. J. Cancer, 96*, 189-195.

O'Connor, J. P., Naish, J. H., Parker, G. J., Waterton, J. C., Watson, Y., Jayson, G. C., . . . Jackson, A. (2009). Preliminary study of oxygen-enhanced longitudinal relaxation in MRI: a potential novel biomarker of oxygenation changes in solid tumors. *Int J Radiat Oncol Biol Phys, 75*(4), 1209-1215. doi:10.1016/j.ijrobp.2008.12.040

O'Connor, J. P. B., Boult, J. K. R., Jamin, Y., Babur, M., Finegan, K. G., Williams, K. J., . . . Robinson, S. P. (2016). Oxygen-Enhanced MRI Accurately Identifies, Quantifies, and Maps Tumor Hypoxia in Preclinical Cancer Models. *Cancer research, 76*(4), 787-795. doi:10.1158/0008-5472.CAN-15-2062

O'Connor, J. P. B., Jackson, A., Parker, G. J. M., Roberts, C., & Jayson, G. C. (2012). Dynamic contrast-enhanced MRI in clinical trials of antivascular therapies. *Nat Rev Clin Oncol, 9*(3), 167-177. doi:http://www.nature.com/nrclinonc/journal/v9/n3/suppinfo/nrclinonc.2012.2_S1.html

Ogul, H., Kantarci, M., Genc, B., Pirimoglu, B., Cullu, N., Kizrak, Y., . . . Karabulut, N. (2014). Perfusion CT imaging of the liver: review of clinical applications. *Diagnostic and Interventional Radiology, 20*(5), 379-389. doi:DOI 10.5152/dir.2014.13396

Page, K., Guttery, D. S., Zahra, N., Primrose, L., Elshaw, S. R., Pringle, J. H., . . . Shaw, J. A. (2013). Influence of plasma processing on recovery and analysis of circulating nucleic acids. *PLoS One, 8*(10), e77963. doi:10.1371/journal.pone.0077963

Pardo, F., Sangro, B., Lee, R. C., Manas, D., Jeyarajah, R., Donckier, V., . . . Schoen, M. (2017). The Post-SIR-Spheres Surgery Study (P4S): Retrospective Analysis of Safety Following Hepatic Resection or Transplantation in Patients Previously Treated with Selective Internal Radiation Therapy with Yttrium-90 Resin Microspheres. *Ann Surg Oncol, 24*(9), 2465-2473. doi:10.1245/s10434-017-5950-z

Pavlides, M., Banerjee, R., Sellwood, J., Kelly, C. J., Robson, M. D., Booth, J. C., . . . Barnes, E. (2016). Multiparametric magnetic resonance imaging predicts clinical outcomes in patients with chronic liver disease. *Journal of Hepatology, 64*(2), 308-315. doi:http://dx.doi.org/10.1016/j.jhep.2015.10.009

Pawlik, T. M., Scoggins, C. R., Zorzi, D., Abdalla, E. K., Andres, A., Eng, C., . . . Vauthey, J.-N. (2005). Effect of Surgical Margin Status on Survival and Site of Recurrence After Hepatic Resection for Colorectal Metastases. *Annals of Surgery, 241*(5), 715-724. doi:10.1097/01.sla.0000160703.75808.7d

Prezzi, D., & Goh, V. (2016). Rectal Cancer Magnetic Resonance Imaging: Imaging Beyond Morphology. *Clinical Oncology, 28*(2), 83-92. doi:10.1016/j.clon.2015.10.010

Primrose, J., Falk, S., Finch-Jones, M., Valle, J., O'Reilly, D., Siriwardena, A., . . . Bridgewater, J. (2014). Systemic chemotherapy with or without cetuximab in patients with resectable colorectal liver metastasis: the New EPOC randomised controlled trial. *Lancet Oncol, 15*(6), 601-611. doi:10.1016/s1470-2045(14)70105-6

Remmele, S., Sprinkart, A. M., Muller, A., Traber, F., von Lehe, M., Gieseke, J., . . . Murtz, P. (2013). Dynamic and simultaneous MR measurement of R1 and R2* changes during respiratory challenges for the assessment of blood and tissue oxygenation. *Magn Reson Med, 70*(1), 136-146. doi:10.1002/mrm.24458

Rial, B., Robson, M. D., Neubauer, S., & Schneider, J. E. (2011). Rapid quantification of myocardial lipid content in humans using single breath-hold 1H MRS at 3 Tesla. *Magn Reson Med, 66*(3), 619-624. doi:10.1002/mrm.23011

Ridge, J. A., Bading, J. R., Gelbard, A. S., Benua, R. S., & Daly, J. M. (1987). Perfusion of colorectal hepatic metastases. Relative distribution of flow from the hepatic artery and portal vein. *Cancer, 59*(9), 1547-1553.

Rubbia-Brandt, L., Audard, V., Sartoretti, P., Roth, A. D., Brezault, C., Le Charpentier, M., . . . Terris, B. (2004). Severe hepatic sinusoidal obstruction associated with oxaliplatin-based chemotherapy in patients with metastatic colorectal cancer. *Ann Oncol, 15*(3), 460-466.

Ruers, T., Punt, C., Van Coevorden, F., Pierie, J. P., Borel-Rinkes, I., Ledermann, J. A., . . . Nordlinger, B. (2012). Radiofrequency ablation combined with systemic treatment versus systemic treatment alone in patients with non-resectable colorectal liver metastases: a randomized EORTC Intergroup phase II study (EORTC 40004). *Ann Oncol, 23*(10), 2619-2626. doi:10.1093/annonc/mds053

Ruers, T., Punt, C. J., van Coevorden, F., Borel Rinkes, I., Ledermann, J. A., Poston, G. J., . . . Nordlinger, B. (2010). Final results of the EORTC intergroup randomized study 40004 (CLOCC) evaluating the benefit of radiofrequency ablation (RFA) combined with chemotherapy for unresectable colorectal liver metastases (CRC LM). *J Clin Oncol (Meeting Abstracts), 28*(15_suppl), 3526-.

Ruers, T., Van Coevorden, F., Punt, C. J. A., Pierie, J.-P. E. N., Borel-Rinkes, I., Ledermann, J. A., . . . Nordlinger, B. (2017). Local Treatment of Unresectable Colorectal Liver Metastases: Results of a Randomized Phase II Trial. *JNCI: Journal of the National Cancer Institute, 109*(9), djx015-djx015. doi:10.1093/jnci/djx015

Rusthoven, K. E., Kavanagh, B. D., Cardenes, H., Stieber, V. W., Burri, S. H., Feigenberg, S. J., . . . Schefter, T. E. (2009). Multi-institutional phase I/II trial of stereotactic body radiation therapy for liver metastases. *Journal of Clinical Oncology, 27*(10), 1572-1578. doi:10.1200/jco.2008.19.6329

Ryan, P., Nanji, S., Pollett, A., Moore, M., Moulton, C. A., Gallinger, S., & Guindi, M. (2010). Chemotherapy-induced liver injury in metastatic colorectal cancer: semiquantitative histologic analysis of 334 resected liver specimens shows that vascular injury but not steatohepatitis is associated with preoperative chemotherapy. *Am J Surg Pathol, 34*(6), 784-791. doi:10.1097/PAS.0b013e3181dc242c

Sahani, D. V., Holalkere, N. S., Mueller, P. R., & Zhu, A. X. (2007). Advanced hepatocellular carcinoma: CT perfusion of liver and tumor tissue - Initial experience. *Radiology, 243*(3), 736-743. doi:DOI 10.1148/radiol.2433052020

Salem, R., & Thurston, K. G. (2006). Radioembolization with yttrium-90 microspheres: a state-of-the-art brachytherapy treatment for primary and secondary liver malignancies: part 3: comprehensive literature review and future direction. *J Vasc Interv Radiol, 17*. doi:10.1097/01.rvi.0000236744.34720.73

Saltz, L. B., Clarke, S., Diaz-Rubio, E., Scheithauer, W., Figer, A., Wong, R., . . . Cassidy, J. (2008). Bevacizumab in combination with oxaliplatin-based chemotherapy as first-line therapy in metastatic colorectal cancer: a randomized phase III study. *J Clin Oncol, 26*(12), 2013-2019. doi:10.1200/jco.2007.14.9930

Sangro, B., Gil-Alzugaray, B., Rodriguez, J., Sola, I., Martinez-Cuesta, A., Viudez, A., . . . Bilbao, J. I. (2008). Liver disease induced by radioembolization of liver tumors: description and possible risk factors. *Cancer, 112*(7), 1538-1546. doi:10.1002/cncr.23339

Schmiegel, W., Scott, R. J., Dooley, S., Lewis, W., Meldrum, C. J., Pockney, P., . . . Fox, S. B. (2017). Blood-based detection of RAS mutations to guide anti-EGFR therapy in colorectal cancer patients: concordance of results from circulating tumor DNA and tissue-based RAS testing. *Molecular oncology, 11*(2), 208-219. doi:10.1002/1878-0261.12023

Schnitzbauer, A. A., Lang, S. A., Goessmann, H., Nadalin, S., Baumgart, J., Farkas, S. A., . . . Schlitt, H. J. (2012). Right portal vein ligation combined with in situ splitting induces rapid left lateral liver lobe hypertrophy enabling 2-staged extended right hepatic resection in small-for-size settings. *Ann Surg, 255*(3), 405-414. doi:10.1097/SLA.0b013e31824856f5

Seymour, L., Bogaerts, J., Perrone, A., Ford, R., Schwartz, L. H., Mandrekar, S., . . . group, R. w. (2017). iRECIST: guidelines for response criteria for use in trials testing immunotherapeutics. *The Lancet. Oncology, 18*(3), e143-e152. doi:10.1016/S1470-2045(17)30074-8

Sharma, M. R., Maitland, M. L., & Ratain, M. J. (2012). RECIST: No Longer the Sharpest Tool in the Oncology Clinical Trials Toolbox—Point. *Cancer Res, 72*(20), 5145-5149. doi:10.1158/0008-5472.can-12-0058

Sharma, R. A., Van Hazel, G. A., Morgan, B., Berry, D. P., Blanshard, K., Price, D., . . . Steward, W. P. (2007). Radioembolization of liver metastases from colorectal cancer using yttrium-90 microspheres with concomitant systemic oxaliplatin, fluorouracil, and leucovorin chemotherapy. *Journal of Clinical Oncology, 25*(9), 1099-1106. doi:Doi 10.1200/Jco.2006.08.7916

Sharma, R. A., Wasan, H. S., Van Hazel, G. A., Heinemann, V., Sharma, N. K., Taieb, J., . . . Gibbs, P. (2017). Overall survival analysis of the FOXFIRE prospective randomized studies of first-line selective internal radiotherapy (SIRT) in patients with liver metastases from colorectal cancer. *Journal of Clinical Oncology, 35*(15_suppl), 3507-3507. doi:10.1200/JCO.2017.35.15_suppl.3507

Silvennoinen, M. J., Kettunen, M. I., & Kauppinen, R. A. (2003). Effects of hematocrit and oxygen saturation level on blood spin-lattice relaxation. *Magn Reson Med, 49*(3), 568-571. doi:10.1002/mrm.10370

Simkens, L. H., van Tinteren, H., May, A., ten Tije, A. J., Creemers, G. J., Loosveld, O. J., . . . Koopman, M. (2015). Maintenance treatment with capecitabine and bevacizumab in metastatic colorectal cancer (CAIRO3): a phase 3 randomised controlled trial of the Dutch Colorectal Cancer Group. *Lancet, 385*(9980), 1843-1852. doi:10.1016/s0140-6736(14)62004-3

Simmonds, P. C., Primrose, J. N., Colquitt, J. L., Garden, O. J., Poston, G. J., & Rees, M. (2006). Surgical resection of hepatic metastases from colorectal cancer: A systematic review of published studies. *Br J Cancer, 94*(7), 982-999.

Siravegna, G., Mussolin, B., Venesio, T., Marsoni, S., Seoane, J., Dive, C., . . . Bardelli, A. (2019). How liquid biopsies can change clinical practice in oncology. *Annals of Oncology, 30*(10), 1580-1590. doi:10.1093/annonc/mdz227

Stangl, R., Altendorf-Hofmann, A., Charnley, R. M., & Scheele, J. (1994). Factors influencing the natural history of colorectal liver metastases. *Lancet, 343*(8910), 1405-1410.

Strasberg, S. M. (2007). Terminology of Liver Anatomy and Resections: The Brisbane 2000 Terminology. In P.-A. Clavien, M. G. Sarr, Y. Fong, & P. Georgiev (Eds.), *Atlas of Upper Gastrointestinal and Hepato-Pancreato-Biliary Surgery* (pp. 313-317). Berlin, Heidelberg: Springer Berlin Heidelberg.

Strasberg, S. M., Belghiti, J., Clavien, P. A., Gadzijev, E., Garden, J. O., Lau, W. Y., . . . Strong, R. W. (2000). The Brisbane 2000 Terminology of Liver Anatomy and Resections. *HPB, 2*(3), 333-339. doi:10.1016/S1365-182X(17)30755-4

Strasberg, S. M., & Phillips, C. (2013). Use and dissemination of the brisbane 2000 nomenclature of liver anatomy and resections. *Ann Surg, 257*(3), 377-382. doi:10.1097/SLA.0b013e31825a01f6

Strickler, J. H., Loree, J. M., Ahronian, L. G., Parikh, A. R., Niedzwiecki, D., Pereira, A. A. L., . . . Kopetz, S. (2018). Genomic Landscape of Cell-Free DNA in Patients with Colorectal Cancer. *Cancer discovery, 8*(2), 164-173. doi:10.1158/2159-8290.CD-17-1009

Tanis, E., Nordlinger, B., Mauer, M., Sorbye, H., van Coevorden, F., Gruenberger, T., . . . Ruers, T. J. (2014). Local recurrence rates after radiofrequency ablation or resection of colorectal liver metastases.

Analysis of the European Organisation for Research and Treatment of Cancer #40004 and #40983. *European Journal of Cancer, 50*(5), 912-919. doi:10.1016/j.ejca.2013.12.008

Thng, C. H., Koh, T. S., Collins, D. J., & Koh, D. M. (2010). Perfusion magnetic resonance imaging of the liver. *World J Gastroenterol, 16*(13), 1598-1609.

Tie, J., Kinde, I., Wang, Y., Wong, H. L., Roebert, J., Christie, M., . . . Gibbs, P. (2015). Circulating Tumor DNA as an Early Marker of Therapeutic Response in Patients with Metastatic Colorectal Cancer. *Annals of Oncology*. doi:10.1093/annonc/mdv177

Tie, J., Wang, Y., Tomasetti, C., Li, L., Springer, S., Kinde, I., . . . Gibbs, P. (2016). Circulating tumor DNA analysis detects minimal residual disease and predicts recurrence in patients with stage II colon cancer. *Science translational medicine, 8*(346), 346ra392-346ra392. doi:10.1126/scitranslmed.aaf6219

Tofts, P. S. (1999). Estimating kinetic parameters from dynamic contrast-enhanced T(1)-weighted MRI of a diffusable tracer: standardized quantities and symbols. *J. Magn. Reson. Imaging, 10*, 223-232.

Tofts, P. S., Brix, G., Buckley, D. L., Evelhoch, J. L., Henderson, E., Knopp, M., . . . Weisskoff, R. M. (1999). Estimating kinetic parameters from dynamic contrast-enhanced T(1)-weighted MRI of a diffusable tracer: Standardized quantities and symbols. *Journal of Magnetic Resonance Imaging, 10*(3), 223-232. doi:Doi 10.1002/(Sici)1522-2586(199909)10:3<223::Aid-Jmri2>3.0.Co;2-S

Townsend, A., Price, T., & Karapetis, C. (2009). Selective internal radiation therapy for liver metastases from colorectal cancer. *Cochrane Database Syst Rev*(4), Cd007045. doi:10.1002/14651858.CD007045.pub2

Van Cutsem, E., Kohne, C. H., Hitre, E., Zaluski, J., Chang Chien, C. R., Makhson, A., . . . Rougier, P. (2009). Cetuximab and chemotherapy as initial treatment for metastatic colorectal cancer. *N Engl J Med, 360*(14), 1408-1417. doi:10.1056/NEJMoa0805019

van Hazel, G. A., Heinemann, V., Sharma, N. K., Findlay, M. P. N., Ricke, J., Peeters, M., . . . Gibbs, P. (2016). SIRFLOX: Randomized Phase III Trial Comparing First-Line mFOLFOX6 (Plus or Minus Bevacizumab) Versus mFOLFOX6 (Plus or Minus Bevacizumab) Plus Selective Internal Radiation Therapy in Patients With Metastatic Colorectal Cancer. *Journal of Clinical Oncology*. doi:10.1200/jco.2015.66.1181

Vauthey, J. N., Pawlik, T. M., Ribero, D., Wu, T. T., Zorzi, D., Hoff, P. M., . . . Abdalla, E. K. (2006). Chemotherapy regimen predicts steatohepatitis and an increase in 90-day mortality after surgery for hepatic colorectal metastases. *J Clin Oncol, 24*(13), 2065-2072. doi:10.1200/jco.2005.05.3074

Wang, L. M., Jani, A. R., Hill, E. J., & Sharma, R. A. (2013). Anatomical basis and histopathological changes resulting from selective internal radiotherapy for liver metastases. *Journal of Clinical Pathology, 66*(3), 205-211. doi:10.1136/jclinpath-2012-201231

Wasan, H. S., Gibbs, P., Sharma, N. K., Taieb, J., Heinemann, V., Ricke, J., . . . Westcott, M. (2017). First-line selective internal radiotherapy plus chemotherapy versus chemotherapy alone in patients with liver metastases from colorectal cancer (FOXFIRE, SIRFLOX, and FOXFIRE-Global): a combined analysis of three multicentre, randomised, phase 3 trials. *The Lancet Oncology, 18*(9), 1159-1171. doi:10.1016/S1470-2045(17)30457-6

White, J., Carolan-Rees, G., Dale, M., Morgan, H. E., Patrick, H. E., See, T. C., . . . Sharma, R. A. (2019). Analysis of a National Programme for Selective Internal Radiation Therapy for Colorectal Cancer Liver Metastases. *Clinical Oncology, 31*(1), 58-66. doi:10.1016/j.clon.2018.09.002

White, J., Carolan-Rees, G., Dale, M., Patrick, H. E., See, T. C., Bell, J. K., . . . Sharma, R. A. (2019). *Journal of Vascular and Interventional Radiology, 30*(8), 1185-1192. doi:10.1016/j.jvir.2019.03.018

Winter, H., Kaisaki, P. J., Harvey, J., Giacopuzzi, E., Ferla, M. P., Pentony, M. M., . . . McCullagh, J. S. O. (2019). Identification of Circulating Genomic and Metabolic Biomarkers in Intrahepatic Cholangiocarcinoma. *Cancers (Basel), 11*(12). doi:10.3390/cancers11121895

Winter, H., Mirecka, J., Papiez, B., Irving, B., Jenkinson, M., Chappell, M., . . . Schnabel, J. (2018). Clinical feasibility of texture analysis in DCE MRI of patients receiving selective internal radiation therapy. *European Journal of Surgical Oncology, 44*, S30-S31. doi:10.1016/j.ejso.2018.01.551

Winter, H., Rassam, J., Virdee, P. S., Goldin, R., Pitcheshwar, P., Weaver, K., . . . Sharma, R. A. (2019). Hepatic Resection Following Selective Internal Radiation Therapy for Colorectal Cancer Metastases in the FOXFIRE Clinical Trial: Clinical Outcomes and Distribution of Microspheres. *Cancers, 11*(8), 1155. doi:10.3390/cancers11081155

Wong, S. Q., Raleigh, J. M., Callahan, J., Vergara, I. A., Ftouni, S., Hatzimihalis, A., . . . Dawson, S.-J. (2017). Circulating Tumor DNA Analysis and Functional Imaging Provide Complementary Approaches for Comprehensive Disease Monitoring in Metastatic Melanoma. *JCO Precision Oncology*(1), 1-14. doi:10.1200/PO.16.00009

Yamamoto, K., Sherman, I., Phillips, M. J., & Fisher, M. M. (1985). Three-dimensional observations of the hepatic arterial terminations in rat, hamster and human liver by scanning electron microscopy of microvascular casts. *Hepatology, 5*(3), 452-456.

Young, I. R., Clarke, G. J., Bailes, D. R., Pennock, J. M., Doyle, F. H., & Bydder, G. M. (1981). Enhancement of relaxation rate with paramagnetic contrast agents in NMR imaging. *J Comput Tomogr, 5*(6), 543-547.

Zaharchuk, G., Busse, R. F., Rosenthal, G., Manley, G. T., Glenn, O. A., & Dillon, W. P. (2006). Noninvasive oxygen partial pressure measurement of human body fluids in vivo using magnetic resonance imaging. *Acad Radiol, 13*(8), 1016-1024. doi:10.1016/j.acra.2006.04.016

Zhang, X. M., Yu, D., Zhang, H. L., Dai, Y., Bi, D., Liu, Z., . . . Li, C. (2008). 3D dynamic contrast-enhanced MRI of rectal carcinoma at 3T: correlation with microvascular density and vascular endothelial growth factor markers of tumor angiogenesis. *J Magn Reson Imaging, 27*(6), 1309-1316. doi:10.1002/jmri.21378

Zhong, L., Wang, W. J., & Xu, J. R. (2009). Clinical application of hepatic CT perfusion. *World J Gastroenterol, 15*(8), 907-911.

Zweifel, M., & Padhani, A. R. (2010). Perfusion MRI in the early clinical development of antivascular drugs: decorations or decision making tools? *Eur. J. Nucl. Med. Mol. Imaging, 37*(Suppl. 1), 164-182.

Supplementary Table 1. Clinical feasibility of serial pCT at 4 time-points in patients randomised to chemotherapy (Arm A) and SIRT or chemotherapy alone, from Jan 2011 – Oct 2014. Patient P1048 was withdrawn. One patient died from disease progression and two did not attend for last scan. Patient P1319 was unable to have second pCT due to inability to establish IV access.

Trial number	Baseline pCT	Cycle 2 pCT	SIRT received	Cycle 3 pCT	Cycle 5 pCT
P1048	Y	N	N	N	N
P1053	Y	Y	Y	Y	Y
P1056	Y	Y	Arm A	Y	Y
P1085	Y	Y	Y	Y	Y
P1099	Y	Y	Arm A	Y	Y
P1105	Y	Y	Y	Y	Y
P1109	Y	Y	Arm A	Y	Y
P1130	Y	Y	Arm A	Y	Y
P1154	Y	Y	Y	Y	Y
P1170	Y	Y	Arm A	Y	Y
P1172	Y	Y	Arm A	Y	Y
P1182	Y	Y	Y	Y	Y
P1200	Y	Y	Y	Y	Y
P1204	Y	Y	Arm A	Y	Y
P1241	Y	Y	Arm A	Y	Y
P1248	Y	Y	Arm A	Y	N
P1263	Y	Y	Arm A	Y	Y
P1277	Y	Y	Y	Y	N
P1278	Y	Y	Y	Y	Y
P1286	Y	Y	Y	Y	Y
P1319	Y	N	Arm A	Y	Y
P1324	Y	Y	Y	Y	Y
P1329	Y	Y	Arm A	Y	Y
P1354	Y	Y	Y	Y	Y
P1287	Y	Y	Y	Y	Y
P1337	Y	Y	Arm A	Y	Y
P1359	Y	Y	Y	Y	Y
P1325	Y	Y	Arm A	Y	N
P1360	Y	Y	Y	Y	Y

Y- yes; N - no

Supplementary Table 2. Line listing of mCRC patient characteristics and tumour radiology data at baseline.

Patient	Cohort	Sex	Age (y)[1]	Therapy2	pCT									DCE MRI		
					BF	BV	HAF	MSI	MTT	PEI	PS	TTP	Tmax	Ktrans	ve	kep
P1048	FOXFIRE	Female	64	SIRT												
P1053	FOXFIRE	Male	48	SIRT	71.44	10.54	0.39	0.83	14.88	0.08	11.77	10.54	32.86			
P1056	FOXFIRE	Male	63	Chemo	69.89	8.83	0.24	0.89	11.68	0.06	18.05	8.09	28.65			
P1085	FOXFIRE	Female	56	SIRT	94.12	15.60	0.54	1.13	13.81	0.11	8.83	8.90	34.09			
P1099	FOXFIRE	Female	43	Chemo	80.33	17.52	0.63	1.02	15.12	0.10	48.16	15.18	35.60			
P1105	FOXFIRE	Male	49	SIRT	77.99	7.77	0.26	0.44	9.57	0.05	3.51	8.46	33.35			
P1109	FOXFIRE	Male	66	Chemo	89.80	13.27	0.34	0.77	16.57	0.09	9.59	12.32	38.11			
P1130	FOXFIRE	Male	60	Chemo	102.95	7.21	0.35	0.85	8.78	0.10	6.38	6.67	32.56			
P1154	FOXFIRE	Female	63	SIRT												
P1170	FOXFIRE	Male	53	Chemo	116.78	10.95	0.19	0.69	10.70	0.17	11.59	8.74	35.67			
P1172	FOXFIRE	Male	72	Chemo	134.10	10.34	0.28	1.04	9.44	0.13	18.37	7.81	39.99			
P1182	FOXFIRE	Male	67	SIRT	79.24	8.05	0.41	0.63	11.10	0.09	6.80	7.83	32.73			
P1200	FOXFIRE	Male	46	SIRT	98.44	14.73	0.39	1.13	12.28	0.13	15.60	8.31	32.25			
P1204	FOXFIRE	Male	71	Chemo	146.35	9.69	0.32	0.85	7.59	0.11	15.07	6.94	34.94			
P1241	FOXFIRE	Female	42	SIRT	120.00	28.35	0.16		15.60	3.02	87.31	9.85	0.00			
P1248	FOXFIRE	Male	67	Chemo	77.02	6.05	0.23	0.51	10.14	0.06	7.03	7.68	31.42			
P1263	FOXFIRE	Male	58	Chemo	66.78	8.12	0.54	0.63	12.09	0.17	11.33	7.57	30.08			
P1277	FOXFIRE	Male	66	SIRT	77.34	9.46	0.32	0.92	11.83	0.08	15.88	8.44	32.75			
P1278	FOXFIRE	Male	52	SIRT	53.78	4.20	0.20	0.40	11.28	0.05	5.07	7.72	32.76			
P1286	FOXFIRE	Female	67	SIRT	88.77	10.29	0.23	1.38	8.57	0.09	13.31	8.33	31.63			
P1287	FOXFIRE	Male	56	SIRT	40.89	9.90	0.44	0.50	23.82	0.14	7.94	15.71	76.55			
P1319	FOXFIRE	Female	59	Chemo	155.50	9.43	0.21	1.48	9.11	0.09	8.78	7.09	33.00			
P1324	FOXFIRE	Male	59	SIRT	92.50	17.86	0.50		11.72	2.13	42.60	7.40	0.00			
P1325	FOXFIRE	Female	55	Chemo	432.65	47.57	0.09	2.61	5.88	0.37	22.29	4.93	33.61			
P1329	FOXFIRE	Male	66	Chemo	110.26	11.17	0.36	1.07	10.16	0.11	13.70	8.06	34.64			
P1337	FOXFIRE	Male	63	Chemo	100.20	14.74	0.88	0.94	14.72	0.22	7.07	9.73	49.94			
P1354	FOXFIRE	Female	59	SIRT	206.72	60.35	0.45		14.87	0.03	85.92	8.66	0.00			
P1359	FOXFIRE	Male	53	SIRT												
P1360	FOXFIRE	Male	73	Chemo	78.73	10.80	0.17	0.61	12.98	0.07	12.34	9.95	33.41			

Supplementary Table 2. Line listing of mCRC patient characteristics and tumour radiology data at baseline.

Patient	Cohort	Sex	Age (y)[1]	Therapy2	pCT									DCE MRI		
					BF	BV	HAF	MSI	MTT	PEI	PS	TTP	Tmax	Ktrans	ve	kep
P1501	Non-FF	Female	52	SIRT	90.71	16.54	0.47	8.44	16.67	0.27	16.49	9.71	1.63	0.32	0.34	0.86
P1502	Non-FOXFIRE	Female	70	SIRT	66.13	8.78	0.43	0.63	14.50	0.07	9.45	10.52	37.76	0.70	1.08	0.66
P1503	Non-FOXFIRE	Male	67	SIRT	90.72	10.94	0.59	1.47	8.82	0.14	10.11	6.39	28.28	0.54	0.78	0.66
P1504	Non-FOXFIRE	Male	76	SIRT	105.20	9.31	0.70	2.13	7.34	0.14	4.62	6.23	23.37	0.32	0.50	0.69
P1505	Non-FOXFIRE	Male	70	SIRT	76.47	7.66	0.36	0.74	10.95	0.07	8.71	8.66	32.83	0.27	0.52	0.64
P1506	Non-FOXFIRE	Male	57	SIRT	94.91	12.66	0.42	0.95	10.49	0.14	9.63	7.09	33.47			
P1507	Non-FOXFIRE	Female	55	SIRT												
P1509	Non-FOXFIRE	Male	53	SIRT	99.70	16.56	0.33	1.32	12.02	0.15	29.05	8.52	29.86	0.93	0.89	1.09
P1510	Non-FOXFIRE	Male	78	SIRT												
P1511	Non-FOXFIRE	Male	56	SIRT	81.25	11.04	0.37	1.27	13.33	0.16	12.44	8.73	31.04	1.07	1.40	0.63
P1512	Non-FOXFIRE	Female	50	SIRT	67.02	12.40	0.49		12.99	0.25	41.35	11.24	0.00			
P1513	Non-FOXFIRE	Male	83	SIRT	96.83	10.19	0.30	1.19	9.25	0.07	22.13	9.53	34.93	0.69	0.91	0.76
P1514	Non-FOXFIRE	Male	73	SIRT	190.25	29.31	0.68	0.97	12.35	0.15	6.74	8.89	33.41	0.98	1.46	0.52
P1517	Non-FOXFIRE	Male	69	SIRT	49.35	5.82	0.29	0.60	12.21	0.05	8.18	8.24	28.99	0.22	0.45	0.51
P1518	Non-FOXFIRE	Male	55	SIRT	58.61	10.58	0.40	0.83	15.40	0.14	16.12	9.65	34.21	0.31	0.58	0.64
P1519	Non-FOXFIRE	Female	61	SIRT	63.10	6.28	0.14	1.24	6.03	0.06	3.64	6.20	20.96			
P1520	Non-FOXFIRE	Female	37	SIRT	102.82	11.04	0.47	1.06	9.81	0.15	13.73	7.19	34.63	1.42	1.27	1.40
P1521	Non-FOXFIRE	Female	44	SIRT	93.70	17.74	0.44	1.13	15.72	0.20	24.59	9.52	33.49	0.61	0.86	0.76
P1523	Non-FOXFIRE	Male	55	SIRT	139.73	12.77	0.39	1.45	8.82	0.16	10.83	6.77	34.05	0.79	0.83	0.68
P1524	Non-FOXFIRE	Female	68	SIRT										0.35	0.88	0.39
P1525	Non-FOXFIRE	Male	32	SIRT	235.70	19.13	0.27	1.60	8.06	0.19	39.51	9.09	31.56	0.21	1.29	0.17
P1527	Non-FOXFIRE	Male	33	SIRT	89.18	15.39	0.62	1.04	14.41	0.09	8.85	8.76	32.67			
P1528	Non-FOXFIRE	Male	67	SIRT	48.34	10.93	0.47	0.74	15.14	0.07	7.97	9.60	30.36			
P1529	Non-FOXFIRE	Male	67	SIRT	86.51	7.26	0.21	0.71	10.11	0.09	7.52	7.86	30.24			

[1] Age given in years at the time of registration

[2] Assigned treatment

[3] MRI performed in the non-FOXFIRE patients only

Supplementary Figure 1. Zonal Analysis of mean microsphere density/mm2. Microsphere density measured at 1 mm and 2 mm zones from tumour margin. The zones were measured at 0-1 mm, 1-2 mm within tumour margin, central tumour and zones outside tumour margin at 0-1 mm, 1-2 mm and adjacent background liver. Work completed with Prof Goldin's laboratory.

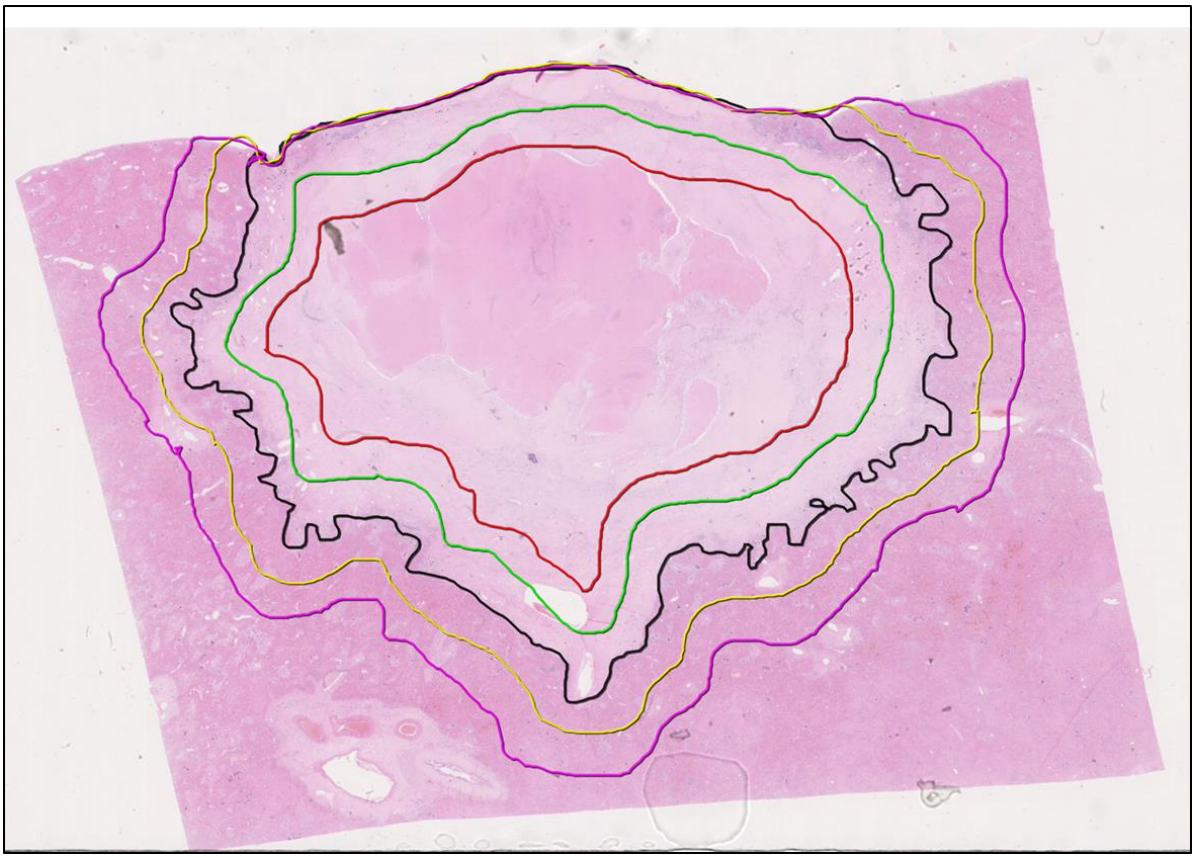

Zone	0-1 mm	1-2 mm	Tumour centre	0-1 mm	1-2 mm	Adjacent background liver
	Inside tumour margin ←			Outside tumour margin →		
Mean microsphere density / mm^2	6.10	3.21	1.05	1.99	1.02	1.05

Appendix 1: Full papers published during the DPhil.

1. Winter H, Kaisaki P, Harvey J, Giacopuzzi E, Ferla M, Pentony M, Knight S, Sharma RA, Taylor JC, McCullagh J. Identification of Circulating Genomic and Metabolic Biomarkers in Intrahepatic Cholangiocarcinoma. *Cancers* 2019, 11(12), 1895; https://doi.org/10.3390/cancers11121895.
2. Winter H, Rassam J, Virdee P, Goldin R, et al. Hepatic resection following selective internal radiation therapy for colorectal cancer metastases in the FOXFIRE clinical trial: clinical outcomes and distribution of microspheres. *Cancers* (Basel). 2019;11(8):1155.
3. Kannan P, Kretzschmar W, Winter H, Warren D, Bates R, Allen P, Syed N, Irving B, Papiez B, et al. Functional parameters derived from magnetic resonance imaging reflect vascular morphology in preclinical tumours and in human liver metastases. *Clinical Cancer Research* 2018.
4. Lyon P, Winter H, Herbschleb K, et al. Long-term radiological and histological outcomes following selective internal radiation therapy to liver metastases from breast cancer. *Radiology Case Reports* 2018; 13 (6): 1259-1266.
5. Winter H, Boardman P, Morgan D, Greenhalgh T, Sharma RA. Advances in SIRT for primary and secondary liver cancer. *Rad* 2016; 42 (496): 17-18.
6. Shiao J, Winter H, Sharma RA. Landmark study raises the bar for interventional oncology. *Future Oncology* 2016; 12 (15): 1747-1749.

Appendix 2: Abstracts presented during the DPhil.

1. Winter H, Kaisaki P, Knight S, Harvery J, Sharma R, McCullagh, Taylor J. Circulating tumour DNA in patients with intrahepatic cholangiocarcinoma – detection of an IDH1 mutation and elevated 2-hydroxyglutarate. *Eur J Surg Onc* 2018; 44: S31.
2. Abbott E, Falzone F, Winter H, Greenhalgh T, Kartsonaki C, Craig, A, Sharma RA, Vallis K. Absorbed dose from ^{90}Y SIRT is correlated with individual lesion response in colorectal cancer patients. *Eur J Surg* Onc 2018; 44: S53.
3. Winter H, Kaisaki P, Carter R, Cutts A, Greenhalgh T, Schuh A, Sharma RA, Taylor JC. Sequencing cfDNA in patients with advanced colorectal cancer receiving SIRT. *J Clin Onc* 2017; 35, (Supp 4S: 646).
4. Winter H. Monitoring and Sequencing Cell-Free DNA in Patients Receiving Selective Internal Radiation. Oral presentation Molecular Diagnostics, Lisbon, Portugal 2017.
5. Winter h, Mireka J, Papiez B, Irving B, Jenkinson M, Chappell M, Schnabel J.. Clinical feasibility of texture analysis in DCE MRI of patients receiving SIRT. *Eur J Surg Onc*: 43(11); 2228.
6. Shiao J, Winter H, Greenhalgh, Virdee P, Little M, Boardman P, Sharma RA.. Assocaition of neutrophil-lymphocyte ratio with survival outcome sin metastatic colorectal cancer patients treated with SIRT. *Int J Rad Onc Physics* 2017: 99(2); E188.
7. Winter H, Kaisaki P, Cutts A, Greenhalgh T, Schuh A, Taylor J, Sharma RA. Monitoring cell free DNA in patients receiving SIRT for liver metastases and intrahepatic cholangiocarcinoma. *European Journal of Cancer* 2016; 61 (Suppl. 1: 834).
8. Shiao J, Winter H, Greenhalgh T, Sharma RA. Analysis of imaging and liver function tests in patients with liver metastases treated with SIRT. Cancer Research UK Oxford Centre Symposium 2016.
9. Winter H, Pavlides M, Greenhalgh T, Anderson E, Piechnik S, Gleeson F, Sharma RA, Bulte D. Quantitative T1 mapping of colorectal liver metastases with inhaled oxygen. Cancer Research UK Biomarker meeting, University of Cambridge 2016.
10. Winter H. Circulating cell free DNA in patients receiving selective internal radiation therapy. Oral presentation Molecular Diagnostics, Lisbon, Portugal 2016.
11. Winter H, Pavlides M, Sharma RA, Gleeson F, Silva M, Ferreira V, Wang LM, Barnes E, Piechnik S, Neubauer S. T1 mapping with shMOLLI using supplemental oxygen – a new cancer imaging tool. Imaging festival, University of Oxford 2015.
12. Abbot E, Craig A, Franklin J, Denis-Bacelar A, Syed N, Flux G, Winter H, Sharma RA, Vallis K, Falzone N. A method towards patient-specific dosimetry of 90Y SIRT in the treatment of liver metastases. CRUK Oxford conference June 2015.
13. Winter H, Hill E, Syed N, Chung D et al. PERFORM: An imaging study of arterial blood flow to liver metastases before and after selective internal radiotherapy. European Association for the Study of Liver, *J Hepatol* 2015; 62: S859.